**Multi-sensory gamma stimulation ameliorates Alzheimer's-associated pathology and improves cognition**

by

Anthony J. Martorell
B.S. The University of Tampa (2012)

Submitted to the Department of Brain and Cognitive Sciences in Partial Fulfillment of the Requirements for the Degree of

Doctor of Philosophy

at the

MASSACHUSETTS INSTITUTE OF TECHNOLOGY

June 2019



Signature redacted

Signature of Author ..... .....
Department of Brain and Cognitive Sciences
February 28th, 2019

Signature redacted

Certified by ..... .....
Li-Huei Tsai, PhD.
Director, the Picower Institute for Learning and Memory
Picower Professor of Neuroscience
Thesis Supervisor

Signature redacted

Accepted by ..... .....
Matthew A. Wilson, PhD.
Sherman Fairchild Professor of Neuroscience
Director of Graduate Education for Brain and Cognitive Sciences

**Multi-sensory gamma stimulation ameliorates Alzheimer's-associated pathology and improves cognition**

by

Anthony J. Martorell

Submitted to the Department of Brain and Cognitive Sciences on February 14, 2019
in Partial Fulfillment of the Requirements for the Degree of
Doctor of Philosophy in Neuroscience

## Abstract

Changes in gamma activity (30-90 Hz) have been observed in humans and animal-models of Alzheimer's disease (AD). Examining the relationship between gamma oscillations and disease pathology is a significant problem in neuroscience. Recent work using a non-invasive light flicker at 40 Hz, termed Gamma ENtrainment Using Sensory stimulus, or 'GENUS', was shown to impact pathology in the visual cortex of AD-mouse models. However, it is not known whether other sensory modalities at 40 Hz can change pathology in higher order brain regions, or affect cognition, in AD-like animal models. In this thesis, I combine *in vivo* electrophysiology, biochemical and imaging techniques, and behavioral assays to understand the effects of multi-sensory gamma stimulation in AD-like animals. I first show that auditory tone stimulation at 40 Hz (auditory GENUS) can drive gamma frequency neural activity in auditory cortex (AC) and hippocampal CA1. I then demonstrate that seven days of auditory GENUS results in improved spatial and recognition memory and reduced amyloid load in AC and hippocampus of 5XFAD mice. These changes in activation responses were evident in microglia, astrocytes, and vasculature. Additionally, auditory GENUS reduced phosphorylated tau in the tau P301S model. Finally, I demonstrate that combined auditory and visual GENUS, but not either alone, decreases amyloid and produces a microglial-clustering response in the medial prefrontal cortex. Whole brain analysis using SHIELD processing revealed widespread reduction of amyloid plaques throughout neocortex after multi-sensory GENUS. These findings suggest that GENUS can be achieved through multiple sensory modalities with wide-ranging effects across multiple brain areas to improve cognitive function.

Thesis supervisor: Li-Huei Tsai, PhD.
Title: Director, the Picower Institute for Learning and Memory
Picower Professor of Neuroscience

**Table of Contents**

## Acknowledgments

I have a deep sense of gratitude for my thesis advisor, Li-Huei Tsai. When I entered Li-Huei's lab as a technician, I did not think I would be leaving with my PhD. Li-Huei has taken invaluable time to guide me, mentor me, and mold me from the naïve student I was to the scientist I am today. If I have just the smallest fraction of her hard work or determination, I am better for it.

I still remember being awfully nervous approaching my committee member, Ed Boyden, to ask if I could rotate in his lab. His charisma and unique and exciting ideas were (and still are) invigorating, and my time working with him was a treasure.

I am extremely thankful for my committee member Emery Brown for his time and dedication towards my project, and contributing discussions.

Annabelle and Abby, my thesis would absolutely not have been possible without you two. I am so lucky and honored to have had the chance to work with such bright minds such as yours, thank you for sticking with me.

Hannah, this thesis would also not have been possible without you. I am so grateful to have been mentored by you, and also consider you my friend.

Meeting Ho-Jun was a life-saver, I could not have performed 40 Hz stimulation without you, thank you for taking ownership of all things digital, and having the patience to walk me through it.

Jennie, thank you for your undying dedication and hard work toward my thesis, and for being a constant source of laughter and all things strange. We spent many long and painful nights together in lab, and I wouldn't have had it any other way.

Fatema and David, thank you for doing pretty much all the hard and at times, grilling work, and for being patient with me while I ramble on with experiments. Special thanks to Fatema and her major help with imaging experiments and for talking to me when things were rough.

Scarlett, I am so grateful to have had a bay mate that was a Latina, I could endlessly talk with, and support each other. I am lucky to consider you my friend.

Ying and Erica, you have helped my thesis in more ways than you know. Thank you for providing help when I needed things NOW.

To my Thursday buddy, Alicia, we share many memories. We have been there through it all (and drank most of it).

To my first PI, Eric Freundt, you showed me the way. We did tissue culture without gloves, it was hardcore.

To Carolina, my friend, my sister, thank you for always being by my side. You have been with me through the hardest parts of my life, and the best, and I am so grateful to continue growing with you.

To my mother and grandmother, words cannot express my gratitude and admiration for the sacrifices you have done for me and my sister, and for being with me no matter what.

Frank, thank you for loving me, inspiring me, and always supporting me. Your love encourages me to live my life with happiness, you have my heart.

# Chapter 1: Introduction

## 1.1 Gamma-activity dysfunction in Alzheimer's disease

### 1.1.1 Overview of neural synchrony

In the early 20th century, while neuroscience was undergoing a paradigm shift toward behaviorism, the German physician Hans Berger (1873-1941) covertly worked in his laboratory in an effort to understand the mechanisms behind telepathy (Buzsaki, 2006). He erroneously reasoned that the human brain could connect with other minds through the generation of electromagnetic forces, and consequently devised experiments which consisted of what we now consider a rudimentary version of the electroencephalogram (EEG). While his efforts to prove the ability of thought-transference failed, he demonstrated for the first time electrical activity recorded from the occipital region of the skull from awake patients. In his pioneering 1929 paper, he described the nature of the recorded electrical oscillations as "... larger first order waves [alpha] with an average duration of 90 milliseconds and smaller second order waves [beta] of an average duration of 35 milliseconds" (Berger, 1929).

Today, we understand that the oscillations Berger witnessed decades ago are rhythmic fluctuations of electrical activity that reflect underlying neuronal synchronization (Sohal, 2016). This generation of neural synchrony is essentially established through a discrete temporal window and is determined by the biophysical properties of a neuron or a neuronal pool. This window period can be the time within which one input from an earlier event is retained, and alters the response to subsequent inputs (e.g. postsynaptic potentials). Thus, a rhythmic event is moderated by the temporal window in which time of the postsynaptic potential, brought about by one input, decays back to baseline; this period of decay can be referred to as the membrane

or decay-time constant (Buzsáki and Draguhn, 2004). The oscillation frequency band of a neuron, or a group of neurons, can be measured by the duration of this constant, where the shorter the time-window (in tens of milliseconds), the higher the frequency oscillation.

Neuronal networks in the mammalian brain display several oscillatory bands ranging from 0.05 Hz to 200 Hz (Bartos et al., 2007). These frequencies form a linear progression on a logarithmic scale, and separate into various frequency bands, and are often associated with different brain states. These frequencies can temporarily coexist in the same or in different brain structures, and can interact with each other (Buzsáki and Wang, 2012, Fries et al., 2001). As such, brain oscillators share both harmonic and relaxation features (i.e. neural 'jumps' following inputs, causing phases to shift), which contribute to the potential of oscillation phase synchronies (Somers and Kopell, 1993). For example, the hippocampus exhibits predominant theta oscillations (5-10 Hz) that resemble sinusoid patterns of harmonic oscillators; their behavior is predictable from short-term observations, however their phases poorly synchronize. On the other hand, the same neurons can generate oscillations with relaxation oscillator characteristics, synchronizing oscillation phases robustly. The combined features of oscillator characteristics allow brain rhythms to be predictable and their phases easy to reset during various cognitive tasks (Somers and Kopell, 1993, Buzsáki and Draguhn, 2004).

### 1.1.2 Gamma oscillations in sensory cortex

Various cognitively-focused activities and environmental stimuli as well as endogenous spike-patterns can evoke neural oscillations in the gamma-frequency range (30-90 Hz) (Fries, 2009, Yamamoto et al., 2014, Jensen et al., 2007, Sederberg et al., 2007). Gamma oscillations can be defined as synchronous barrages of excitation and inhibition between reciprocally connected cells, namely fast-spiking inhibitory neurons and excitatory pyramidal neurons (Fries et al., 2007, Cardin et al., 2009b). A gamma-cycle of a cell assembly relies on several neural biophysical properties, including the time-decay constant of gamma-aminobutyric acid $(GABA)_A$ and α-amino-3-hydroxy-5-methyl-4-isoxazolepropionic acid (AMPA) receptors, ranging from 10-33 ms (Buzsáki and Wang, 2012). It was through early pharmacological manipulations, mathematical modeling, and electrophysiological observations that we observed the common denominators for gamma oscillations, namely inhibitory interneurons and their respective $GABA_A$ synapses, and excitatory input from pyramidal cells (Buzsaki, 2006).

In general, gamma oscillations can emerge in a network model that consists primarily of interconnected inhibitory neurons, a $GABA_AR$ time-decay constant, and an energy input sufficient to drive spiking in the interneurons (excitatory neurons) (Buzsáki and Wang, 2012). As such, synchronous IPSPs are generated as interneurons spike together, thus inhibiting connected partner neurons. Following a $GABA_A$ receptor-mediated hyperpolarization time-decay period, these inhibited interneurons discharge again following an energy input and continue the synchronous IPSP cycle (Kopell, 2009). Because the time-decay constant is the limiting factor in regards to when interneurons can discharge again, it essentially sets the inter-spike-interval between spikes, a major determining factor of the frequency (Hz) range being generated. This

mutual inhibition among interneurons and the resulting gamma rhythm can be sustained by the activation of metabotropic glutamate receptors (Buzsaki, 2006).

Gamma rhythms have been characterized in various animals and in many brain regions, though primarily in the neocortex. A seminal example is from Gray and Singer in 1989 where they demonstrate sustained visual stimulation evoked an LFP-gamma signature in the visual cortex of primates, as well as oscillation phase-locking (Gray and Singer, 1989). Other examples of gamma signatures have been reported in the visual cortex of humans (Hall et al., 2005, Hoogenboom et al., 2010, van Pelt et al., 2012) and rodents (Nase et al., 2003, Niell and Stryker, 2010), auditory cortex of humans (Pantev et al., 1991, Edwards et al., 2005), primates (Brosch et al., 2002, Lakatos et al., 2005, Fukushima et al., 2012), and rodents (Sukov and Barth, 1998, Macdonald et al., 1998, Headley and Weinberger, 2011), and the somatosensory cortex of humans (Bauer et al., 2006, Gross et al., 2007, Zhang et al., 2012) and rodents (Jones and Barth, 1997, Hamada et al., 1999, Sirota et al., 2008).

### 1.1.3 Proposed functions of gamma oscillations – and controversy

There are two major theories regarding the 'function' of gamma oscillations in the brain, the first (and oldest) theorem is binding by bottom-up connectivity, famously proposed by Wolf Singer in 1993 at the Society for Neuroscience meeting, and second is the spike-timing dependent plasticity phenomenon (Fries, 2009, Sohal, 2016).

Binding by bottom-up connectivity proposes that separate independent features of a stimulus (i.e. visual stimulus, such as one polka-dot on a skirt) are processed and bound together into a coherent pattern, shape, or entity (i.e. a skirt with many polka-dots). Essentially, representations of various features of the visual world via independent neuronal assemblies can be bound together harmoniously in the time domain through oscillatory synchrony, and in this case, gamma rhythms. A neurophysiological explanation of this proposal was first suggested by David Hubel and Torsten Wiesel in Harvard Medical School, where following the presentation of a moving bar, neurons in the visual cortex of cats and primates discharged only in a restricted part of the visual field in a phase-dependent fashion (Hubel and Wiesel, 1968). These cells were named 'simple cells', whereas another class of neurons called 'complex cells' had bigger receptive fields and no phase-dependence. The simplified conclusion from these observations was that the visual system processed information through a feedforward, hierarchical system, where each step is responsible for more complex input features. However, this proposal has philosophical objections, mainly that a primarily feedforward model of sensory processing does not allow for the combination of current inputs with previous experiences. This is due to its unidirectional flow of information; feedforward networks cannot learn with network growth, and thus higher order systems with emergent properties require feedback (Berger, 2006).

An alternative to this model is binding by temporal coherence (Sohal, 2016, Milner, 1974). The general idea of this model is that spatially distributed neuronal groups synchronize their responses when active by a single object. In contrast to the binding by bottom-up connectivity hypothesis, this idea proposes that connectivity from different stimuli 'representations' are no longer the main variable, instead it is the temporal synchrony of neurons that represent various features of the stimulus. The fundamental, and most important difference, between the two ideas is that binding by temporal coherence works through synchronicity, and as such, can offer a larger coding capacity for feature combinations. Experimental support for temporal synchrony was provided by Singer and Gray in 1989 where they recorded multi-unit activity and local field potentials from single electrodes in the visual cortex of cats. During a display of moving bars, they observed an increase in gamma band oscillations (30-60 Hz), often phase-locked, and only present during the stimulus and rarely spontaneously (Rager and Singer, 1998a, Gray and Singer, 1989).

An intriguing addition to the potential function of gamma oscillations is the effect it may have on synaptic strengths of existing neuronal connections. Methods for affecting synaptic strength may involve sufficiently strong depolarization of the postsynaptic neuron, and timing between presynaptic activity and discharge of the postsynaptic neuron (Levy and Steward, 1983). Both of these methods are affected by gamma-oscillation-mediated synchronization. Interestingly, the critical temporal window of synaptic plasticity has been shown to correspond to the length of the gamma cycle (10-30 ms). Referred to as spike-timing-dependent plasticity, the essential idea is that gamma oscillations can modify synaptic connections (Bibbig et al., 2001). These synaptic modifications, via gamma-oscillation-induced synchrony, can potentially help

strengthen different assemblies representing stimuli features. In turn, these changes increase the probability that the same assemblies are activated upon future presentations of the same or similar stimuli. Moreover, the assembly bound by gamma-oscillation-induced synchrony can reconstruct representations by partial cues due to the already gamma-modified connections (Berger, 2006).

The role of gamma rhythms in information processing and its implications in cognition remains debated and an open question. Various groups have proposed gamma oscillations to be a broad and non-specific signal of low-level cortical interactions, arguing that its low power, conduction delays, and biased spike-related activity make it unsuitable for a role in cognitive functions (Jia et al., 2013, Ray and Maunsell, 2015, Burns et al., 2011). Various investigators have critiqued the 'binding by temporal coherence' theories by indicating that properties of gamma rhythms are not stable enough to coordinate information between brain regions (Shadlen and Movshon, 1999). In one example, stimulus-evoked gamma oscillations in the primate visual cortex did not have their phase and frequency conserved and was inconsistent over the stimulation period, furthermore the recorded and filtered LFP data were statistically indistinguishable from broadband noise (Burns et al., 2011). However, gamma may still have a role in communication even if the frequency over time is variable, as long as it maintains coherence across areas. In a study by Roberts et al in 2013, they demonstrated that while the frequency of gamma slightly changed throughout the stimulus period, the frequency fluctuations were highly correlated between the primate V1 and V2 (Roberts et al., 2013). In general, skeptics have every right to point out that many theories of gamma's functions in communication and cognition are too high-level. It may be necessary as we continue with oscillations research to

remember that the fundamental mechanisms of oscillations, if any, are unknown; however, the study of its correlations with behavior, and importantly experimental manipulations on oscillations and their effects on behavior, are worthy of understanding, and perhaps through our investigations we will gain deeper understandings of its functions.

### 1.1.4 Effects of amyloid pathology on synaptic function

Amyloid-beta (β) production and the amyloid-$\beta_{1-42}$/amyloid-$\beta_{1-40}$ ratio, which influence the formation of pathogenic oligomers as well as plaque deposition, are mainly regulated by neuronal action potential firing (Kamenetz et al., 2003, Bero et al., 2011). Increasing the rates of regular or burst firing enhances amyloid-$\beta_{1-40}$ and amyloid-$\beta_{1-42}$ production in an activity-dependent manner; regular firing proportionally increases both amyloid-$\beta_{1-40}$ and amyloid-$\beta_{1-42}$ levels. This has been demonstrated *in vivo*, through mouse whisker stimulation and amyloid microdialysis in the barrel cortex, and *in* vitro, through pharmacological manipulations of synaptic activity using organotypic hippocampal slices of AD-mice (Cirrito et al., 2005, Bero et al., 2011, Selkoe et al., 1996). Amyloid-β peptides (including amyloid-$\beta_{1-42}$/amyloid-$\beta_{1-40}$) are proteolytically cleaved from the amyloid precursor protein (APP) by β-site APP cleaving enzyme 1 (BACE1, also known as β-secretase) and γ-secretase, and exist in various peptide states such as monomers (unstable), oligomers, fibrils and plaques (highly stable) (Selkoe et al., 1996). Pathology, or the accumulation of these proteins, can be caused by hereditary genetic mutations, mainly *APP* duplications, or mutations in the catalytic subunits of γ-secretase, PSEN1 and PSEN2. Sporadic AD however, which accounts for 95% of the AD population, is mainly thought to be caused by genetic alterations in apolipoprotein 4 (APOE4), and/or other metabolic or immune genes (Canter et al., 2016).

Pathological accumulation of amyloid-β has been extensively shown to induce abnormalities in synaptic functions *in vivo* and *in vitro* (Palop and Mucke, 2016, Li et al., 2009, Yankner and Lu, 2009). In 2009, a seminal paper by Li et al showed that soluble amyloid oligomers from several sources (synthetic, cell culture, and human brain) enhanced long-term depression

(LTD) in the hippocampus. They observed that soluble amyloid peptides altered glutamate recycling at the synapse by inhibiting glutamate uptake, resulting in glutamate spillover to extra- or perisynaptic GluN2B-containing NMDARs, thus promoting synapse depression. In the brains of AD mouse models, hypersynchrony has been observed, which unlike normal fluctuations in network synchrony that are associated with changes in brain states, hypersynchrony is a phenomenon in which aberrant synchronization of neuronal networks results in epileptiform discharges (Palop and Mucke, 2016). In turn, chronic epileptic activity is thought to aggravate the production and accumulation of amyloid-β. Interestingly, patients who had mild cognitive impairment (MCI) or early AD with epilepsy, cognitive decline was reported near the onset of seizure activity.

### 1.1.5 Network dysfunction and AD

Attention-demanding and cognitive tasks, such as sensory processing, memory encoding, and spatial recognition, are associated with the coordination and synchrony of neuronal groups (Fries, 2009, Kim et al., 2016, Sederberg et al., 2007, Sohal et al., 2009, Jensen et al., 2007). In animal models and humans, these tasks increase functional MRI (fMRI) signals in specific brain regions, and a reduction in others, such as the default mode network (DMN) (Sperling et al., 2010, Palop and Mucke, 2016, Gillespie et al., 2016, Verret et al., 2012b). The DMN consists of the precuneus, posterior cingulate cortex, lateral and inferior parietal cortex, and regions of the temporal and medial prefrontal cortex, and is primarily active during inwardly oriented mental activity (i.e. recall of a memory) and deactivated during outward mental tasks (i.e. encoding of a memory) (Palop and Mucke, 2016). In AD, as well as other cognitive disorders, deactivation of the DMN has been demonstrated to be impaired during learning. In one study, AD patients tasked with a face-name association test showed significant deactivation deficits, as measured by fMRI BOLD signal, in the precuneus when compared to age-matched controls (Sperling et al., 2010). Another study evaluated whole brain activity via MEG in AD patients during a no-task eyes-closed condition. They observed reduced synchronization and power in the gamma band in AD patients, when compared to healthy controls (Stam et al., 2002).

Because synchrony is thought to regulate the function of network activity, abnormal activation or deactivation of brain regions during cognitive tasks may be a result from synchrony deficits. Studies using AD-like mice have shown that spontaneous epileptiform discharges emerge primarily during resting periods, when the intensity of gamma oscillations is low. When pharmacological inductions of gamma are increased or decreased *in vivo*, epileptic activity

decreased or increased, respectively (Maheshwari et al., 2016). This correlation between network hypersynchrony and reduced gamma power has been linked across multiple conditions, and behavior-induced increases in gamma power have been shown to reduce AD-epileptiform activity (Vossel et al., 2013, Matsumoto et al., 2013). Moreover, general decreases in gamma activity, as measured by EEG, have been reported in various mouse models of AD (Verret et al., 2012b).

### 1.2 Non-invasive light flicker stimulation at 40 Hz and its effect on AD pathology

Previous work from Jessica Cardin et al has shown that manipulation of oscillations through optogenetic techniques can lead to the induction of very specific frequencies *in vivo* (Cardin et al., 2009a). Importantly, she demonstrated that in order to drive gamma activity (40 Hz), fast-spiking (FS) parvalbumin-positive (PV)- interneurons, and not CamKII-positive excitatory neurons, were essential to be stimulated at 40 Hz. Years later, and seminal to this thesis, Iaccarino et al demonstrated that optogenetic induction of 40 Hz for 1 hr in the hippocampus resulted in increased LFP power at 40 Hz, and a significant decrease in amyloid-$\beta_{1-42}$ and amyloid-$\beta_{1-40}$ in the familial AD mouse model, 5XFAD (Iaccarino et al., 2016a). Associated with this decrease in amyloid load was a change in microglia response, the primary immune cell of the brain. Essentially, RNA-sequencing of microglia following optogenetic stimulation indicated increased expression of genes responsible for microglia activation and phagocytic transformation.

Iaccarino et al further designed a non-invasive method to induce gamma activity in the mouse visual cortex via a light flicker at 40 Hz. This method was inspired by Charles Gray and Wolf Singer during their time at Max-Planck Institute, where they demonstrated the ability to induce specific oscillations in the cat visual cortex depending the frequency of bars being displayed. Similar to the results of optogenetic induction, visual stimulation at 40 Hz for 1 hr p/day for 7 days resulted in increased LFP power at 40 Hz, and reduced amyloid plaque load in the visual cortex of aged 5XFAD mice. Immunohistochemistry analysis in the visual cortex indicated a profound change in microglia response, specifically showing an increase in the number and soma size of microglia, as well as an increase in amyloid-microglia colocalization, potentially indicating increased amyloid uptake. Additionally, they observed the reduction of

specific phosphorylated tau epitopes, another AD-related pathogenic marker, in the tauopathy mouse model, tau P301S.

### 1.3 Thesis overview

Rhythmic neural activity in the gamma range (30-90 Hz) is proposed to be important for numerous higher-order cognitive functions (Fries, 2009), and has been shown to be disrupted in several AD mouse models (Verret et al., 2012a, Gillespie et al., 2016) including in young 5XFAD mice, months before the onset of Aβ accumulation and major cognitive impairment (Iaccarino et al., 2016b). We and others have shown that gamma oscillations can be evoked optogenetically (Cardin et al., 2009b, Sohal et al., 2009), or in a non-invasive manner, which we term Gamma ENtrainment Using Sensory stimuli (GENUS), via a light programmed to flicker at 40 Hz (Rager and Singer, 1998b, Iaccarino et al., 2016b, Singer et al., 2018). In our previous study (Iaccarino et al., 2016), we applied visual GENUS to entrain gamma oscillations in the primary visual cortex (VC), and found a reduction in amyloid load and morphological changes in microglia - such as enlarged soma size and increased co-localization with Aβ - that are consistent with transition of these brain immune cells to an engulfing state (Saijo and Glass, 2011, Walker and Lue, 2015). These findings demonstrated that 40 Hz light flicker stimulation can affect local network activity and induce a protective molecular and cellular response in VC in 5XFAD mice.

However, AD is a circuit-wide disease affecting multiple brain centers that are critical for learning and memory, such as the hippocampus (HPC), as well as regions involved in other higher-order brain functions, such as the medial prefrontal cortex (mPFC) (Seeley et al., 2009, Sperling et al., 2010, Yamamoto et al., 2014, Spellman et al., 2015, Kim et al., 2016). Thus, many outstanding questions for the application of GENUS to ameliorate AD-related pathologies and dysfunction remain. First, can other sensory modalities induce GENUS beyond primary sensory brain areas? Second, could GENUS improve cognitive function in an AD mouse model? Third, are

there beneficial cellular and molecular effects following auditory GENUS? And finally, could multi-sensory stimuli affect AD pathology in further downstream brain regions?

In my thesis, we tested the possibility of evoking gamma entrainment by stimulation through the auditory system with a 40 Hz train of tones (**Chapter 2**). We show that auditory GENUS significantly improved several cognitive tasks known to be associated with hippocampal function (**Chapter 3**). This effect concurrently occurred with microglia responses consistent with increased engulfment and reduced amyloid load in the auditory cortex and hippocampus of 5XFAD mice. Auditory GENUS also increased the number of reactive astrocytes and prompted a vasculature response in these brain regions (**Chapter 4**). Finally, we found that beyond AC and HPC, combined auditory and visual GENUS induced a microglia-clustering response in mPFC, and reduced amyloid load not just in AC, HPC, and mPFC but throughout the neocortex (**Chapter 5**). My thesis demonstrates a non-invasive approach to elicit system-wide effects on AD-related pathology and improvements in cognition in an AD-mouse model.

## 1.4 References


BARTOS, M., VIDA, I. & JONAS, P. 2007. Synaptic mechanisms of synchronized gamma oscillations in inhibitory interneuron networks. *Nat Rev Neurosci,* 8, 45-56.

BAUER, M., OOSTENVELD, R., PEETERS, M. & FRIES, P. 2006. Tactile spatial attention enhances gamma-band activity in somatosensory cortex and reduces low-frequency activity in parieto-occipital areas. *J Neurosci,* 26, 490-501.

BERGER, H. *Arch.* 1929. *Psychiatr. Nervenkr.* 87, 527.

BERO, A. W., YAN, P., ROH, J. H., CIRRITO, J. R., STEWART, F. R., RAICHLE, M. E., LEE, J. M. & HOLTZMAN, D. M. 2011. Neuronal activity regulates the regional vulnerability to amyloid-β deposition. *Nat Neurosci,* 14, 750-6.

BIBBIG, A., FAULKNER, H. J., WHITTINGTON, M. A. & TRAUB, R. D. 2001. Self-organized synaptic plasticity contributes to the shaping of gamma and beta oscillations in vitro. *J Neurosci,* 21, 9053-67.

BROSCH, M., BUDINGER, E. & SCHEICH, H. 2002. Stimulus-related gamma oscillations in primate auditory cortex. *J Neurophysiol,* 87, 2715-25.

BURNS, S. P., XING, D. & SHAPLEY, R. M. 2011. Is gamma-band activity in the local field potential of V1 cortex a "clock" or filtered noise? *J Neurosci,* 31, 9658-64.

BUZSÁKI, G. & DRAGUHN, A. 2004. Neuronal oscillations in cortical networks. *Science,* 304, 1926-9.

BUZSÁKI, G. & WANG, X. J. 2012. Mechanisms of gamma oscillations. *Annu Rev Neurosci,* 35, 203-25.

CANTER, R. G., PENNEY, J. & TSAI, L.-H. 2016. The road to restoring neural circuits for the treatment of Alzheimer's disease. *Nature,* 539, 187-196.

CARDIN, J. A., CARLÉN, M., MELETIS, K., KNOBLICH, U., ZHANG, F., DEISSEROTH, K., TSAI, L.-H. & MOORE, C. I. 2009a. Driving fast-spiking cells induces gamma rhythm and controls sensory responses. *Nature,* 459, 663-667.

CARDIN, J. A., CARLÉN, M., MELETIS, K., KNOBLICH, U., ZHANG, F., DEISSEROTH, K., TSAI, L. H. & MOORE, C. I. 2009b. Driving fast-spiking cells induces gamma rhythm and controls sensory responses. *Nature,* 459, 663-7.

CIRRITO, J. R., YAMADA, K. A., FINN, M. B., SLOVITER, R. S., BALES, K. R., MAY, P. C., SCHOEPP, D. D., PAUL, S. M., MENNERICK, S. & HOLTZMAN, D. M. 2005. Synaptic activity regulates interstitial fluid amyloid-beta levels in vivo. *Neuron,* 48, 913-22.

EDWARDS, E., SOLTANI, M., DEOUELL, L. Y., BERGER, M. S. & KNIGHT, R. T. 2005. High gamma activity in response to deviant auditory stimuli recorded directly from human cortex. *J Neurophysiol,* 94, 4269-80.

FRIES, P. 2009. Neuronal gamma-band synchronization as a fundamental process in cortical computation. *Annu Rev Neurosci,* 32, 209-24.

FRIES, P., NIKOLIĆ, D. & SINGER, W. 2007. The gamma cycle. *Trends Neurosci,* 30, 309-16.

FRIES, P., REYNOLDS, J. H., RORIE, A. E. & DESIMONE, R. 2001. Modulation of oscillatory neuronal synchronization by selective visual attention. *Science,* 291, 1560-3.

FUKUSHIMA, M., SAUNDERS, R. C., LEOPOLD, D. A., MISHKIN, M. & AVERBECK, B. B. 2012. Spontaneous high-gamma band activity reflects functional organization of auditory cortex in the awake macaque. *Neuron,* 74, 899-910.

GILLESPIE, A. K., JONES, E. A., LIN, Y. H., KARLSSON, M. P., KAY, K., YOON, S. Y., TONG, L. M., NOVA, P., CARR, J. S., FRANK, L. M. & HUANG, Y. 2016. Apolipoprotein E4 Causes Age-Dependent Disruption of Slow Gamma Oscillations during Hippocampal Sharp-Wave Ripples. *Neuron,* 90, 740-51.

GRAY, C. M. & SINGER, W. 1989. Stimulus-specific neuronal oscillations in orientation columns of cat visual cortex. *Proc Natl Acad Sci U S A,* 86, 1698-702.

GROSS, J., SCHNITZLER, A., TIMMERMANN, L. & PLONER, M. 2007. Gamma oscillations in human primary somatosensory cortex reflect pain perception. *PLoS Biol,* 5, e133.

HALL, S. D., HOLLIDAY, I. E., HILLEBRAND, A., SINGH, K. D., FURLONG, P. L., HADJIPAPAS, A. & BARNES, G. R. 2005. The missing link: analogous human and primate cortical gamma oscillations. *Neuroimage,* 26, 13-7.

HAMADA, Y., MIYASHITA, E. & TANAKA, H. 1999. Gamma-band oscillations in the "barrel cortex" precede rat's exploratory whisking. *Neuroscience,* 88, 667-71.

HEADLEY, D. B. & WEINBERGER, N. M. 2011. Gamma-band activation predicts both associative memory and cortical plasticity. *J Neurosci,* 31, 12748-58.

HOOGENBOOM, N., SCHOFFELEN, J. M., OOSTENVELD, R. & FRIES, P. 2010. Visually induced gamma-band activity predicts speed of change detection in humans. *Neuroimage,* 51, 1162-7.

HUBEL, D. H. & WIESEL, T. N. 1968. Receptive fields and functional architecture of monkey striate cortex. *J Physiol,* 195**,** 215-43.

IACCARINO, H. F., SINGER, A. C., MARTORELL, A. J., RUDENKO, A., GAO, F., GILLINGHAM, T. Z., MATHYS, H., SEO, J., KRITSKIY, O., ABDURROB, F., ADAIKKAN, C., CANTER, R. G., RUEDA, R., BROWN, E. N., BOYDEN, E. S. & TSAI, L.-H. 2016a. Gamma frequency entrainment attenuates amyloid load and modifies microglia. *Nature,* 540**,** 230-235.

JENSEN, O., KAISER, J. & LACHAUX, J. P. 2007. Human gamma-frequency oscillations associated with attention and memory. *Trends Neurosci,* 30**,** 317-24.

JIA, X., XING, D. & KOHN, A. 2013. No consistent relationship between gamma power and peak frequency in macaque primary visual cortex. *J Neurosci,* 33**,** 17-25.

JONES, M. S. & BARTH, D. S. 1997. Sensory-evoked high-frequency (gamma-band) oscillating potentials in somatosensory cortex of the unanesthetized rat. *Brain Res,* 768**,** 167-76.

KAMENETZ, F., TOMITA, T., HSIEH, H., SEABROOK, G., BORCHELT, D., IWATSUBO, T., SISODIA, S. & MALINOW, R. 2003. APP processing and synaptic function. *Neuron,* 37**,** 925-37.

KIM, H., ÄHRLUND-RICHTER, S., WANG, X., DEISSEROTH, K. & CARLÉN, M. 2016. Prefrontal Parvalbumin Neurons in Control of Attention. *Cell,* 164**,** 208-18.

LAKATOS, P., SHAH, A. S., KNUTH, K. H., ULBERT, I., KARMOS, G. & SCHROEDER, C. E. 2005. An oscillatory hierarchy controlling neuronal excitability and stimulus processing in the auditory cortex. *J Neurophysiol,* 94**,** 1904-11.

LEVY, W. B. & STEWARD, O. 1983. Temporal contiguity requirements for long-term associative potentiation/depression in the hippocampus. *Neuroscience,* 8**,** 791-7.

LI, S., HONG, S., SHEPARDSON, N. E., WALSH, D. M., SHANKAR, G. M. & SELKOE, D. 2009. Soluble oligomers of amyloid Beta protein facilitate hippocampal long-term depression by disrupting neuronal glutamate uptake. *Neuron,* 62**,** 788-801.

MACDONALD, K. D., FIFKOVA, E., JONES, M. S. & BARTH, D. S. 1998. Focal stimulation of the thalamic reticular nucleus induces focal gamma waves in cortex. *J Neurophysiol,* 79**,** 474-7.

MAHESHWARI, A., MARKS, R. L., YU, K. M. & NOEBELS, J. L. 2016. Shift in interictal relative gamma power as a novel biomarker for drug response in two mouse models of absence epilepsy. *Epilepsia,* 57**,** 79-88.

MATSUMOTO, J. Y., STEAD, M., KUCEWICZ, M. T., MATSUMOTO, A. J., PETERS, P. A., BRINKMANN, B. H., DANSTROM, J. C., GOERSS, S. J., MARSH, W. R., MEYER, F. B. & WORRELL, G. A. 2013. Network oscillations modulate interictal epileptiform spike rate during human memory. *Brain,* 136**,** 2444-56.

MILNER, P. M. 1974. A model for visual shape recognition. *Psychol Rev,* 81**,** 521-35.

NASE, G., SINGER, W., MONYER, H. & ENGEL, A. K. 2003. Features of neuronal synchrony in mouse visual cortex. *J Neurophysiol,* 90**,** 1115-23.

NIELL, C. M. & STRYKER, M. P. 2010. Modulation of visual responses by behavioral state in mouse visual cortex. *Neuron,* 65**,** 472-9.

PALOP, J. J. & MUCKE, L. 2016. Network abnormalities and interneuron dysfunction in Alzheimer disease. *Nat Rev Neurosci,* 17**,** 777-792.

PANTEV, C., MAKEIG, S., HOKE, M., GALAMBOS, R., HAMPSON, S. & GALLEN, C. 1991. Human auditory evoked gamma-band magnetic fields. *Proc Natl Acad Sci U S A,* 88**,** 8996-9000.

RAGER, G. & SINGER, W. 1998a. The response of cat visual cortex to flicker stimuli of variable frequency. *European Journal of Neuroscience,* 10**,** 1856-1877.

RAGER, G. & SINGER, W. 1998b. The response of cat visual cortex to flicker stimuli of variable frequency. *Eur J Neurosci,* 10**,** 1856-77.

RAY, S. & MAUNSELL, J. H. 2015. Do gamma oscillations play a role in cerebral cortex? *Trends Cogn Sci,* 19**,** 78-85.

ROBERTS, M. J., LOWET, E., BRUNET, N. M., TER WAL, M., TIESINGA, P., FRIES, P. & DE WEERD, P. 2013. Robust gamma coherence between macaque V1 and V2 by dynamic frequency matching. *Neuron,* 78**,** 523-36.

SAIJO, K. & GLASS, C. K. 2011. Microglial cell origin and phenotypes in health and disease. *Nat Rev Immunol,* 11**,** 775-87.

SEDERBERG, P. B., SCHULZE-BONHAGE, A., MADSEN, J. R., BROMFIELD, E. B., MCCARTHY, D. C., BRANDT, A., TULLY, M. S. & KAHANA, M. J. 2007. Hippocampal and neocortical gamma oscillations predict memory formation in humans. *Cereb Cortex,* 17**,** 1190-6.

SEELEY, W. W., CRAWFORD, R. K., ZHOU, J., MILLER, B. L. & GREICIUS, M. D. 2009. Neurodegenerative diseases target large-scale human brain networks. *Neuron,* 62**,** 42-52.

SELKOE, D. J., YAMAZAKI, T., CITRON, M., PODLISNY, M. B., KOO, E. H., TEPLOW, D. B. & HAASS, C. 1996. The role of APP processing and trafficking pathways in the formation of amyloid beta-protein. *Ann N Y Acad Sci,* 777, 57-64.

SHADLEN, M. N. & MOVSHON, J. A. 1999. Synchrony unbound: a critical evaluation of the temporal binding hypothesis. *Neuron,* 24, 67-77, 111-25.

SINGER, A., MARTORELL, A., DOUGLAS, J. M., ABDURROB, F., ATTOKAREN, M., TIPTON, J., MATHYS, H., ADAIKKAN, C. & TSAI, L.-H. 2018. Non-invasive 40 Hz light flicker to reduce amyloid load and recruit microglia. *Nature Methods*.

SIROTA, A., MONTGOMERY, S., FUJISAWA, S., ISOMURA, Y., ZUGARO, M. & BUZSÁKI, G. 2008. Entrainment of neocortical neurons and gamma oscillations by the hippocampal theta rhythm. *Neuron,* 60, 683-97.

SOHAL, V. S. 2016. How Close Are We to Understanding What (if Anything) γ Oscillations Do in Cortical Circuits? *J Neurosci,* 36, 10489-10495.

SOHAL, V. S., ZHANG, F., YIZHAR, O. & DEISSEROTH, K. 2009. Parvalbumin neurons and gamma rhythms enhance cortical circuit performance. *Nature,* 459, 698-702.

SOMERS, D. & KOPELL, N. 1993. Rapid synchronization through fast threshold modulation. *Biol Cybern,* 68, 393-407.

SPELLMAN, T., RIGOTTI, M., AHMARI, S. E., FUSI, S., GOGOS, J. A. & GORDON, J. A. 2015. Hippocampal-prefrontal input supports spatial encoding in working memory. *Nature,* 522, 309-14.

SPERLING, R. A., DICKERSON, B. C., PIHLAJAMAKI, M., VANNINI, P., LAVIOLETTE, P. S., VITOLO, O. V., HEDDEN, T., BECKER, J. A., RENTZ, D. M., SELKOE, D. J. & JOHNSON, K. A. 2010. Functional alterations in memory networks in early Alzheimer's disease. *Neuromolecular Med,* 12, 27-43.

STAM, C. J., VAN CAPPELLEN VAN WALSUM, A. M., PIJNENBURG, Y. A., BERENDSE, H. W., DE MUNCK, J. C., SCHELTENS, P. & VAN DIJK, B. W. 2002. Generalized synchronization of MEG recordings in Alzheimer's Disease: evidence for involvement of the gamma band. *J Clin Neurophysiol,* 19, 562-74.

SUKOV, W. & BARTH, D. S. 1998. Three-dimensional analysis of spontaneous and thalamically evoked gamma oscillations in auditory cortex. *J Neurophysiol,* 79, 2875-84.

VAN PELT, S., BOOMSMA, D. I. & FRIES, P. 2012. Magnetoencephalography in twins reveals a strong genetic determination of the peak frequency of visually induced γ-band synchronization. *J Neurosci,* 32, 3388-92.

VERRET, L., MANN, E. O., HANG, G. B., BARTH, A. M., COBOS, I., HO, K., DEVIDZE, N., MASLIAH, E., KREITZER, A. C., MODY, I., MUCKE, L. & PALOP, J. J. 2012a. Inhibitory interneuron deficit links altered network activity and cognitive dysfunction in Alzheimer model. *Cell,* 149, 708-21.

VERRET, L., MANN, EDWARD O., HANG, GIAO B., BARTH, ALBERT M. I., COBOS, I., HO, K., DEVIDZE, N., MASLIAH, E., KREITZER, ANATOL C., MODY, I., MUCKE, L. & PALOP, JORGE J. 2012b. Inhibitory Interneuron Deficit Links Altered Network Activity and Cognitive Dysfunction in Alzheimer Model. *Cell,* 149, 708-721.

VOSSEL, K. A., BEAGLE, A. J., RABINOVICI, G. D., SHU, H., LEE, S. E., NAASAN, G., HEGDE, M., CORNES, S. B., HENRY, M. L., NELSON, A. B., SEELEY, W. W., GESCHWIND, M. D., GORNO-TEMPINI, M. L., SHIH, T., KIRSCH, H. E., GARCIA, P. A., MILLER, B. L. & MUCKE, L. 2013. Seizures and epileptiform activity in the early stages of Alzheimer disease. *JAMA Neurol,* 70, 1158-66.

WALKER, D. G. & LUE, L. F. 2015. Immune phenotypes of microglia in human neurodegenerative disease: challenges to detecting microglial polarization in human brains. *Alzheimers Res Ther,* 7, 56.

YAMAMOTO, J., SUH, J., TAKEUCHI, D. & TONEGAWA, S. 2014. Successful execution of working memory linked to synchronized high-frequency gamma oscillations. *Cell,* 157, 845-57.

YANKNER, B. A. & LU, T. 2009. Amyloid beta-protein toxicity and the pathogenesis of Alzheimer disease. *J Biol Chem,* 284, 4755-9.

ZHANG, Z. G., HU, L., HUNG, Y. S., MOURAUX, A. & IANNETTI, G. D. 2012. Gamma-band oscillations in the primary somatosensory cortex--a direct and obligatory correlate of subjective pain intensity. *J Neurosci,* 32, 7429-38.

## Chapter 2: 40 Hz auditory stimulation modulates spiking activity in AC and CA1[1]

### 2.1 40 Hz auditory stimulation paradigm during electrophysiology recordings and recording landmarks

We first determined whether auditory tone stimulation could produce GENUS in auditory cortex (AC), hippocampal subregion CA1, and in medial prefrontal cortex (mPFC). We presented animals with trains of tones at 20 Hz, 40 Hz, 80 Hz, or with trains of randomly spaced tones (1 ms-long, 10 kHz tones played every 12.5 ms, 25 ms, 50 ms, or with random inter-tone intervals, henceforward referred to as "auditory flicker stimulation", see **Methods**). During tone presentation we performed electrophysiological recordings using 32 channel silicon probes in AC, CA1, and mPFC of 3-8 month old male wild-type (C57BL6J) mice running or resting on a spherical treadmill. To locate AC a series of 50 ms auditory mapping tones, henceforward referred to as "mapping stimuli," were played at varying depths until a transient LFP response was detected around 20 ms after tone onset as observed in prior studies (Barth and Di, 1990, Szymanski et al., 2009, Farley et al., 2010) (**Supplement Figure 1A**). CA1 was located based on electrophysiological hallmarks, and mPFC recording location was confirmed with histology after the final recording in each animal (**Supplement Figure 1H and O**).

[1] The findings in this chapter were in press at the time of thesis submission (Martorell, Paulson, et al., *Cell*, 2019).

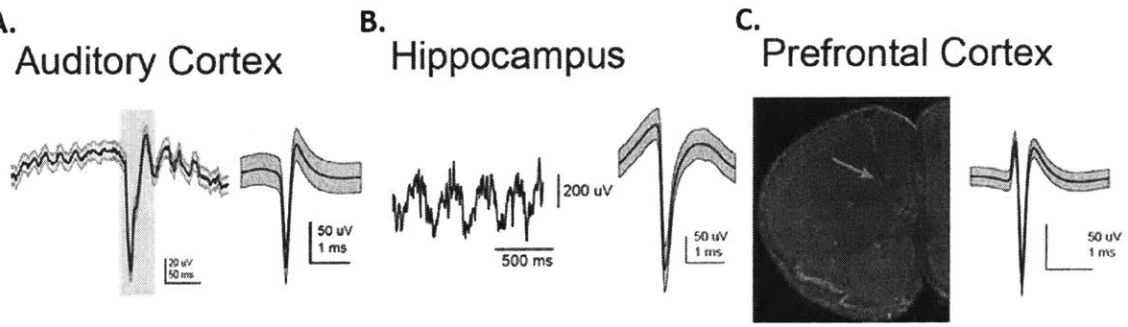


**Figure 1.1. Electrophysiological and histological hallmarks during recordings** A) Mean LFP response to auditory mapping tones used to detect auditory cortex (*left*). The blue region indicates when the 50 ms mapping tone played. Example of a clustered putative single unit (*right*). B) Example of theta rhythm, a hallmark of hippocampus, used to detect CA1. C) Histology image showing probe trace and recording location in mPFC. Red arrow indicates recording location.

### 2.2 40 Hz auditory stimulation modulates spiking activity in AC, CA1, and mPFC

After we reached the target region, animals were presented with interleaved periods of quiet and auditory flicker stimuli while neural activity was recorded. Stimulus blocks rotated between 20 Hz, 40 Hz, 80 Hz, and random auditory flicker stimuli. The firing rate of putative single units increased and decreased periodically with each tone thereby entraining to the 40 Hz auditory flicker stimulation (**Figure 1A, G, and M; Figure 1B, H, and N, blue**). Units were also modulated by random stimulation: when all random pulses were aligned, there was a change in firing rate modulation following the stimuli, indicating that single units responded to the random stimuli pulses. However, the random train of auditory tones did not induce periodic firing modulation because the stimuli themselves were not periodic (**Figure 1B, H, and N, orange**). Entrainment to flicker stimulation varied between single units, in both phase distribution and amplitude. During flicker stimulation, neurons fired as a function of the stimulus, but they did not fire on every cycle and often fired at a wide range of phases: in response to 40 Hz auditory stimulation most neurons fired every 0-22 pulses in AC, 0-30 pulses in CA1, and 0-34 pulses in

mPFC ($1^{st}$ - $3^{rd}$ quartiles reported; **Figure 1B, H, and N; Figure 1E, K, and Q**). The interval between peaks in firing rate during the auditory flicker stimulation was around 25 ms (equivalent to 40 Hz) in the majority of single units; 75% in AC, 79% in CA1, and 74% in mPFC (**Figure 1C, I, and O**). In contrast, during baseline periods with no tones and periods with random tones the interval between peaks had a broad distribution with less than 11% of cells in AC, 12% of cells in CA1, and 16% of cells in mPFC having peak intervals of around 25 ms (i.e. the firing rate was not modulated at 40 Hz; **Figure 1C, I, and O**). Modulation strength was quantified by considering single unit firing rate as a function of the stimulus phase and calculating its vector strength (VS) (**Figure 1D, J, and P, *left***). Vector strength values range from 0 to 1, with 0 representing a uniform distribution of firing that is not modulated by the stimulus (VS = 0) and 1 representing a distribution in which a neuron only fired to a specific stimulus phase (VS = 1). The distribution of vector strengths of single-unit response to 40 Hz auditory stimulation ranged from 0.02-0.09 in AC, 0.02-0.07 in CA1, and 0.02-0.07 in mPFC, and was significantly higher than no stimulation, as well as than that of random stimulation ($1^{st}$ – $3^{rd}$ quartiles reported; **Figure 1D, I, and N, *center***). Random stimulation vector strengths were also significantly higher than the no stimulation condition, because vector strength measures modulation by a stimulus. However, vector strength does not quantify periodicity of modulation, and while random stimulation did elicit a single unit response, it did not induce periodic firing modulation. Similarly, the distribution of Rayleigh statistics for single units during 40 Hz auditory stimulation was significantly higher than that of the no stimulation and random stimulation controls (**Figure 1D, J and P, *right***).

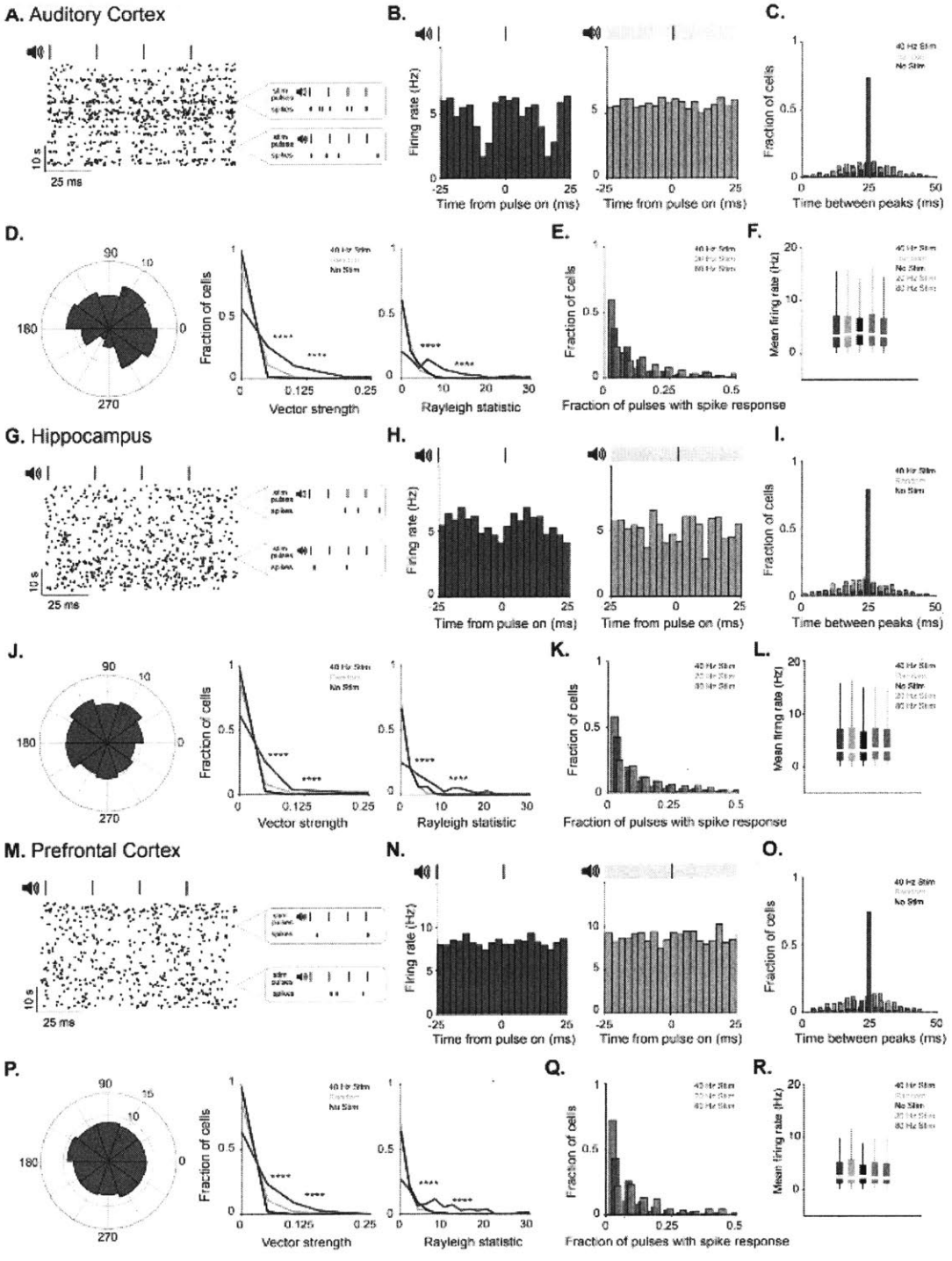
A. Auditory Cortex
B.
C.
D.
E.
F.
G. Hippocampus
H.
I.
J.
K.
L.
M. Prefrontal Cortex
N.
O.
P.
Q.
R.
10 s
25 ms
Firing rate (Hz)
Time from pulse on (ms)
Fraction of cells
Time between peaks (ms)
Vector strength
Rayleigh statistic
Fraction of pulses with spike response
Mean firing rate (Hz)
40 Hz Stim
No Stim

**Figure 1.2. 40 Hz auditory stimulation modulates spiking activity in AC, CA1, and mPFC** A) Example putative single unit spiking response to 40 Hz auditory stimulation with many 10 second stimulation blocks shown wrapped every 100 ms, *left*. Examples of spiking response to four consecutive pulses, *right*. B) Firing rate modulation of unit shown in **A** during 40 Hz auditory (blue) and random stimulation (orange) in AC. Blue ticks, auditory pulses; light blue bar, randomly distributed pulses. C) Intervals between peaks in firing rate in AC for no (grey, labeled no stim), random (orange, labeled random), and 40 Hz auditory stimulation (dark blue, labeled 40 Hz stim) conditions for all single units (n = 292 units in 9 recording sessions in 5 mice. Proportion of intervals around inter-stimulus interval: P = 0 40 Hz vs. No stim, P = 0 40 Hz vs. Random; z-Test for two proportions. For all statistics reported, results are significant after controlling for multiple comparisons using the Bonferroni correction unless otherwise stated). D) Example polar plot of firing rate modulation relative to stimulus onset during 40 Hz auditory stimulation (*left,* stimulus onset at 0), vector strengths of single unit firing rate modulation during 40 Hz auditory, random, and no stimulation (*center,* ****P<0.00005 40 Hz vs. No Stim, 40 Hz vs. Random; Kolmogorov-Smirnov test; 9 units had 40 Hz stim VS values greater than 0.25; 6 units had random stim VS values greater than 0.25), and Rayleigh statistic values of single unit firing rate modulation (*right*, ****P<0.00005 40 Hz vs. No Stim, 40 Hz vs. Random; Kolmogorov-Smirnov test; 40 units had 40 Hz stim RS values greater than 30; 2 units had random stim RS values greater than 30). E) Fraction of pulses with spiking response from single units in AC for 20 Hz, 40 Hz, and 80 Hz auditory stimulation. F) Mean firing rates between stimulation conditions in AC. G) Same as A for CA1. H) Same as B for CA1. I) Same as C for CA1 (n = 338 units in 10 recording sessions in 5 mice. P = 0 40 Hz vs. No stim, P = 0 40 Hz vs. Random; z-Test for two proportions). J) Same as D for CA1 (center, ****P<0.00005 40 Hz vs. No Stim, 40 Hz vs. Random; Kolmogorov-Smirnov test; 11 units and 2 units had VS values > 0.25 during 40 Hz or random, respectively; right, ****P<0.00005 40 Hz vs. No Stim, 40 Hz vs. Random; Kolmogorov-Smirnov test; 7 units had 40 Hz stim RS values > 30). K) Same as E for CA1. L) Same as F for CA1. M) Same as A for mPFC. N) Same as B for mPFC. O) Same as C for mPFC (n = 115 units in 7 recording sessions in 4 mice. P = 0 40 Hz vs. No stim, P = 0 40 Hz vs. Random; z-Test for two proportions). P) Same as D for mPFC (center, ****P<0.00005 40 Hz vs. No Stim, 40 Hz vs. Random; Kolmogorov-Smirnov test; right, ****P<0.00005 40 Hz vs. No Stim, 40 Hz vs. Random; Kolmogorov-Smirnov test; 2 units had 40 Hz stim RS values > 30). Q) Same as E for mPFC. R) Same as F for mPFC.

Differences in vector strength and Rayleigh statistics between stimulation conditions within single units show than neurons were more strongly modulated by periodic stimuli, and that single units were significantly more strongly modulated by lower frequencies of stimulation (**Supplement Figure 1G, N, and U**). The mean firing rate of single neurons was similar between 40 Hz auditory flicker stimulation and controls of no stimulation, random stimulation, 20 Hz and 80 Hz auditory flicker stimulation (**Figure 1F, L, and R; Supplement Figure 1D, K, and R**). Local field potentials in AC displayed elevated power at 40 Hz during the auditory flicker stimulation, but the effects varied between recording locations, recording sessions, and response latency to mapping tones (**Supplement Figure 1B, I, and P**). These findings suggest that 40 Hz auditory flicker stimulation induces GENUS robustly in AC, CA1, and mPFC.

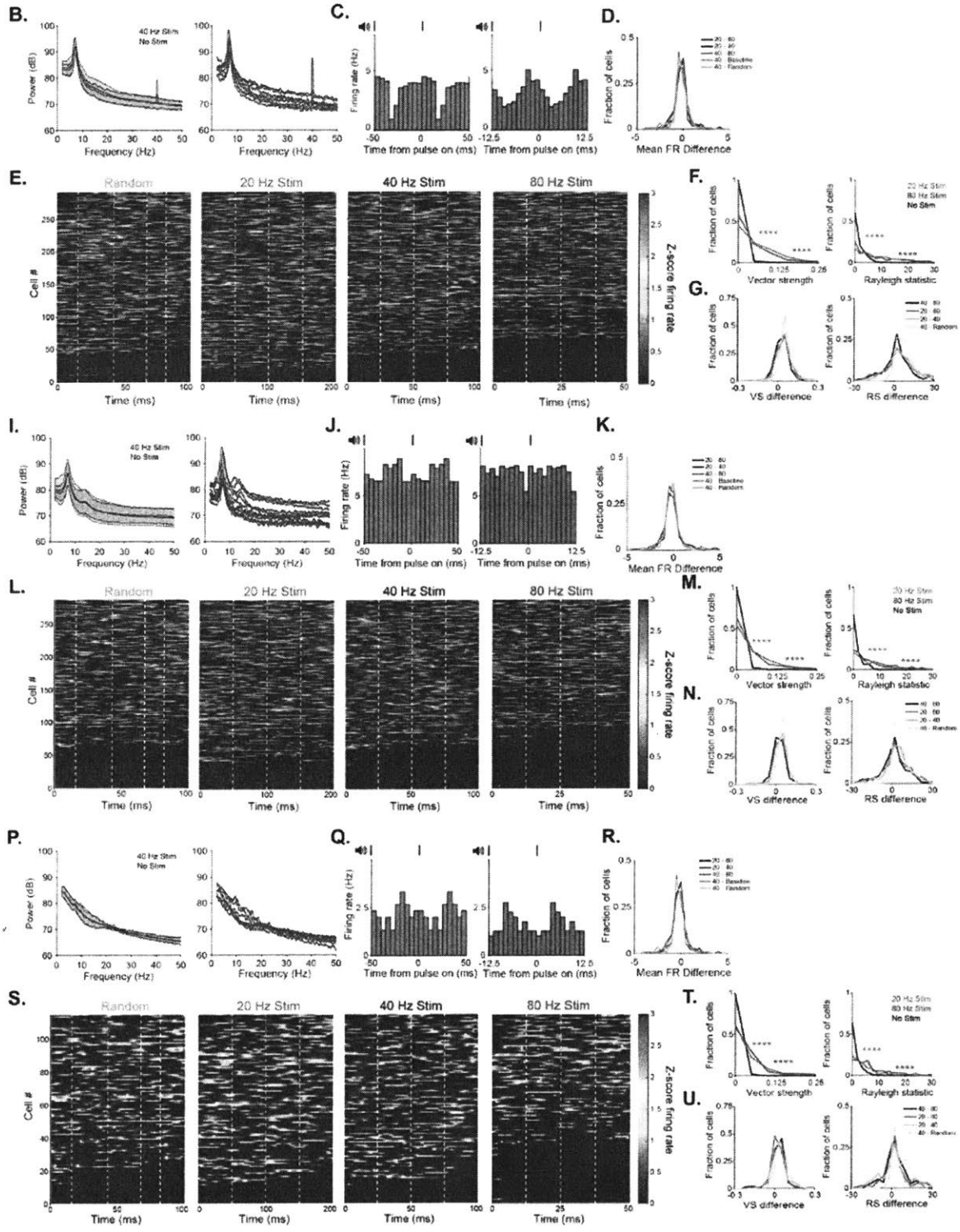
B.
C.
D.
E.
F.
G.
I.
J.
K.
L.
M.
N.
P.
Q.
R.
S.
T.
U.
Random
20 Hz Stim
40 Hz Stim
80 Hz Stim
No Stim
Power (dB)
Frequency (Hz)
Firing rate (Hz)
Time from pulse on (ms)
Fraction of cells
Mean FR Difference
Cell #
Time (ms)
Z-score firing rate
Vector strength
Rayleigh statistic
VS difference
RS difference

**Supplement figure 1. 20 Hz and 80 Hz auditory stimulation modulates activity in AC, CA1, and mPFC** B) Power spectral density (PSD) response to 40 Hz auditory flicker stimuli and no stimulation periods, with mean and standard deviation across recording days (left), power spectrum LFP response to auditory flicker of all recording days in AC (recording site with largest 40 Hz peak during 40 Hz auditory flicker per recording depth is shown, see Methods) (right). C) Firing rate modulation of a putative single unit in response to 20 Hz audio flicker stimulation (left, green) and 80 Hz auditory flicker (right, purple). D) Mean firing rate difference between multiple stimulation conditions of single units in AC centers around 0 Hz (P>0.01 20 Hz – 40 Hz, n.s. after controlling for five comparisons; ****P<0.00002 40 Hz – no stimulation; all others n.s.; Wilcoxon signed rank test for zero median. In all statistical tests, significance remains after controlling for multiple comparisons using the Bonferroni correction, unless otherwise stated). E) Firing rate response of all isolated single units in AC to Random, 20 Hz, 40 Hz, and 80 Hz auditory stimulation. Z-scored response to four consecutive stimulus cycles is shown. Units are ordered by their average stimulus phase preference in the analyzed four cycles. White dashed lines indicate auditory pulse timing. F) Vector strength distribution of 20 Hz and 80 Hz auditory stimulation vs. no stimulation condition (left, ****P<0.00005 20 Hz vs. No Stim, 80 Hz vs. No Stim; Kolmogorov-Smirnov test; 11 units had 20 Hz stim VS values greater than 0.25; 6 units had 80 Hz stim VS values greater than 0.25) and Rayleigh statistic distribution of 20 Hz and 80 Hz auditory stimulation vs. no stimulation (right, ****P<0.00005 20 Hz vs. No Stim, 80 Hz vs. No Stim; Kolmogorov-Smirnov test; 74 units had 20 Hz stim RS values greater than 30; 41 units had 80 Hz stim RS values greater than 30). G) Distribution of within cell differences in vector strength values between all frequencies of auditory stimulation (left, ****P<0.000025 20 Hz - 80 Hz, 20 Hz – 40 Hz, 40 Hz – Random; 40 Hz – 80 Hz n.s.; Wilcoxon signed rank test for zero median). Within cell differences in Rayleigh statistic values between all frequencies of auditory stimulation (right, ****P<0.000025 20 Hz - 80 Hz, 20 Hz – 40 Hz, 40 Hz – Random; 40 Hz – 80 Hz n.s.; Wilcoxon signed rank test for zero median). I) Same as B for CA1. J) Same as C for CA1. K) Same as D for CA1 (P>0.01 40 Hz – no stimulation, n.s. after controlling for five comparisons; all others n.s.; Wilcoxon signed rank test for zero median). L) Same as E for CA1. M) Same as F for CA1 (left, ****P<0.00005, 20 Hz vs. No Stim, 80 Hz vs. No Stim; Kolmogorov-Smirnov test; 12 units had 20 Hz stim VS values greater than 0.25; 10 units had 80 Hz stim VS values greater than 0.25; right, ****P<0.00005, 20 Hz vs. No Stim, 80 Hz vs. No Stim; Kolmogorov-Smirnov test; 4 units had 20 Hz stim RS values greater than 30; 5 units had 80 Hz stim RS values greater than 30). N) Same as G for CA1 (left, **P<0.0025 20 Hz – 80 Hz; ***P<0.00025 20 Hz – 40 Hz; ****P<0.000025 40 Hz – random, 40 Hz – 80 Hz n.s.; Wilcoxon signed rank test for zero median; right, P>0.0125 20 Hz - 80 Hz, n.s. after controlling for four comparisons; **P<0.0025 20 Hz – 40 Hz, ****P<0.000025 40 Hz – Random, 40 Hz – 80 Hz n.s.; Wilcoxon signed rank test for zero median). P) Same as B for mPFC. Q) Same as C for mPFC. R) Same as D for mPFC (right, n.s.; Wilcoxon signed rank test for zero median). S) Same as E for mPFC. T) Same as F for mPFC (left, ****P<0.00005 20 Hz vs. No Stim, 80 Hz vs. No Stim; Kolmogorov-Smirnov test; 4 units had 20 Hz stim VS values greater than 0.25; right, ****P<0.00005 20 Hz vs. No Stim, 80 Hz vs. No Stim; Kolmogorov-Smirnov test; 5 units had 20 Hz stim RS values greater than 30; 3 units had 80 Hz stim RS values greater than 30). U) Same as G for mPFC (left, ****P<0.000025 40 Hz – random, all others n.s.; Wilcoxon signed rank test for zero median; right, ****P<0.000025 40 Hz – Random, all others n.s.; Wilcoxon signed rank test for zero median).

## Chapter 3: Auditory GENUS improves memory performance in 5XFAD mice [2]

Given that auditory GENUS is able to influence hippocampal neural activity, we next assessed its effects on hippocampus-dependent learning and memory in 6-month-old 5XFAD mice (**Figure 2A**). We used 6-month-old 5XFAD animals as that is when behavioral impairments first become evident (Oakley et al., 2006). We previously reported that a single, 1 hr long visual GENUS session did not affect amyloid load in visual cortex (VC) of 6-month-old 5XFAD mice, whereas 1 hr of daily visual stimulation for 7 days elicited a significant reduction (Iaccarino et al., 2016). Thus, we performed 1-week of auditory GENUS for all subsequent experiments; specifically, mice were placed in a quiet chamber and exposed to a train of 1 ms-long 10 kHz auditory tones for 1 hr/day for 7 days at a frequency of 40 Hz (thus, 40 (10 kHz) tones/second). We began by habituating the mice to the behavior chamber 24 hours prior to testing novel object recognition (NOR) and novel object location (NOL) memory performance (Leger et al., 2017, see **Methods**), which evaluate the ability to remember the identity or placement of an object in a specific context, a behavior known to be affected in human AD subjects (Han et al., 2017). These tests measure behavior performance using a recognition index, which is the percent of time spent exploring the novel object or object in new location, respectively, over the entire duration of exploration (Leger et al., 2013).

During habituation, neither auditory GENUS, random frequency, nor non-stimulated groups showed significant changes in average velocity, total distance, time spent in the center, or time spent in the periphery, indicating the three groups did not show differences in general

[2] The findings in this chapter were in press at the time of thesis submission (Martorell, Paulson, et al., *Cell*, 2019).

activity or anxiety-like behavior (**Supplement Figure 2E-H**). Following auditory GENUS, 5XFAD mice exhibited a significantly higher recognition index of 65.50 ± 1.40% for object and 61.41 ± 2.0% for location memory tasks, whereas the non-stimulated and random frequency control groups did not display a preference for the novel object nor the newly-displaced object in the two tests, respectively (**Figure 2B and E**). There was no significant difference in distance traveled or average velocity during the task periods between 40 Hz and random frequency stimulated mice when compared to non-stimulated mice, indicating that these effects were not due to general differences in activity (**Figures 2C, D, F, and G**). The amount of time spent exploring the novel and familiar objects during NOR was examined; we observed that mice following auditory GENUS spent a significantly higher amount of time with the novel object whereas the non-stimulated and random frequency control groups did not exhibit an exploration preference (**Supplement Figure 2A)**. Similarly, we observed that mice following auditory GENUS spent a significantly higher amount of time with an object in a novel location (NOL), whereas the non-stimulated and random frequency control groups did not exhibit an exploration preference (**Supplement Figure 2C**). As an additional control measure to examine differences in exploration activity, we measured the amount of time (min) mice spent to reach the object exploration requirement of 20 s during the object tasks. We observed no significant difference in the time taken to reach the object exploration requirement between 40 Hz and random frequency stimulated mice when compared to non-stimulated mice (**Supplement Figure 2B and D**).

To further characterize the effects of auditory GENUS on hippocampus-dependent behavior, we performed the Morris water maze test, which measures the ability to remember the location of a hidden platform with respect to surrounding context cues (Morris, 1984,

Vorhees and Williams, 2006). Mice gradually learn the location of the hidden platform over successive trials, and their spatial memory of the platform location is measured by the escape latency, which is the amount of time it takes for the individual mouse to find the hidden platform. During the training phase, all three groups were able to successfully learn the location of the hidden platform, however the escape latency for the group receiving auditory GENUS was consistently and significantly shorter than both the non-stimulated and random frequency control groups (**Figure 2H**). There was no significant difference in swim velocity between 40 Hz and random frequency stimulated mice when compared to non-stimulated mice (**Supplement Figure 2I**). During the probe trial, or when the hidden platform is removed from the tank, mice that received auditory GENUS spent a significantly longer period of time exploring the quadrant containing the missing platform, and displayed a higher number of crossings over the previous platform location, but not the random frequency control group, when compared to the non-stimulated control (**Figure 2I and J**).

As a final behavioral measure, we examined the activity of 5XFAD mice during 1-hr auditory GENUS, no stimulation, or random frequency stimulation and observed no significant differences in average velocity (cm/s) and distance traveled (cm) (**Supplement Figure 2J and K**). To explore whether there are differences in 'sleep' states, or periods of quiescence, we measured the amount of time mice spent under 2cm/s during the 1-hr stimulation groups. We observed no significant difference between 40 Hz and random frequency stimulated mice when compared to non-stimulated mice (**Supplement Figure 2L**).

To determine whether auditory GENUS can affect wild-type (WT) cognitive tasks, we performed the same behavioral tests as we previously carried out in AD mice – NOR, NOL, and

the Morris water maze following 7 days of 40 Hz auditory stimulation, random frequency stimulation, or no stimulation. We found no significant difference in the recognition index between mice with 40 Hz and random frequency stimulation when compared to non-stimulated mice in both NOR and NOL tests, and no significant difference in the training curves during the Morris water maze between 40 Hz and random groups when compared to non-stimulated mice (data not shown). Together, these results show that auditory GENUS can improve recognition and spatial memory in 6-month-old 5XFAD mice.

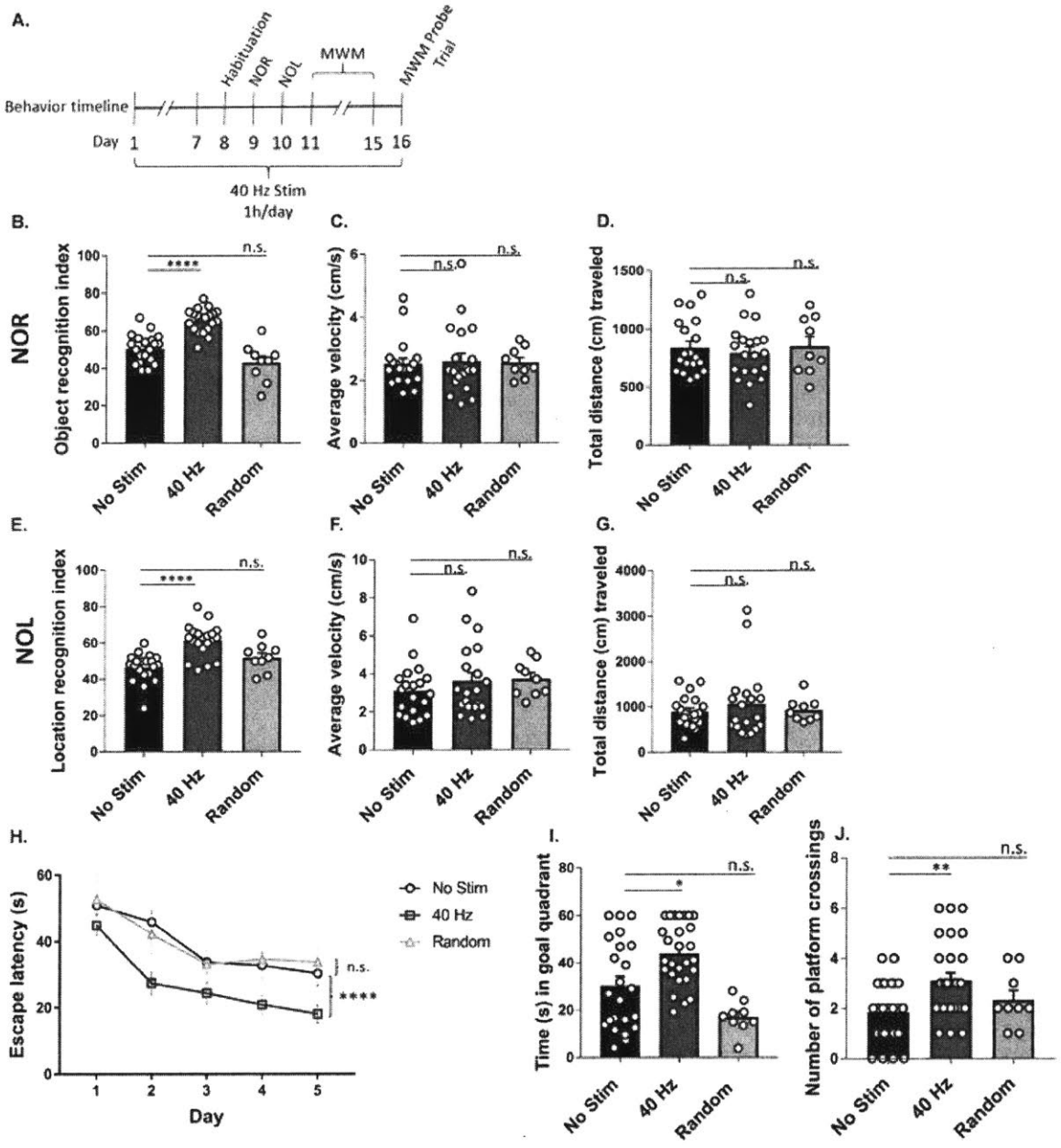
A.
Habituation
NOR
NOL
MWM
MWM Probe Trial
Behavior timeline
Day 1 7 8 9 10 11 15 16
40 Hz Stim
1h/day
B.
C.
D.
NOR
Object recognition index
Average velocity (cm/s)
Total distance (cm) traveled
n.s.
****
No Stim
40 Hz
Random
E.
F.
G.
NOL
Location recognition index
Average velocity (cm/s)
Total distance (cm) traveled
H.
Escape latency (s)
Day
No Stim
40 Hz
Random
I.
Time (s) in goal quadrant
*
J.
Number of platform crossings
**

**Figure 2. Auditory GENUS improves recognition and spatial memory tasks in 5XFAD mice**
A) Timeline of behavior experiments for 5XFAD auditory GENUS mice. B) Recognition index of novel object recognition (NOR) test of 5XFAD auditory GENUS mice (n=20 mice in no stim group [black], n=20 mice in 40 Hz group [blue], n=9 in random frequency group [orange], circles indicate 'n', mean s.e.m. in bar graphs, ****P<0.0001, n.s.= not significant, Kruskal-Wallis test with Dunn's multiple comparison test). C) Average velocity (cm/s) during novel object recognition test (n=20 mice in no stim group, n=20 mice in 40 Hz group, n=9 in random frequency group, mean s.e.m. in bar graphs, n.s.= not significant, Kruskal-Wallis test with Dunn's multiple comparison test). D) Total distance (cm) traveled during novel object recognition test (n=20 mice in no stim group, n=20 mice in 40 Hz group, n=9 in random frequency group, mean s.e.m. in bar graphs, n.s.= not significant, Kruskal-Wallis test with Dunn's multiple comparison test). E) Recognition index of novel object location (NOL) test of 5XFAD auditory GENUS mice (n=20 mice in no stim group, n=20 mice in 40 Hz group, n=9 in random frequency group, mean s.e.m. in bar graphs, ****P<0.0001, n.s.= not significant, Kruskal-Wallis test with Dunn's multiple comparison test). F) Average velocity (cm/s) during novel object location test (n=20 mice in no stim group, n=20 mice in 40 Hz group, n=9 in random frequency group, mean s.e.m. in bar graphs, n.s.= not significant, Kruskal-Wallis test with Dunn's multiple comparison test). G) Total distance (cm) traveled during novel object location test (n=20 mice in no stim group, n=20 mice in 40 Hz group, n=9 in random frequency group, mean s.e.m. in bar graphs, n.s.= not significant, Kruskal-Wallis test with Dunn's multiple comparison test). H) Escape latencies (s) of 5XFAD non-stimulated, random frequency, and 40 Hz auditory stimulated mice in the Morris Water Maze (n=25 mice in no stim group, n=28 mice in 40 Hz group, n= 9 in random frequency group, mean s.e.m. in bar graphs, ****P<0.0001, n.s.= not significant, 2-way ANOVA with Tukey's multiple comparison test). I) Time (s) spent swimming in the goal quadrant during the probe trial (n=25 mice in no stim group, n=28 mice in 40 Hz group, n= 9 in random frequency group, mean s.e.m. in bar graphs, *P<0.05, Kruskal-Wallis test with Dunn's multiple comparison test). J) Number of platform crossings during the probe trial (n=25 mice in no stim group, n=28 mice in 40 Hz group, n= 9 in random frequency group, mean s.e.m. in bar graphs, **P<0.01, Kruskal-Wallis test with Dunn's multiple comparison test).

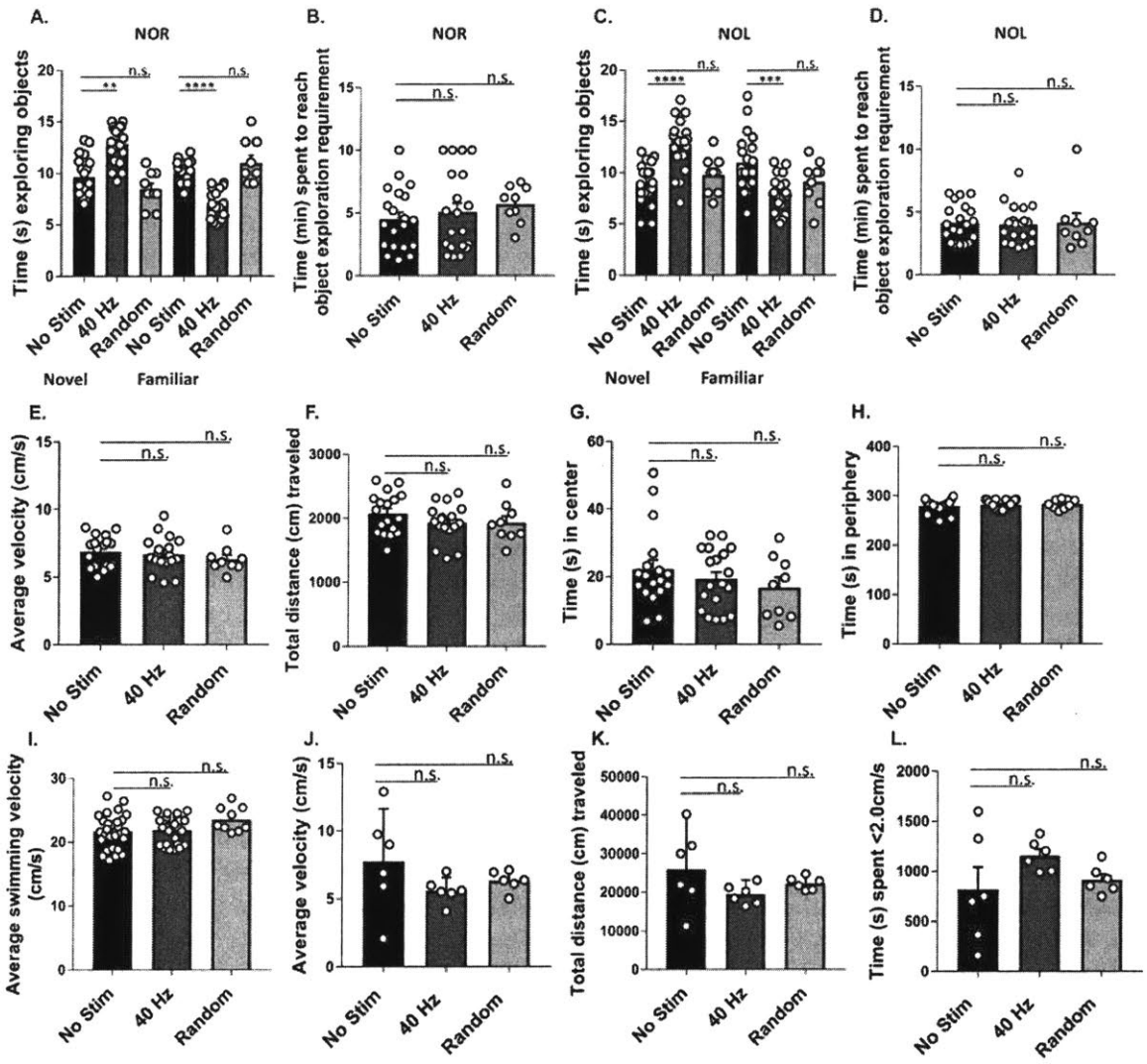
A.
NOR
Time (s) exploring objects
n.s.
**
****
No Stim
40 Hz
Random
Novel
Familiar
B.
NOR
Time (min) spent to reach object exploration requirement
C.
NOL
Time (s) exploring objects
***
D.
NOL
Time (min) spent to reach object exploration requirement
E.
Average velocity (cm/s)
F.
Total distance (cm) traveled
G.
Time (s) in center
H.
Time (s) in periphery
I.
Average swimming velocity (cm/s)
J.
Average velocity (cm/s)
K.
Total distance (cm) traveled
L.
Time (s) spent <2.0cm/s

**Supplement figure 2. Auditory GENUS does not affect mouse behavior** A) Time (seconds) spent exploring familiar and novel objects during NOR test of 5XFAD non-stimulated, 40 Hz, and random frequency stimulated mice (n=20 mice in no stim group, n=20 mice in 40 Hz group, n=9 in random frequency group, mean s.e.m. in bar graphs, **P<0.01, ****p<0.0001, n.s.= not significant, Kruskal-Wallis test with Dunn's multiple comparison test). B) Time (min) mice required during NOR test to reach the total object exploration requirement of 20s (n=20 mice in no stim group, n=20 mice in 40 Hz group, n=9 in random frequency group, mean s.e.m. in bar graphs, n.s.= not significant, Kruskal-Wallis test with Dunn's multiple comparison test). C) Time (seconds) spent exploring object in familiar and novel location during NOL test of 5XFAD non-stimulated, 40 Hz, and random frequency stimulated mice (n=20 mice in no stim group, n=20 mice in 40 Hz group, n=9 in random frequency group, mean s.e.m. in bar graphs, ***P<0.001, ****p<0.0001, n.s.= not significant, Kruskal-Wallis test with Dunn's multiple comparison test). D) Time (min) mice required during NOL test to reach the total object exploration requirement of 20s (n=20 mice in no stim group, n=20 mice in 40 Hz group, n=9 in random frequency group, mean s.e.m. in bar graphs, n.s.= not significant, Kruskal-Wallis test with Dunn's multiple comparison test). E) Average velocity (cm/s) during habituation (n=20 mice in no stim group, n=20 mice in 40 Hz group, n=9 in random frequency group, mean s.e.m. in bar graphs, n.s.= not significant, Kruskal-Wallis test with Dunn's multiple comparison test). F) Total distance (cm) traveled during habituation (n=20 mice in no stim group, n=20 mice in 40 Hz group, n=9 in random frequency group, mean s.e.m. in bar graphs, n.s.= not significant, Kruskal-Wallis test with Dunn's multiple comparison test). G) Time (seconds) spent in the center of the behavior chamber during habituation (n=20 mice in no stim group, n=20 mice in 40 Hz group, n=9 in random frequency group, mean s.e.m. in bar graphs, n.s.= not significant, Kruskal-Wallis test with Dunn's multiple comparison test). H) Time (seconds) spent in the periphery of the behavior chamber during habituation (n=20 mice in no stim group, n=20 mice in 40 Hz group, n=9 in random frequency group, mean s.e.m. in bar graphs, n.s.= not significant, Kruskal-Wallis test with Dunn's multiple comparison test). I) Average swimming velocity (cm/s) during Morris water maze (n=25 mice in no stim group, n=28 mice in 40 Hz group, n= 9 in random frequency group, mean s.e.m. in bar graphs, n.s.= not significant, Kruskal-Wallis test with Dunn's multiple comparison test). J) Average velocity (cm/s) during 1-hour no stimulation, auditory GENUS, or random frequency stimulation (n=6 mice in no stim group, n=6 mice in 40 Hz group, n= 6 in random frequency group, mean s.e.m. in bar graphs, n.s.= not significant, Kruskal-Wallis test with Dunn's multiple comparison test). K) Total distance (cm) traveled during 1-hour no stimulation, auditory GENUS, or random frequency stimulation (n=6 mice in no stim group, n=6 mice in 40 Hz group, n= 6 in random frequency group, mean s.e.m. in bar graphs, n.s.= not significant, Kruskal-Wallis test with Dunn's multiple comparison test). L) Time (seconds) spend under 2 cm/s during 1-hour no stimulation, auditory GENUS, or random frequency stimulation (n=6 mice in no stim group, n=6 mice in 40 Hz group, n= 6 in random frequency group, mean s.e.m. in bar graphs, n.s.= not significant, Kruskal-Wallis test with Dunn's multiple comparison test).

## Chapter 4: Auditory GENUS reduces AD-associated pathology and induces glia-vasculature response in AC and hippocampus of AD-like mice [3]

### 4.1 Auditory GENUS reduces amyloid load in AC and hippocampus of AD-like mice

The beneficial effects of auditory GENUS on cognitive function led us to investigate whether underlying amyloid pathology could be modified in the 5XFAD mouse model. Previously, we showed the ameliorative effect of visual GENUS on amyloid load in younger 3-month-old mice (Iaccarino et al., 2016). Here, our aim was to further study the effect of auditory GENUS on 6-month old mice, which are in a more progressive state of AD and exhibit higher amyloid plaque loads. Mice were placed in a quiet chamber and exposed to a series of different auditory tone-train frequencies, including 40 Hz, 8Hz, 80Hz, random frequency stimulation (see **Methods**), or to no stimulation. 24 hrs after the completion of the 7-day stimulation, we analyzed amyloid load in AC and whole hippocampus (HPC) by Aβ enzyme-linked immunosorbent assay (ELISA) (See **Methods**).

Following 40 Hz auditory stimulation, we observed that soluble $A\beta_{1-42}$ levels were reduced by 51.84±4.98% in AC and 46.89 ±3.89% in HPC, whereas soluble $A\beta_{1-40}$ levels in AC and HPC were reduced by 20.65 ±3.21% and 34.15 ± 4.83%, respectively, and not in other frequency control groups, when compared to non-stimulated control (**Figure 3A and Supplement Figure 3A**). Similarly, insoluble $A\beta_{1-42}$ levels were reduced by 36.68 ±3.21% in AC and 43.84 ±2.42% in HPC (**Figure 3B**). Insoluble $A\beta_{1-40}$ was not detectable via ELISA in both auditory GENUS or no stimulation controls. Our results indicate that the observed reduction in amyloid is specific to 40

[3] The findings in this chapter were in press at the time of thesis submission (Martorell, Paulson, et al., *Cell*, 2019).

Hz stimulation as neither 8 Hz, 80Hz, nor random frequency stimulation significantly change Aβ levels when compared to non-stimulation control. To determine whether these effects apply to other AD-mouse models, and whether our results are specific to our 5XFAD model, we examined Aβ levels of 6-month-old APP/PS1 transgenic mice, a well-validated AD model, following 7 days of auditory GENUS. We found that soluble $A\beta_{1-42}$ was significantly reduced by 48.39±3.50% in AC and by 35.54±4.27% in HPC when compared to no stimulation control (**Supplement Figure 3B**).

We next examined plaque load in the 5XFAD mouse model with immunohistochemical analysis using a β-amyloid specific antibody (Cell Signaling Technology; D54D2) (**Figure 3C and D)**. Plaque number was significantly reduced following 7 days of auditory GENUS, by 45.73±2.818% and 59.30±2.083% in AC and CA1 respectively, compared to no stimulation controls (**Figure 3E**). Plaque size was also significantly reduced, by 54.37±5.603% and 40.70±5.321% in AC and CA1, respectively (**Figure 3F**). Analysis of $A\beta_{1-42}$ specific immunostaining indicated a substantial reduction in $A\beta_{1-42}$ deposits by 45.35±0.011% and 43.21±0.0285% in AC and CA1, respectively (**Figure 3G-I**). To examine the dynamics of plaque load after 40 Hz stimulation, we performed immunohistochemistry analysis using a β-amyloid specific antibody (Cell Signaling Technology; D54D2) in 5XFAD mice that were first subjected to a week of auditory GENUS and then left unstimulated for the next 7 days. We observed slight decreases in average plaque number, area, and amyloid intensity, however these differences were not significant (**See Supplement Figure 3F-H**).

To examine plaque load following auditory GENUS in another AD model, we used 9-month-old APP/PS1 mice, as 6-month-old mice do not exhibit significant plaque development. We observed plaque number was significantly reduced in AC by 52.65 ± 7.53% and CA1 by 62.90

± 15.5%. Plaque size was significantly reduced in AC by 67.90 ± 6.18% and CA1 by 64.06 ± 15.2%. Analysis of $A\beta_{1-42}$ specific immunostaining using an $A\beta_{1-42}$ antibody (BioLegend; 12F4) indicated a substantial reduction in $A\beta_{1-42}$ deposits by 38.77 ± 4.21% and 47.63 ± 6.08% in AC and CA1, respectively, compared to no-stimulation control (**Supplement Figure 3C-E**). Collectively, these results demonstrate that auditory GENUS can entrain gamma activity in AC and CA1 and reduce amyloid load in AD mouse models.

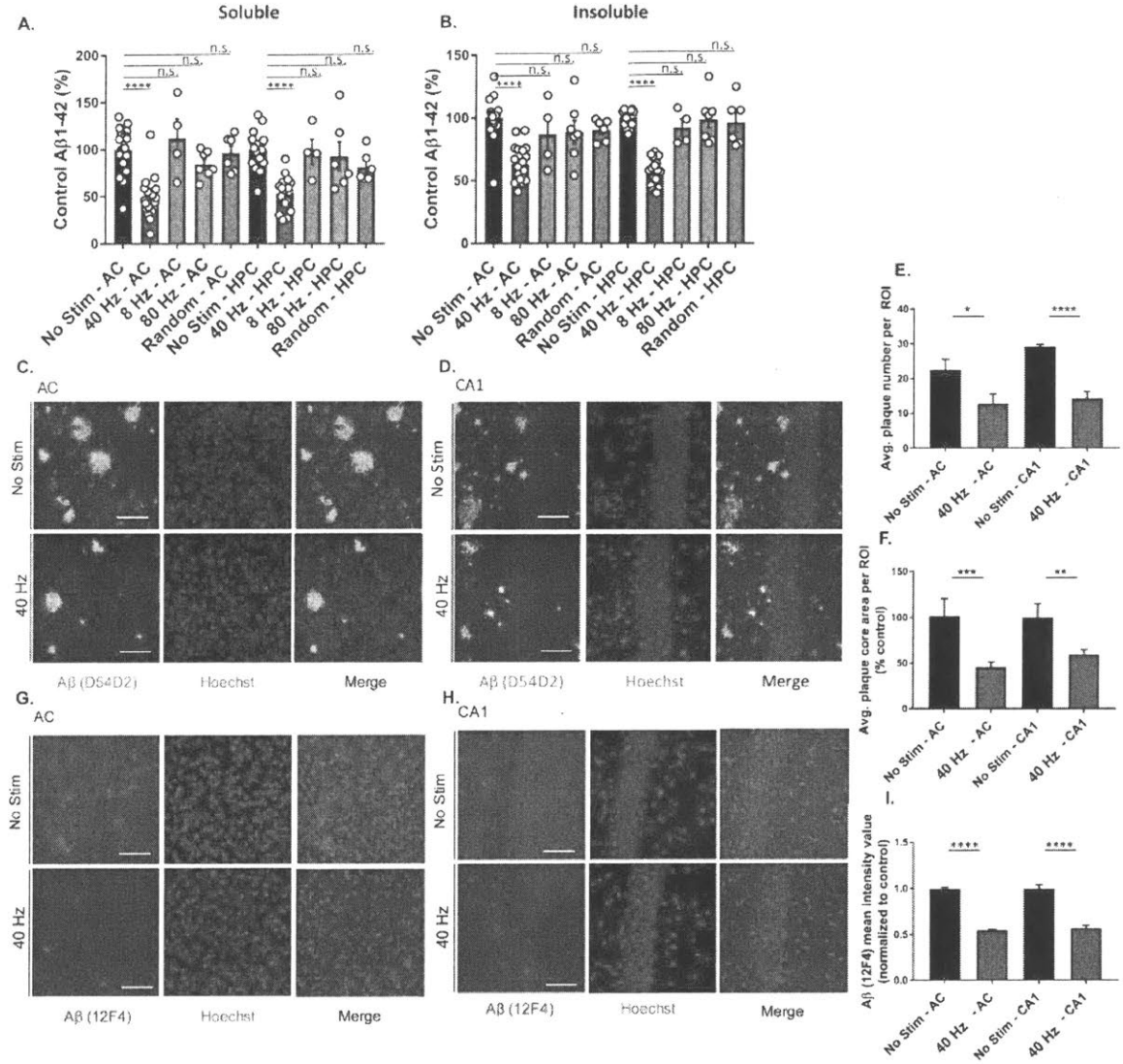

**Figure 3. Auditory GENUS reduces amyloid load in AC and HPC in 5XFAD mice**
A) Relative soluble Aβ1-42 levels in auditory cortex (AC) and hippocampus (HPC) in 6-month-old 5XFAD mice following 40 Hz, 8 Hz, 80 Hz, or random frequency auditory stimulation for 1 hour per day for 7 days, normalized to non-stimulation control (n=19 mice in no stim group, n=19 mice in 40 Hz group, n=4 mice in 8 Hz group, n=7 in 80 Hz group, n=6 in random frequency group, mean s.e.m. in bar graphs, ****P<0.0001, n.s.= not significant, Kruskal-Wallis test with Dunn's multiple comparison test). B) As in A for insoluble Aβ1-42. C) Immunohistochemistry with anti-Aβ (D54D2, green) antibody in 6-month-old AC of 5XFAD mice after auditory GENUS or no stimulation, for 1 hour per day for 7 days (n=7 mice per group, scale bar, 50 μm). D) As in C for CA1. E) Average number of Aβ-positive plaques in AC and CA1 (n=7 mice per group, mean s.e.m. in bar graphs, *P<0.05, ****P<0.0001; unpaired Mann-Whitney Test). F) Average area of Aβ-positive plaques in AC and CA1 (n=7 mice mice per group, mean s.e.m. in bar graphs, **P<0.01, ***P<0.001; unpaired Mann-Whitney Test). G) Immunohistochemistry with anti-Aβ (12F4, red) antibody in 6-month-old AC of 5XFAD mice after auditory GENUS or no stimulation, for 1 hour per day for 7 days (Inset, 20x, scale bar, 50 μm). H) As in G for CA1. I) Aβ (12F4) mean intensity value (12F4 antibody) normalized to non-stimulated controls (n=7 mice per group, mean s.e.m. in bar graphs, ****P<0.0001, unpaired Mann-Whitney Test).

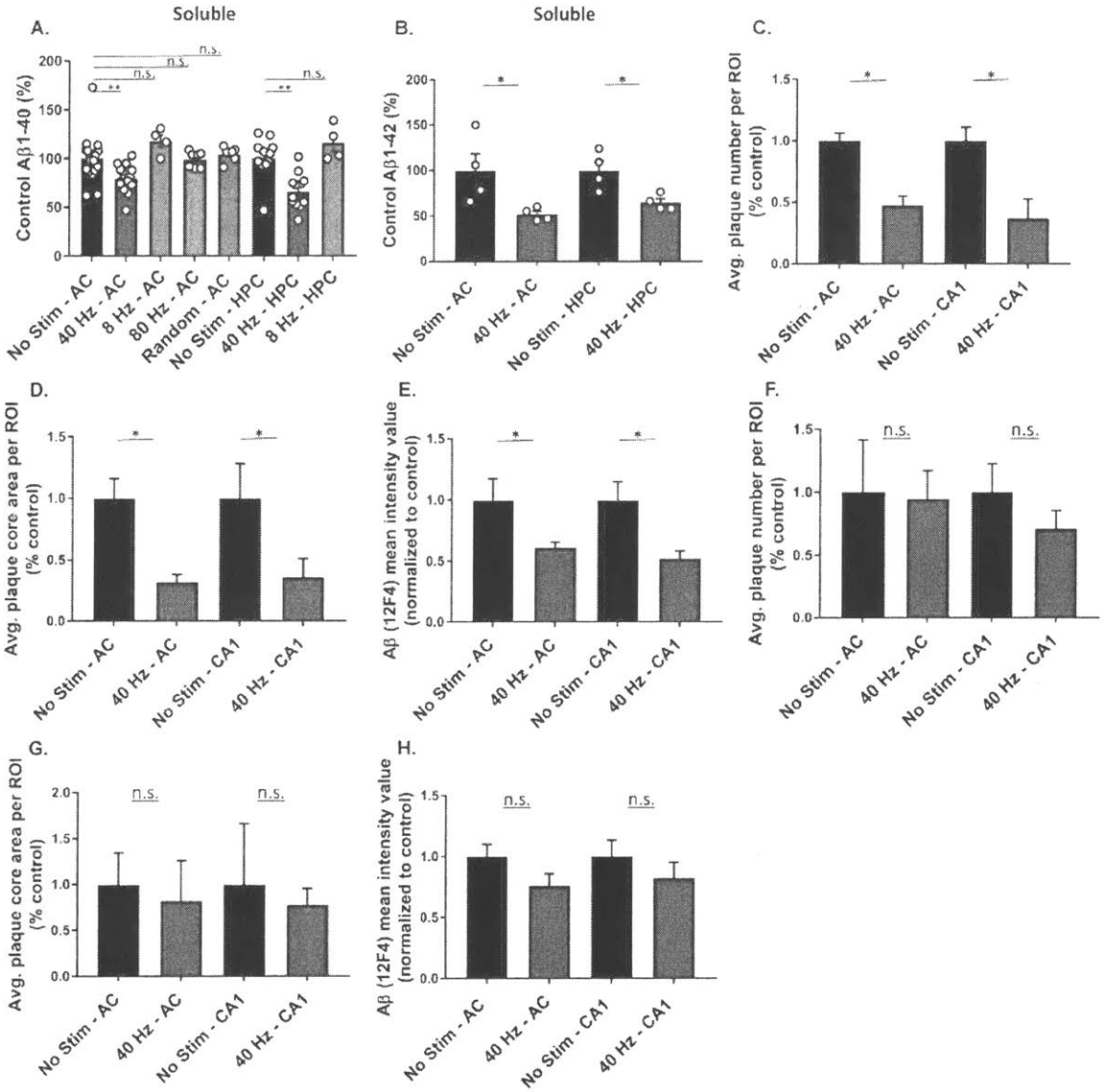
A.
Soluble
Control Aβ1-40 (%)
n.s.
n.s.
n.s.
n.s.
**
**
No Stim - AC
40 Hz - AC
8 Hz - AC
80 Hz - AC
Random - AC
No Stim - HPC
40 Hz - HPC
8 Hz - HPC
B.
Soluble
Control Aβ1-42 (%)
*
*
No Stim - AC
40 Hz - AC
No Stim - HPC
40 Hz - HPC
C.
Avg. plaque number per ROI (% control)
*
*
No Stim - AC
40 Hz - AC
No Stim - CA1
40 Hz - CA1
D.
Avg. plaque core area per ROI (% control)
*
*
No Stim - AC
40 Hz - AC
No Stim - CA1
40 Hz - CA1
E.
Aβ (12F4) mean intensity value (normalized to control)
*
*
No Stim - AC
40 Hz - AC
No Stim - CA1
40 Hz - CA1
F.
Avg. plaque number per ROI (% control)
n.s.
n.s.
No Stim - AC
40 Hz - AC
No Stim - CA1
40 Hz - CA1
G.
Avg. plaque core area per ROI (% control)
n.s.
n.s.
No Stim - AC
40 Hz - AC
No Stim - CA1
40 Hz - CA1
H.
Aβ (12F4) mean intensity value (normalized to control)
n.s.
n.s.
No Stim - AC
40 Hz - AC
No Stim - CA1
40 Hz - CA1

**Supplement figure 3. Auditory GENUS ameliorates plaque load in APP/PS1 mice**
A) Relative soluble Aβ1-40 levels in auditory cortex (AC) and hippocampus (HPC) in 6-month-old 5XFAD mice following 40 Hz, 8 Hz, 80 Hz, or random frequency auditory stimulation for 1 hour per day for 7 days, normalized to non-stimulation control (note: ELISA for 80 Hz and random frequency HPC samples were unsuccessful and were unable to be reported, n=19 mice in no stim group, n=19 mice in 40 Hz group, n=4 mice in 8 Hz group, n=7 in 80 Hz group, n=6 in random frequency group, mean s.e.m. in bar graphs, **P<0.01, n.s.= not significant, Kruskal-Wallis test with Dunn's multiple comparison test). B) Relative soluble Aβ1-42 levels in auditory cortex (AC) and hippocampus (HPC) in 6-month-old APP/PS1 mice following auditory GENUS for 1 hour per day for 7 days, normalized to non-stimulation control (n=4 mice in no stim group, n=4 mice in 40 Hz group, mean s.e.m. in bar graphs, *P<0.05, unpaired Mann-Whitney test). C) Average plaque number in AC and CA1 ('region of interest', ROI) in 9-month old APP/PS1 mice following auditory GENUS for 1 hour per day for 7 days, normalized to non-stimulation control (n=5 mice in no stim group, n=5 mice in 40 Hz group, mean s.e.m. in bar graphs, *P<0.05, unpaired Mann-Whitney test). D) Average plaque core area in AC and CA1 in 9-month old APP/PS1 mice following auditory GENUS for 1 hour per day for 7 days, normalized to non-stimulation control (n=5 mice in no stim group, n=5 mice in 40 Hz group, mean s.e.m. in bar graphs, *P<0.05, unpaired Mann-Whitney test). E) Aβ (12F4) mean intensity value (12F4 antibody) in AC and CA1 in 9-month old APP/PS1 mice following auditory GENUS for 1 hour per day for 7 days, normalized to non-stimulation control (n=5 mice in no stim group, n=5 mice in 40 Hz group, mean s.e.m. in bar graphs, *P<0.05, unpaired Mann-Whitney test). F) Average plaque number in AC and CA1 in 6-month old 5XFAD mice following 7 days no stimulation post-auditory GENUS for 1 hour per day for 7 days, normalized to non-stimulation control (n=6 mice in no stim group, n=6 mice in 40 Hz group, mean s.e.m. in bar graphs, n.s.= not significant, unpaired Mann-Whitney test). G) Average plaque core area in AC and CA1 in 6-month old 5XFAD mice following 7 days no stimulation post-auditory GENUS for 1 hour per day for 7 days, normalized to non-stimulation control (n=6 mice in no stim group, n=6 mice in 40 Hz group, mean s.e.m. in bar graphs, n.s.= not significant, unpaired Mann-Whitney test). H) Aβ (12F4) mean intensity value (12F4 antibody) in AC and CA1 in 6-month old 5XFAD mice following 7 days no stimulation post-auditory GENUS for 1 hour per day for 7 days, normalized to non-stimulation control (n=6 mice in no stim group, n=6 mice in 40 Hz group, mean s.e.m. in bar graphs, n.s.= not significant, unpaired Mann-Whitney test).

## 4.2 Auditory GENUS reduces tau phosphorylation and seeding in AC and hippocampus

Another classical pathological hallmark of AD is the accumulation of phosphorylated tau aggregates (Grundke-Iqbal et al., 1986, Ihara et al., 1986, Ittner and Götz, 2011). Tau phosphorylation at specific amino acid residues associated with AD has been demonstrated to alter its cytoskeletal support functions and to reduce its solubility, and is thus suggested to be a major neuronal insult (Bramblett et al., 1993, Vanmechelen et al., 2000). To investigate whether auditory GENUS could impact pathology in another AD-associated mouse model, we used Tau P301S mice (Yoshiyama et al., 2007). Because tau P301S mice begin exhibiting spatial and contextual learning deficits at 6-months-old (Takeuchi et al., 2011), we examined whether auditory GENUS could lead to a reduction in phosphorylated tau in AC and HPC in 6-month-old tau P301S mice. Immunohistochemical analysis of brain slices from these mice (Supplement Figure 3.2 A,B,D, and E) indicated that auditory GENUS reduced tau phosphorylation at threonine-181 (T181) by 36.20±2.828% (AC) and 38.70±2.737% (CA1), and at serine-396 (S396) by 37.90±3.469% (AC) and 40.80±4.528% (CA1) (Supplement Figure 3.2C and F).

Western blot (WB) experiments confirmed the immunohistochemistry results of tau phosphorylation at S396, showing a 33.83±0.20% and 43.20±1.50% reduction in phosphorylation in AC and whole hippocampus tissue, respectively, when compared with total tau (Supplement Figure 3.2G,H,J, and K). WB analysis indicated a reduction in phosphorylated T181 tau in hippocampus by 34.50±1.61%, although the difference was not significant in AC (Supplement Figure 3.2I and L).

To further examine tau pathology, we performed a tau seeding assay (see Methods, and (Holmes et al., 2014)). to investigate whether changes in proteopathic tau propagation occur in

the AC and hippocampus of P301S mice following 1-week of auditory GENUS. We observed that the average change in FRET signal, which indicates tau seeding activity, was significantly decreased in auditory cortex (72.5 ± 9.2%) and hippocampus (77.5 ± 5.6%) in the 40 Hz group when compared to the non-stimulated group (Supplement Figure 3.2M). Altogether, our results show that auditory GENUS can reduce the levels of AD-related hyperphosphorylated tau epitopes, and that auditory GENUS can affect pathology in a tauopathy mouse model.

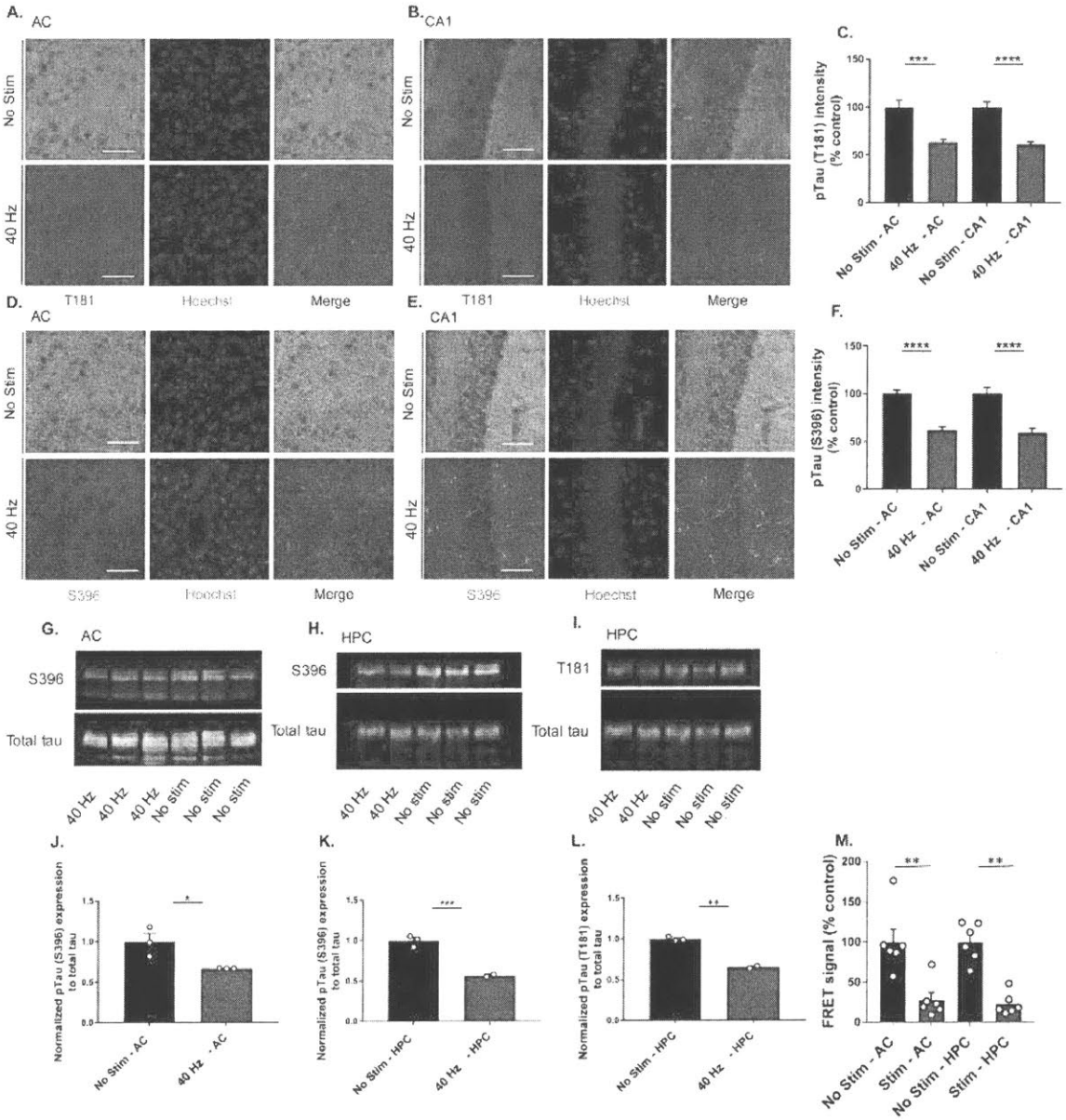
A.
AC
No Stim
40 Hz
T181
Hoechst
Merge
B.
CA1
C.
pTau (T181) intensity (% control)
No Stim - AC
40 Hz - AC
No Stim - CA1
40 Hz - CA1
D.
AC
S396
E.
CA1
F.
pTau (S396) intensity (% control)
G.
AC
S396
Total tau
H.
HPC
I.
HPC
T181
J.
Normalized pTau (S396) expression to total tau
K.
L.
Normalized pTau (T181) expression to total tau
M.
FRET signal (% control)
Stim - AC
Stim - HPC

**Supplement figure 3.2 Auditory GENUS reduces phosphorylated tau and seeding in P301S mice.**

A) Immunohistochemistry with anti-pTau (T181, red) antibodies in AC of 6-month-old P301S mice after 7 days of 1 hour per day no stimulation or auditory GENUS (image taken with 40x objective, scale bar, 50 μm). B) As in A for CA1. C) Relative pTau (T181) intensity levels in AC and CA1 of P301S mice after 7 days of 1 hour per day no stimulation or auditory GENUS normalized to non-stimulation control (n=10 mice per group, ***P<0.001, ****P<0.0001; unpaired Mann-Whitney test). D) Immunohistochemistry with anti-pTau (S396, green) antibodies in AC of 6-month-old P301S mice after 7 days of 1 h per day no stimulation or auditory GENUS (scale bar, 50 μm). E) As in D for CA1. F) Relative pTau (S396) intensity levels in P301S mice in AC and CA1 after 7 days of 1 hour per day no stimulation or auditory GENUS normalized to non-stimulation control (n=10 mice per group, ****P<0.0001; unpaired Mann-Whitney test). G) Representative western blot showing levels of pTau (S396) and total tau in AC of 6-month-old P301S mice after 7 days of 1 hour per day no stimulation or auditory GENUS. H) As in G for hippocampus. I) Representative western blot showing levels of pTau (T181) and total tau in hippocampus of 6-month-old P301S mice after 7 days of 1 hour per day no stimulation or auditory GENUS. J) Relative immunoreactivity of pTau (S396) normalized to total tau in AC of P301S mice (from western blot in G) after 7 days of 1 hour per day no stimulation or auditory GENUS (n=3 mice per group, mean s.e.m. in bar graphs, *P<0.05; unpaired Mann-Whitney test). K) Relative immunoreactivity of pTau (S396) normalized to total tau in HPC of P301S mice (from western blot in H) after 7 days of 1 hour per day no stimulation or auditory GENUS (n=2 mice in 40 Hz group and n=3 in non-stimulation group, mean s.e.m. in bar graphs, ***P<0.001; unpaired Mann-Whitney test).

L) Relative immunoreactivity of pTau (T181) normalized to total tau in hippocampus of P301S mice (from western blot in I) after 7 days of 1 hour per day no stimulation or auditory GENUS (n=2 mice in 40 Hz group and n=3 in non-stimulation group, mean s.e.m. in bar graphs, **P<0.01; unpaired Mann-Whitney test). M) Average change in FRET signal from 2-month-old P301S tau mice following auditory GENUS for 1 hour per day for 7 days, normalized to non-stimulation control (n=6 in no stim group, n=6 in 40 Hz group, mean s.e.m. in bar graphs, **P<0.01, unpaired Mann-Whitney Test).

## 4.2 Auditory GENUS induces a glia response in 5XFAD mice

Accumulating evidence suggests that microglia are responsive to changes in neuronal activity, and play a role in AD pathology (Allen and Barres, 2005, Mosher and Wyss-Coray, 2014, Walker and Lue, 2015). Our ability to reduce amyloid load in AC and HPC led us to examine whether auditory GENUS could stimulate a change in microglia response in 6-month-old 5XFAD mice. Microglia have been shown to change their cellular morphology during activation states involving engulfment (Davies et al., 2016) and indeed, our earlier study demonstrated that 1 hr of visual GENUS was sufficient to induce a morphological change in microglia consistent with activation and increased phagocytic activity in VC (Iaccarino et al., 2016). Using an antibody against the microglia marker Iba1 (Figure 4A and B), we observed approximately 60% more microglia in both AC and CA1 in the auditory GENUS group when compared with no stimulation controls (Figure 4C). Microglia cell body area increased by 70.60±4.78% in AC and 117.17±10.4% in CA1, following auditory GENUS when compared with no stimulation controls (Figure 4D). We further found a decrease in microglia process length by 46.44±3.2% (AC) and 50.875.±4.8% (CA1) as well as a 36.00±9.5% (AC) and 143.813±29.9% (CA1) increase in process arborization, when compared with no stimulation controls (Figure 4E and F). To evaluate microglia uptake of Aβ, we measured the co-localization of Aβ within microglia by co-immunostaining tissue sections with Iba1 and an Aβ antibody specific for $A\beta_{1-42}$ (12F4, see Methods). We observed that the percentage of microglia whose cell bodies were co-localized with Aβ increased by 58.75±1.25% in AC and 61.33±3.71% in CA1 following auditory GENUS when compared with no stimulation controls (Figure 4G).

To examine whether microglia response following auditory GENUS occurs in other AD mouse models, we measured microglia morphology from 9-month old APP/PS1 mice following 7 days of auditory GENUS. Similar to our results seen in 5XFAD microglia following 7 days of auditory GENUS (See Figure 4A-G), we observed a significant increase in microglia cell body diameter and count, as well as a significant decrease in average processes length in AC and CA1 when compared to no stimulation control (Supplement Figure 4A-C).

In order to understand the longitudinal effects of microglia response in 5XFAD mice following auditory GENUS, we examined microglia morphology following 7 days of no stimulation post a week of auditory GENUS. We observed a similar trend as from amyloid (Supplement Figure 3F-H), specifically a non-significant increase in microglia cell body diameter, decrease in average processes length, and increase in microglia count in the auditory cortex (See Supplement Figure 4D-F). We did however see a significant increase (by 41.70 ± 6.75%) in microglia count in CA1 when compared to non-stimulation control.

Astrocytes are another primary glial cell in the central nervous system, and are critical for homeostatic maintenance, synaptic pruning, waste clearance, and other important biological processes such as regulating cerebral blood flow (Chung et al., 2015; Kisler et al., 2017). Reactive-like astrocytes express glial fibrillary acidic protein (GFAP) (Eng et al., 1971). To investigate whether there are any baseline changes in the number of reactive astrocytes between 6-month-old 5XFAD and WT littermate control mice, we performed CLARITY on 100 μm CA1 brain sections stained against GFAP antibodies (Supplement Figure 4G). We observed that 5XFAD mice had a significantly lower number of GFAP-positive astrocytes when compared to WT controls (Supplement Figure 4H). This observation is consistent with reports that show other AD

transgenic mouse models with similar glia atrophy (Rodríguez et al., 2009). To determine whether auditory GENUS could affect the reactivity of astrocytes, we subjected 6-month-old 5XFAD mice to 7 days of either 1 hr/day auditory GENUS or no stimulation control, and then immunostained their brain sections using antibodies against GFAP and S100 calcium-binding protein B (S100B), another protein shown to be expressed in reactive-like astrocytes (Figure 4H and I). Astrocytes positive for GFAP increased by 27.66±0.954% and 18.14±0.799% in AC and CA1, respectively, and S100B-positive astrocytes increased by 21.83±1.07% in AC and 15.57±0.869% in CA1 (Figure 4J and K). This observed change in astrocyte number following auditory GENUS may be indicative of a potential increase in astrocyte survival.

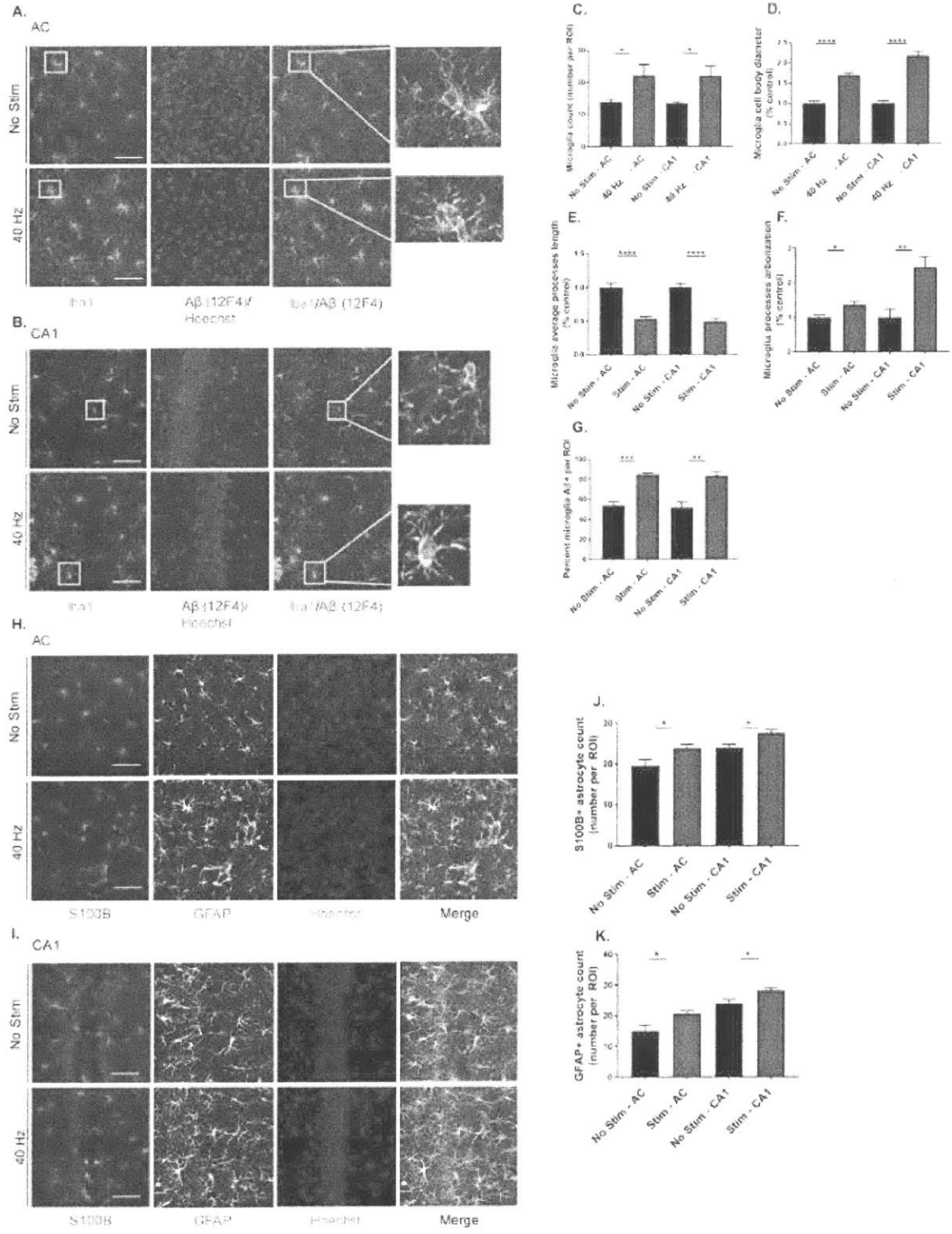
A.
AC
No Stim
40 Hz
Iba1
Aβ (12F4)/ Hoechst
Iba1/Aβ (12F4)
B.
CA1
No Stim
40 Hz
Iba1
Aβ (12F4)/ Hoechst
Iba1/Aβ (12F4)
C.
Microglia count (number per ROI)
No Stim - AC
40 Hz - AC
No Stim - CA1
40 Hz - CA1
D.
Microglia cell body diameter (% control)
No Stim - AC
40 Hz - AC
No Stim - CA1
40 Hz - CA1
E.
Microglia average processes length (% control)
No Stim - AC
Stim - AC
No Stim - CA1
Stim - CA1
F.
Microglia processes arborization (% control)
No Stim - AC
Stim - AC
No Stim - CA1
Stim - CA1
G.
Percent microglia Aβ+ per ROI
No Stim - AC
Stim - AC
No Stim - CA1
Stim - CA1
H.
AC
No Stim
40 Hz
S100B
GFAP
Hoechst
Merge
I.
CA1
No Stim
40 Hz
S100B
GFAP
Hoechst
Merge
J.
S100B+ astrocyte count (number per ROI)
No Stim - AC
Stim - AC
No Stim - CA1
Stim - CA1
K.
GFAP+ astrocyte count (number per ROI)
No Stim - AC
Stim - AC
No Stim - CA1
Stim - CA1

**Figure 4. Auditory GENUS induces glial response in AC and CA1 in 5XFAD mice**
A) Immunohistochemistry with anti-Iba1 (019-19741, green) and anti-Aβ (12F4, red) antibodies in AC of 5XFAD mice after 7 days of 1 hour per day no stimulation or auditory GENUS (n=8 mice per group, scale bar, 50 μm). B) As in A for CA1. C) Number of Iba1-positive microglia in AC and CA1 (n=8 mice per group, mean s.e.m. in bar graphs, *P<0.05; unpaired Mann-Whitney Test). D) Diameter of Iba1-positive microglia cell bodies in AC and CA1 normalized to non-stimulated controls (n=8 mice per group, mean s.e.m. in bar graphs, ****P<0.0001; unpaired Mann-Whitney Test). E) Average length of Iba1-positive microglia primary processes in AC and CA1 normalized to non-stimulated controls (n=8 mice per group, mean s.e.m. in bar graphs, ****P<0.0001; unpaired Mann-Whitney Test). F) Average processes arborization of Iba1-positive microglia in AC and CA1 normalized to non-stimulated controls (n=8 mice per group, mean s.e.m. in bar graphs, *P<0.05, **P<0.01; unpaired Mann-Whitney Test). G) Percentage of Iba1-positive microglia cell bodies that are also Aβ-positive in AC and CA1 (n=8 mice per group, mean s.e.m. in bar graphs, **P<0.01, ***P<0.001; unpaired Mann-Whitney Test). H) Immunohistochemistry with anti-S100B (ab868, purple) and anti-GFAP (ab4674, grey) antibodies in AC of 5XFAD mice after 7 days of 1 hour per day no stimulation or auditory GENUS (n=8 per group, scale bar, 50 μm). I) As in H for CA1. J) Number of S100B-positive astrocytes in AC and CA1 (n=8 mice per group, mean s.e.m. in bar graphs, *P<0.05; unpaired Mann-Whitney Test). K) As in J for GFAP-positive astrocytes.

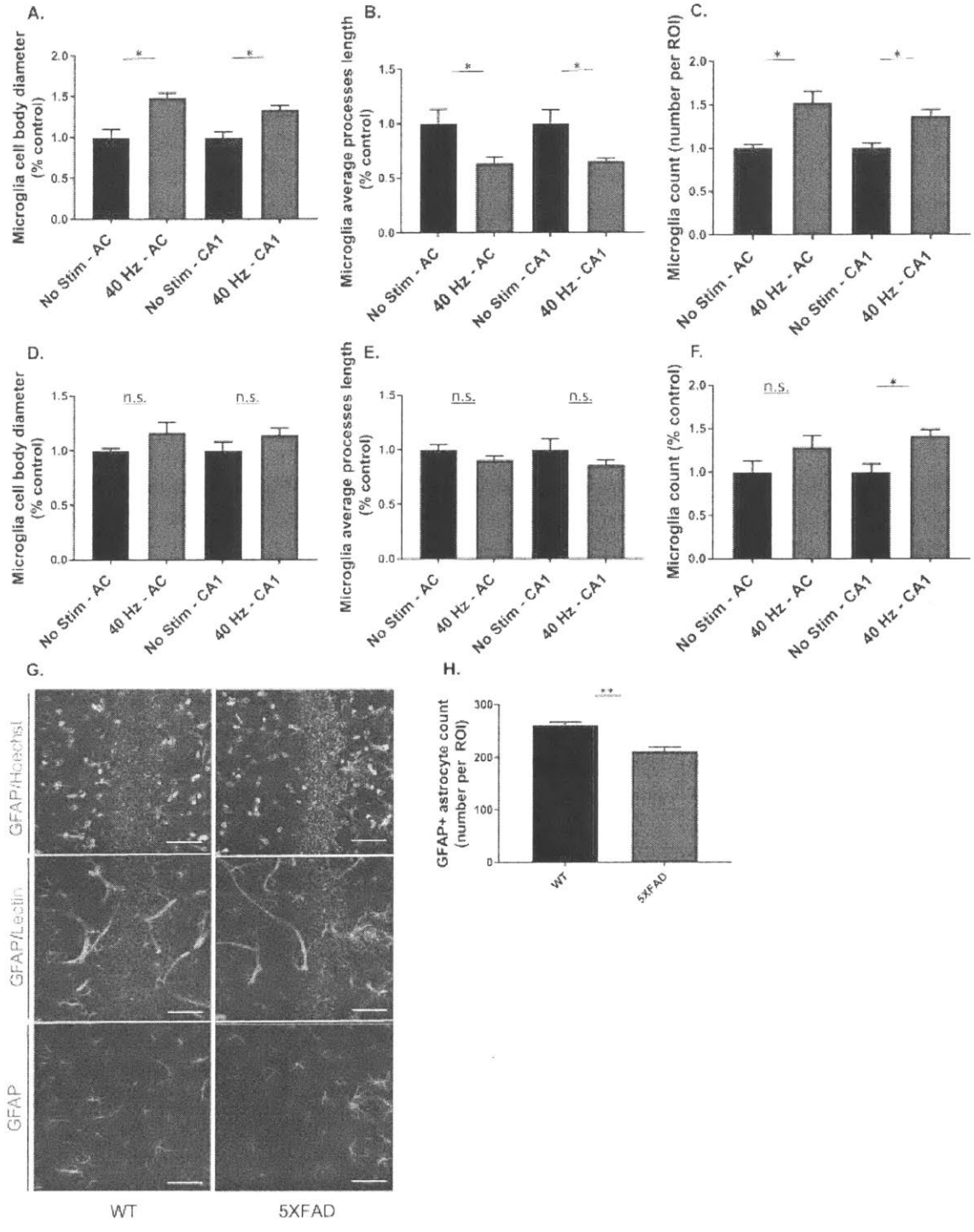
A.
Microglia cell body diameter (% control)
2.0
1.5
1.0
0.5
0.0
*
*
No Stim - AC
40 Hz - AC
No Stim - CA1
40 Hz - CA1
B.
Microglia average processes length (% control)
1.5
1.0
0.5
0.0
*
*
No Stim - AC
40 Hz - AC
No Stim - CA1
40 Hz - CA1
C.
Microglia count (number per ROI)
2.0
1.5
1.0
0.5
0.0
*
*
No Stim - AC
40 Hz - AC
No Stim - CA1
40 Hz - CA1
D.
Microglia cell body diameter (% control)
1.5
1.0
0.5
0.0
n.s.
n.s.
No Stim - AC
40 Hz - AC
No Stim - CA1
40 Hz - CA1
E.
Microglia average processes length (% control)
1.5
1.0
0.5
0.0
n.s.
n.s.
No Stim - AC
40 Hz - AC
No Stim - CA1
40 Hz - CA1
F.
Microglia count (% control)
2.0
1.5
1.0
0.5
0.0
n.s.
*
No Stim - AC
40 Hz - AC
No Stim - CA1
40 Hz - CA1
G.
GFAP/Hoechst
GFAP/Lectin
GFAP
WT
5XFAD
H.
GFAP+ astrocyte count (number per ROI)
300
200
100
0
**
WT
5XFAD

**Supplement Figure 4. Auditory GENUS induces microglia response in APP/PS1 mice.**
A) Diameter of Iba1-positive microglia cell bodies in AC and CA1 in 9-month old APP/PS1 mice following auditory GENUS for 1 hour per day for 7 days, normalized to non-stimulation control (n=5 mice per group, mean s.e.m. in bar graphs, *P<0.05, unpaired Mann-Whitney test). B) Average length of Iba1-positive microglia primary processes in AC and CA1 in 9-month old APP/PS1 mice following auditory GENUS for 1 hour per day for 7 days, normalized to non-stimulation control (n=5 mice per group, mean s.e.m. in bar graphs, *P<0.05, unpaired Mann-Whitney test). C) Number of Iba1-positive microglia in AC and CA1 in 9-month old APP/PS1 mice following auditory GENUS for 1 hour per day for 7 days, normalized to non-stimulation control (n=5 mice per group, mean s.e.m. in bar graphs, *P<0.05, unpaired Mann-Whitney test). D) Diameter of Iba1-positive microglia cell bodies in AC and CA1 in 6-month old 5XFAD mice following 7 days no stimulation post-auditory GENUS for 1 hour per day for 7 days, normalized to non-stimulation control (n=6 mice per group, mean s.e.m. in bar graphs, n.s.= not significant, unpaired Mann-Whitney test). E) Average length of Iba1-positive microglia primary processes in AC and CA1 in 6-month old 5XFAD mice following 7 days no stimulation post-auditory GENUS for 1 hour per day for 7 days, normalized to non-stimulation control (n=6 mice per group, mean s.e.m. in bar graphs, n.s.= not significant, unpaired Mann-Whitney test). F) Number of Iba1-positive microglia in AC and CA1 in 6-month old 5XFAD mice following 7 days no stimulation post-auditory GENUS for 1 hour per day for 7 days, normalized to non-stimulation control (n=6 mice per group, mean s.e.m. in bar graphs, *P<0.05, n.s.= not significant, unpaired Mann-Whitney test). G) Immunohistochemistry of CLARITY treated brain sections with anti-GFAP (ab4674, red) and lectin stain (DL-1174, green) antibodies in CA1 of 6-month-old WT and 5XFAD mice (n=5 mice per group, scale bar, 50 μm). H) Number of GFAP positive cells (per image of interest, using IMARIS) in CA1 of 6-month-old WT and 5XFAD mice (n=5 mice per group, mean s.e.m. in bar graphs, **P<0.01, unpaired Mann-Whitney test).

### 4.3 Auditory GENUS induces vasculature response in 5XFAD mice

Astrocytes are known to play an important role in regulating the brain's vascular network, and accumulating evidence suggests dysfunction of this network in AD may exacerbate pathology (Kyrtsos and Baras, 2015). Amyloid clearance from the brain is multifaceted and various processes via the vasculature have been proposed, such as through the glymphatic system and via transport by the endocytic receptor lipoprotein receptor-related protein 1 (LRP1) (Kyrtsos and Baras, 2015, Storck et al., 2016, Iliff et al., 2012). To investigate potential changes in the vasculature, we first used tomato lectin (*Lycopersicon esculentum*), an effective marker of the blood vessel endothelium to stain 5XFAD brain slices following auditory GENUS (Figure 5A and B). Interestingly, we observed a 49.70 $\pm$7.80% (AC) and 104.70 $\pm$10.96% (CA1) increase in blood vessel diameter following auditory GENUS, when compared with no stimulation controls (Figure 5C).

We further explored whether amyloid-blood vessel interactions change following auditory GENUS. We examined whether auditory GENUS could affect Aβ co-localization with LRP1, which has been shown to play an important role in Aβ transport and systemic elimination through the vasculature (Storck et al., 2016), by staining for LRP1 and Aβ in brain slices from 5XFAD mice that were either exposed to the 1 hr/day auditory GENUS or no stimulation for 7 days (Figure 5D and E). In no stimulation controls, we observed a 8.17$\pm$2.70% (AC) and 6.97$\pm$1.73% (CA1) co-localization of Aβ with LRP1, whereas in the auditory GENUS group, co-localization of Aβ with LRP1 increased significantly to 17.71$\pm$2.78% and 16.50$\pm$3.90% in AC and CA1, respectively (Figure 5F). Together, these results suggest that one explanation for reduced

Aβ levels in AC and CA1 following auditory GENUS may be through increased clearance of Aβ through microglia and changes in the vasculature.

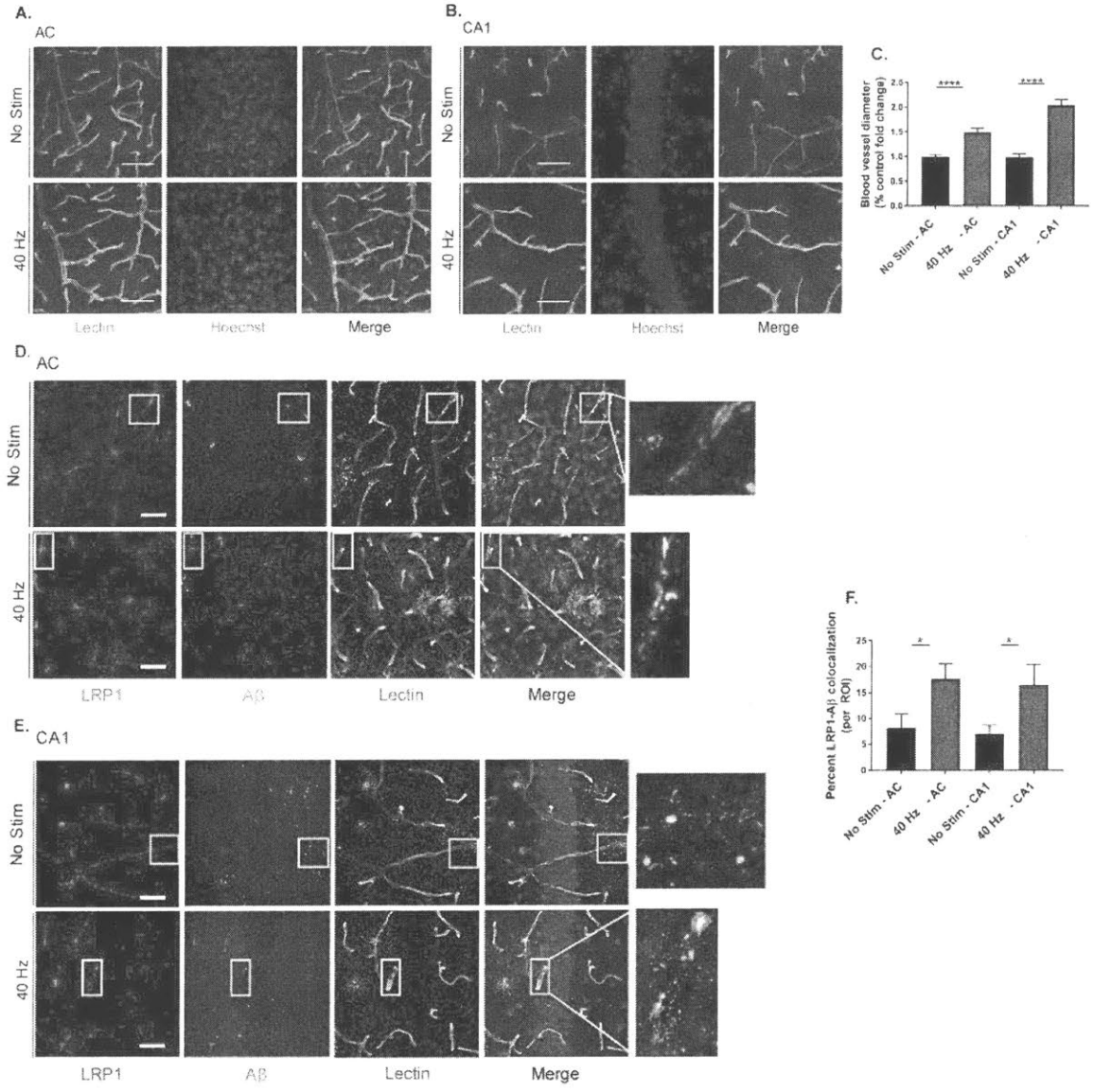

**Figure 5. Auditory GENUS induces vasculature changes.**
A) Immunohistochemistry with lectin stain (DL-1174, green) in AC of 6-month-old 5XFAD mice after 7 days of 1 h per day no stimulation or auditory GENUS (scale bar, 50 μm). B) As in A for CA1. C) Percent fold change in blood vessel diameter in AC and CA1 of 6-month-old 5XFAD mice after 7 days of 1 hour per day no stimulation or auditory GENUS, normalized to no stimulation control (n=7 mice per group, mean s.e.m. in bar graphs, ****P<0.0001; unpaired Mann-Whitney Test). D) Immunohistochemistry with anti-LRP1 (28320, red), anti-Aβ (AB9234, green), and lectin stain (DL-1174, gray) antibodies in AC of 6-month-old 5XFAD mice after 7 days of 1 hour per day no stimulation or auditory GENUS (n=8 mice per group, scale bar, 50 μm). E) As in D for CA1. F) Percentage of Aβ-LRP1 co-localization in AC and CA1 of 5XFAD mice after 7 days of 1 hour per day no stimulation or auditory GENUS (n=8 mice per group, *P<0.05; unpaired Mann-Whitney Test).

## Chapter 5: Combined auditory and visual GENUS induces microglia-clustering response and amyloid reduction in mPFC[4]

### 5.1: 40 Hz combined auditory and visual stimulation modulates spiking activity in AC, CA1, and mPFC.

Our findings thus far demonstrate that auditory GENUS can reduce amyloid levels and induce glial and vasculature changes in cortical sensory areas and in hippocampus. This prompted us to investigate whether combining auditory with visual GENUS could elicit more profound cellular effects. We first determined whether a combination of 40 Hz auditory tone stimulation with 40 Hz light flicker could entrain neural responses in AC, CA1, and mPFC. We presented 3-8 month old male wild-type (C57BL6J) mice with a combination of 1 ms-long auditory tones and 12.5 ms-long light pulses at a frequency of 40 Hz while recording neural activity in AC, CA1, and mPFC using 32-channel silicon probes as animals ran or rested on a spherical treadmill. Single unit firing rate increased and decreased periodically with each tone and light-on period, thus entraining to 40 Hz during combined auditory-visual stimulation (**Figure 6.1A-C, *left)***. Vector strength distributions were significantly higher during 40 Hz auditory-visual stimulation than in random stimulation or no stimulation conditions (**Figure 6.1A-C, *right).*** Therefore, the spiking of single neurons in AC, CA1, and mPFC was entrained to 40 Hz significantly more during auditory-visual stimulation periods than during baseline periods. Local field potentials in AC, HPC, and mPFC displayed elevated power at 40 Hz during audio-visual flicker stimulation, however the effect was very small in mPFC (**Supplement Figure 6.1A, H, and O**). Thus, 40 Hz tone plus light stimulation induced GENUS in AC, CA1, and mPFC.

---

[4] The findings in this chapter were in press at the time of thesis submission (Martorell, Paulson, et al., *Cell*, 2019).

While small, we observe differences between auditory and combined auditory-visual stimulation in mPFC in the local field potential (LFP) response and in single unit mean firing rates. There was a small increase in power in the LFP at 40 Hz during combined stimulation, but not during auditory only stimulation (**Supplement Figure 1P and Figure 6O)**. Additionally, the distribution of mean firing rate differences between combined stimulation and baseline had a median that was significantly different from zero, while this did not differ significantly from zero with auditory only stimulation (**Supplement Figure 1R and Figure 6R**).

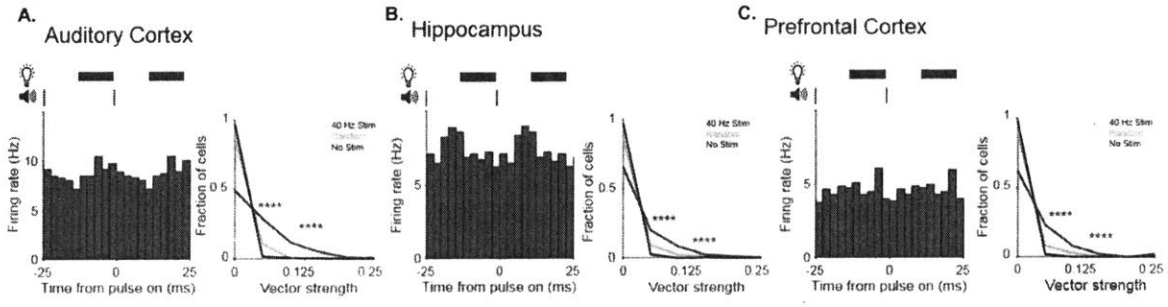


**Figure 6.1 Neuronal firing rate modulation following combined GENUS.**
A) Firing rate modulation of a single unit during 40 Hz audio-visual stimulation (left). Vector strength distribution of 40 Hz audio-visual stimulation, random audio-visual stimulation, and no stimulation periods (right, ****P<0.0001, P = 4x10-71 40 Hz vs. No Stim, P = 3x10-20 40 Hz vs. Random; Kolmogorov-Smirnov test; 9 units had 40 Hz stim VS values greater than 0.25; 3 units had random stim VS values greater than 0.25. In all statistical tests for panels A-C, significance remains after controlling for multiple comparisons using the Bonferroni correction, unless otherwise stated). B) Same as A for CA1 (right, ****P<0.0001, P = 2x10-54 40 Hz vs. No Stim, P = 3x10-12 40 Hz vs. Random; Kolmogorov-Smirnov test; 8 units had 40 Hz stim VS values greater than 0.25; 3 units had random stim VS values greater than 0.25).
C) Same as A for mPFC (right, ****P<0.0001, P = 9x10-29 40 Hz vs. No Stim, P = 9x10-7 40 Hz vs. Random; Kolmogorov-Smirnov test; 5 units had 40 Hz stim VS values greater than 0.25).

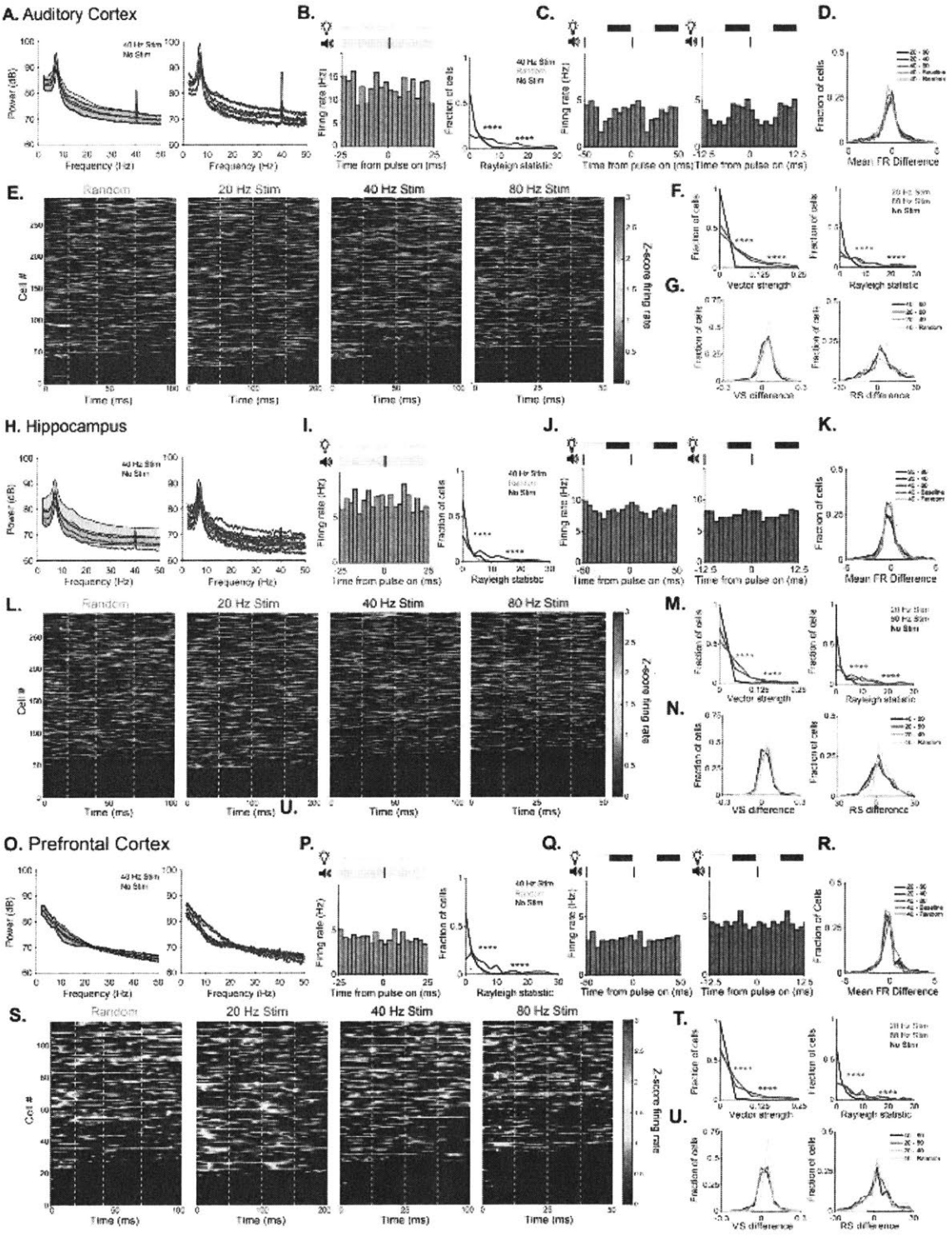
A. Auditory Cortex
B.
C.
D.
E.
Random
20 Hz Stim
40 Hz Stim
80 Hz Stim
F.
G.
H. Hippocampus
I.
J.
K.
L.
M.
N.
O. Prefrontal Cortex
P.
Q.
R.
S.
T.
U.

**Supplement Figure 6. 40 Hz combined auditory and visual stimulation modulates spiking activity in AC, CA1, and mPFC.**

A) Power spectral density (PSD) response to 40 Hz audio-visual flicker stimuli and no stimulation periods, with mean and standard deviation across recording days (left), power spectrum LFP response to audio-visual flicker stimulation of all recording days in AC (recording site with largest 40 Hz peak during 40 Hz audio-visual flicker per recording depth is shown, see Methods) (right). B) Firing rate modulation of putative single unit shown in Figure 6A to audio-visual random stimulation, Rayleigh statistic distribution of single unit response to 40 Hz audio-visual stimulation (right, ****P<0.0001, P = 4x10-71 40 Hz vs. No Stim, P =3x10-20 40 Hz vs. Random; Kolmogorov-Smirnov test; 40 units had 45 Hz stim RS values greater than 30; 5 units had random stim RS values greater than 30. In all statistical tests, significance remains after controlling for multiple comparisons using the Bonferroni correction, unless otherwise stated). C) Firing rate modulation of a putative single unit in response to 20 Hz audio-visual flicker stimulation (left, green) and 80 Hz audio-visual flicker stimulation (right, purple). D) Mean firing rate difference of single units between multiple stimulation conditions in AC centers around 0 Hz (P>0.01 40Hz – no stimulation, n.s. after controlling for five comparisons; all others n.s.; Wilcoxon signed rank test for zero median).

E) Firing rate response of all isolated single units in AC to Random, 20 Hz, 40 Hz, and 80 Hz audio-visual stimulation. Z-scored response to four consecutive stimulus cycles is shown. Units are ordered by their average stimulus phase preference in the analyzed four cycles. White dashed lines indicate auditory pulse timing. F) Vector strength distribution of 20 Hz and 80 Hz audio-visual stimulation vs. no stimulation condition (left, ****P<0.0001, P = 1x10-73 20 Hz vs. No Stim, P = 2x10-60 80 Hz vs. No Stim; Kolmogorov-Smirnov test; 12 units had 20 Hz stim VS values greater than 0.25; 10 units had 80 Hz stim VS values greater than 0.25), and Rayleigh statistic distribution of 20 Hz and 80 Hz audio-visual stimulation vs. no stimulation (right, ****P<0.0001, P = 1x10-56 20 Hz vs. No Stim, P = 5x10-41 80 Hz vs. No Stim; Kolmogorov-Smirnov test; 86 units had 20 Hz stim RS values greater than 30; 35 units had 80 Hz stim RS values greater than 30). G) Distribution of within cell differences in vector strength values between all frequencies of auditory stimulation (left, ***P<0.001 20 Hz – 40 Hz, ****P<0.0001, P = 1x10-6 20 Hz - 80 Hz, P = 2x10-39 40 Hz – Random, 40 Hz – 80 Hz n.s.; Wilcoxon signed rank test for zero median). Within cell differences in Rayleigh statistic values between all frequencies of auditory stimulation (right, ***P>0.000025 20 Hz - 80 Hz, after controlling for four comparisons; ****P<0.0001 P = 5x10-7 20 Hz – 40 Hz, P = 8x10-43 40 Hz – Random; 40 Hz – 80 Hz n.s.; Wilcoxon signed rank test for zero median). H) Same as A for CA1. I) Same as B for CA1 (right, ****P<0.0001, P = 8x10-29 40 Hz vs. No Stim, P =2x10-12 40 Hz vs. Random; Kolmogorov-Smirnov test; 8 units had 40 Hz stim RS values greater than 30). J) Same as C for CA1. K) Same as D for CA1 (P>0.01 40 Hz – no stimulation, n.s. after controlling for five comparisons; all others n.s.; Wilcoxon signed rank test for zero median). L) Same as E for CA1.

M) Same as F for CA1 (left, ****P<0.0001, P = 2x10-63 20 Hz vs. No Stim, P = 2x10-51 80 Hz vs. No Stim; Kolmogorov-Smirnov test; 16 units had 20 Hz stim VS values greater than 0.25; 7 units had 80 Hz stim VS values greater than 0.25; right, ****P<0.0001, P = 9x10-37 20 Hz vs. No Stim, P = 3x10-27 80 Hz vs. No Stim; Kolmogorov-Smirnov test; 21 units had 20 Hz stim RS values greater than 30; 3 units had 80 Hz stim RS values greater than 30). N) Same as G for CA1 (left, ***P<0.001 20 Hz – 40 Hz, ****P<0.001, P = 4x10-7 20 Hz – 80 Hz, P = 4x10-22 40 Hz – random; 40 Hz – 80 Hz n.s.; Wilcoxon signed rank test for zero median; right, **P<0.01 20 Hz – 40 Hz, ****P<0.0001 P = 5x10-30 40 Hz – Random; all others n.s.; Wilcoxon signed rank test for zero median). O) Same as A for mPFC. P) Same as B for mPFC (right, ****P<0.0001, P = 9x10-29 40 Hz vs. No Stim, P =2x10-12 40 Hz vs. Random; Kolmogorov-Smirnov test; 1 unit had a 40 Hz stim RS value greater than 30). Q) Same as C for mPFC. R) Same as D for mPFC (P>0.01 40 Hz – no stimulation, n.s. after controlling for five comparisons; all others n.s.; Wilcoxon signed rank test for zero median). S) Same as E for mPFC. T) Same as F for mPFC (left, ****P<0.0001, P = 1x10-24 20 Hz vs. No Stim, P = 2x10-25 80 Hz vs. No Stim; Kolmogorov-Smirnov test; 4 units had 20 Hz stim VS values greater than 0.25; 1 unit had a 80 Hz stim VS value greater than 0.25; right, ****P<0.0001, P = 4x10-15 20 Hz vs. No Stim, P = 2x10-15 80 Hz vs. No Stim; Kolmogorov-Smirnov test; 5 units had 20 Hz stim RS values greater than 30; 1 unit had a 80 Hz stim RS value greater than 30). U) Same as G for mPFC (left, ****P<0.0001, P = 2x10-14 40 Hz – random; all others n.s.; Wilcoxon signed rank test for zero median; right, ****P<0.0001 P = 1x10-15 40 Hz – Random; all others n.s.; Wilcoxon signed rank test for zero median).

## 5.2: Combined auditory and visual GENUS induces a clustering phenotype response by microglia

Following 1 hr/day for 7 days of combined GENUS, we examined the morphological features of microglia and their interactions with Aβ in AC, VC, and CA1 (**Figure 6D and E**). Because higher-order cognitive regions are known to process multi-modal sensory stimuli (Takehara et al., 2003, Maviel et al., 2004, Euston et al., 2012, Kitamura et al., 2017), we examined whether combined GENUS could elicit a microglia effect in the medial prefrontal cortex (mPFC) as well. We found that microglia exhibited a significant increase in soma area whereas projection length significantly decreased when compared with non-stimulated controls (**Figure 6F and G**). Microglia number also significantly increased following combined GENUS in AC, VC, CA1, and mPFC (**Figure 6H**). Microglia in the auditory or visual stimulation groups alone (**Supplement Figure 7A-D, G, and H**) displayed reduced projection length and enlarged soma area in AC, VC, and CA1, but not in mPFC. In contrast to visual GENUS, auditory GENUS showed a significant increase in microglia count in CA1; but neither auditory nor visual GENUS alone elicited a significant change in microglia count in the mPFC (**Supplement Figure 7E and I**). These findings show that following 1-week of GENUS, only combined auditory and visual stimulation, and not auditory or visual stimulation alone, promoted a microglia response in mPFC.

Interestingly, microglia in the combined GENUS group appeared to show a change in activity by displaying an encapsulating effect surrounding amyloid deposits. To better resolve the clustering microglia-Aβ phenotype, we created three-dimensional (3D) renderings from AC, VC, CA1, and mPFC images, taken from 5XFAD brain slices following combined GENUS and no stimulation control (Shown in '3D reconstruction' column in **Figure 6D and E**). Using IMARIS

imaging software (see **Methods),** we created 3D surfaces of amyloid deposits (red spots) and microglia cells (green spots), and quantified the proximity and number of microglia within a 25 μm radius of an amyloid deposit (*far right* inset, **Figure 6D and E**, example videos showing the clustering microglia-Aβ phenotype following combined GENUS and no stimulation control are provided in **supplementary videos 3 and 4.)** We observed a significant increase of 48.88±0.651% in AC, 31.56±1.11% in VC, and 38.64±0.959% in mPFC in the number of microglia surrounding a 25 μm radius around amyloid plaques following combined GENUS, when compared to no stimulation control (**Figure 6I**). We also observed a non-significant increase in CA1 by 33.05±2.65%. To examine whether the clustering microglia-Aβ phenotype is a specific phenotype following combined GENUS, we analyzed the number of microglia within a 25 μm radius of an amyloid deposit following auditory or visual GENUS alone. We observed no significant difference in the number of microglia per plaque between GENUS and non-stimulated mice (**Supplement Figure 7F and J**).

We next addressed the frequency specificity of microglia response in 6-month-old 5XFAD mice following 7-days of 40 Hz auditory GENUS, combined GENUS, 80 Hz, or random frequency stimulation in AC, CA1, and mPFC. We observed significant increases in microglia cell body diameter and count, as well as a significant decrease in average processes length in AC and CA1 following both 40 Hz auditory stimulation and combined GENUS, but not additional frequencies, when compared to non-stimulation control. Interestingly, only combined GENUS resulted in a microglia response in the mPFC when compared to 40 Hz auditory stimulation, additional frequencies, and non-stimulation controls (**Supplement Figure 7K-M**).

We also examined whether GENUS has frequency specific effects on astrocyte count following 7-days of 40 Hz auditory GENUS, combined GENUS, 80 Hz, or random frequency stimulation in AC and CA1. We observed a significant increase in the number of GFAP-positive astrocytes in both AC (69.2 ± 3.4%) and CA1 (26.7 ± 2.6%) following 40 Hz auditory GENUS, and a significant increase in AC (63.7 ± 4.3%) following 40 Hz combined A+V GENUS, but not in other frequency groups, when compared to mice with no stimulation (**Supplement Figure 7N-O)**. We observed a significant increase in the number of S100B-positive astrocytes in AC (27.8 ± 2.1%) and CA1 (30.2 ± 1.8%) following 40 Hz auditory GENUS, and a non-significant increase in AC (28.2 ± 5.1%) and CA1 (21.6 ± 2.8%) following 40 Hz combined A+V GENUS, but not other frequency groups, when compared to non-stimulated mice.

These results provide an intriguing hypothesis, that combined GENUS enhances glial response through changes in neuronal activity; this idea is supported by studies demonstrating the capability of glia to respond to such changes (Ransohoff and Perry, 2009). Therefore, we conclude combined GENUS induces an extended microglia clustering response in AC, VC and mPFC.

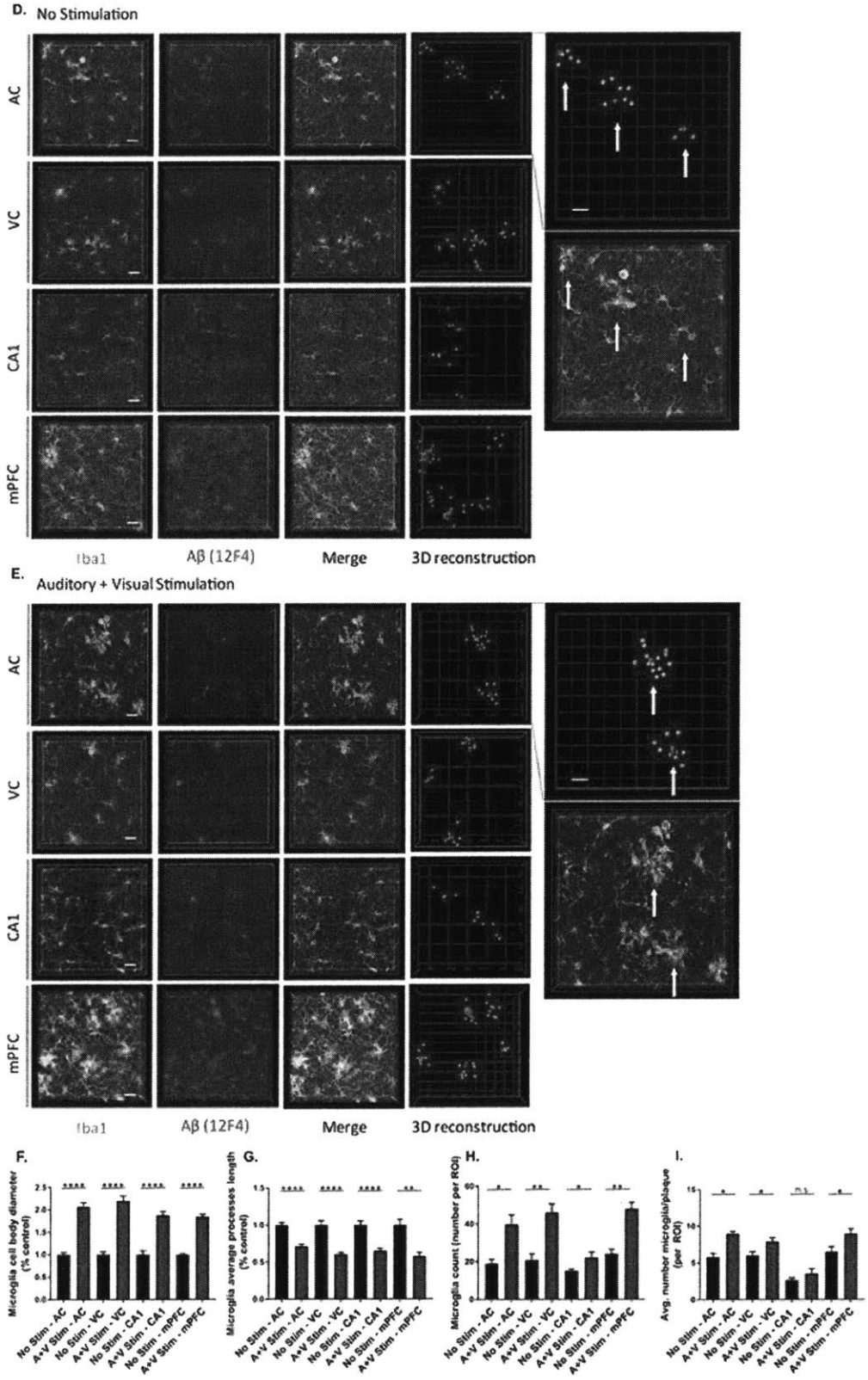
D.
No Stimulation
AC
VC
CA1
mPFC
Iba1
Aβ (12F4)
Merge
3D reconstruction
E.
Auditory + Visual Stimulation
AC
VC
CA1
mPFC
Iba1
Aβ (12F4)
Merge
3D reconstruction
F.
Microglia cell body diameter (% control)
G.
Microglia average processes length (% control)
H.
Microglia count (number per ROI)
I.
Avg. number microglia/plaque (per ROI)
No Stim - AC
A+V Stim - AC
No Stim - VC
A+V Stim - VC
No Stim - CA1
A+V Stim - CA1
No Stim - mPFC
A+V Stim - mPFC

**Figure 6.2 Combined auditory and visual GENUS induces a clustering phenotype response by microglia**

D) Immunohistochemistry and 3D reconstruction using IMARIS (Methods) of anti-Iba1 (019-19741, green) and anti-Aβ (12F4, red) antibodies in AC, VC, CA1, and mPFC of 6-month-old 5XFAD mice after 7 days of 1 hour per day of no stimulation (n=6 mice per group, top inset: example of using IMARIS to quantify the number of microglia surrounding a 25 μm radius around amyloid plaques. Plaques are demonstrated as red dots, microglia as green dots, and white arrows point to clusters. Bottom inset: enlarged merged image from AC. Scale bar, 20 μm). E) As in D for combined GENUS. F) Average microglia cell body diameter in AC, VC, CA1, and mPFC of 6-month-old 5XFAD mice after 7 days of 1 hour per day of no stimulation or combined GENUS (A+V Stim), normalized to no stimulation control (n=6 mice in no control group, n=7 mice in combined GENUS group, mean s.e.m. in bar graphs, ****P<0.0001; unpaired Mann-Whitney test). G) Average microglia process length in AC, VC, CA1, and mPFC of 6-month-old 5XFAD mice after 7 days of 1 hour per day of no stimulation or combined GENUS, normalized to no stimulation control (n=6 mice in no control group, n=7 mice in combined GENUS group, mean s.e.m. in bar graphs, **P<0.01, ****P<0.0001; unpaired Mann-Whitney test). H) Microglia count per region of interest in AC, VC, CA1, and mPFC of 6-month-old 5XFAD mice after 7 days of 1 h per day of no stimulation or combined GENUS (n=6 mice in no control group, n=7 mice in combined GENUS group, mean s.e.m. in bar graphs, *P<0.05, **P<0.01, unpaired Mann-Whitney test). I) Average number of microglia surrounding 25 μm radium of a plaque in AC, VC, CA1, and mPFC following no stimulation or combined GENUS (n=6 mice per group, mean s.e.m. in bar graphs, n.s.= not significant, *P<0.05; unpaired Mann-Whitney test).

## 5.3: Concurrent auditory and visual GENUS, but not auditory or visual alone, reduces amyloid load in the mPFC

Our observation of a microglial response in AC, VC, CA1, and mPFC led us to investigate whether combined GENUS could change amyloid levels in those regions. Immunostaining for Aβ (D54D2) revealed reduced plaque area (AC: 56.34±6.3%; VC: 71.50±6.5%; CA1: 69.73±6.4%) and number (AC: 50.02±3.7%; VC: 50.60±10.9%; CA1: 48.80±11.1%) following combined GENUS, versus no stimulation controls. Combined GENUS uniquely reduced plaque area (59.64±8.7%) and number (48.2±0.07%) in mPFC (**Figure 7A-D**), whereas neither auditory nor visual GENUS alone affected amyloid in mPFC (**Supplement figure 7P-U**). Multi-comparisons between frequencies and between stimuli modalities in the same data set showed that combined GENUS had significant effects in the mPFC when compared to auditory or visual GENUS alone, and summed auditory and visual stimulations (**Supplement Table 1, Supplement figure 7Y and Z**). Amyloid reduction in mPFC is frequency-specific, as we observed no significant differences in amyloid plaque area nor number with 80 Hz A+V or random A+V stimulation (**Figure 7C and D**). We carried out Aβ-ELISA to support our immunostaining results and found that combined GENUS reduced $A\beta_{1\text{-}42}$ levels in AC, HPC, as well as mPFC (soluble $A\beta_{1\text{-}42}$: 59.58±7.2%; insoluble $A\beta_{1\text{-}42}$: 34.17±8.2%) (**Figure 7E and F**) which was not affected by auditory GENUS alone (**Supplement figure 7V and W)**. Additionally, A+V stimulation at 8 Hz and random frequency did not impact $A\beta_{1\text{-}42}$ levels in AC, HPC, and mPFC, compared to no stimulation controls (**Supplement figure 7V and W**). Immunostaining for $A\beta_{1\text{-}42}$ (12F4) showed a unique reduction in amyloid in mPFC after combined GENUS (but not auditory GENUS alone), and no effect of 80 Hz A+V or random frequency A+V stimulation across all three brain regions, compared to their respective no

stimulation controls (**Supplement figure 7X**). In sum, these results demonstrate that combined GENUS uniquely reduces amyloid in mPFC (in contrast to auditory or visual GENUS alone), and that this effect is specific to A+V stimulation at 40 Hz.

Reduced amyloid load in the mPFC suggests that combined GENUS affects broader cortical regions. To determine the overall effect of combined GENUS on amyloid plaque abundance in the whole cortex, we performed whole brain SHIELD processing (**Methods**) in 6-month-old 5XFAD mice following 1-week of combined GENUS and immunostained for amyloid plaques (using D54D2 antibody) (**Figure 7G and H**). Using light sheet microscopy to analyze plaques in 3D, we found a 37% and 34% reduction in total plaque volume and number, respectively, in the neocortex when compared to non-stimulation control (**Figure 7I and J**, example videos showing 3D whole brain SHIELD samples immunostained for plaques following combined GENUS and no stimulation control are provided in **supplementary videos 5 and 6).** Together, these results indicate that combined GENUS significantly reduces amyloid plaque load across the neocortex of the 5XFAD mouse model.

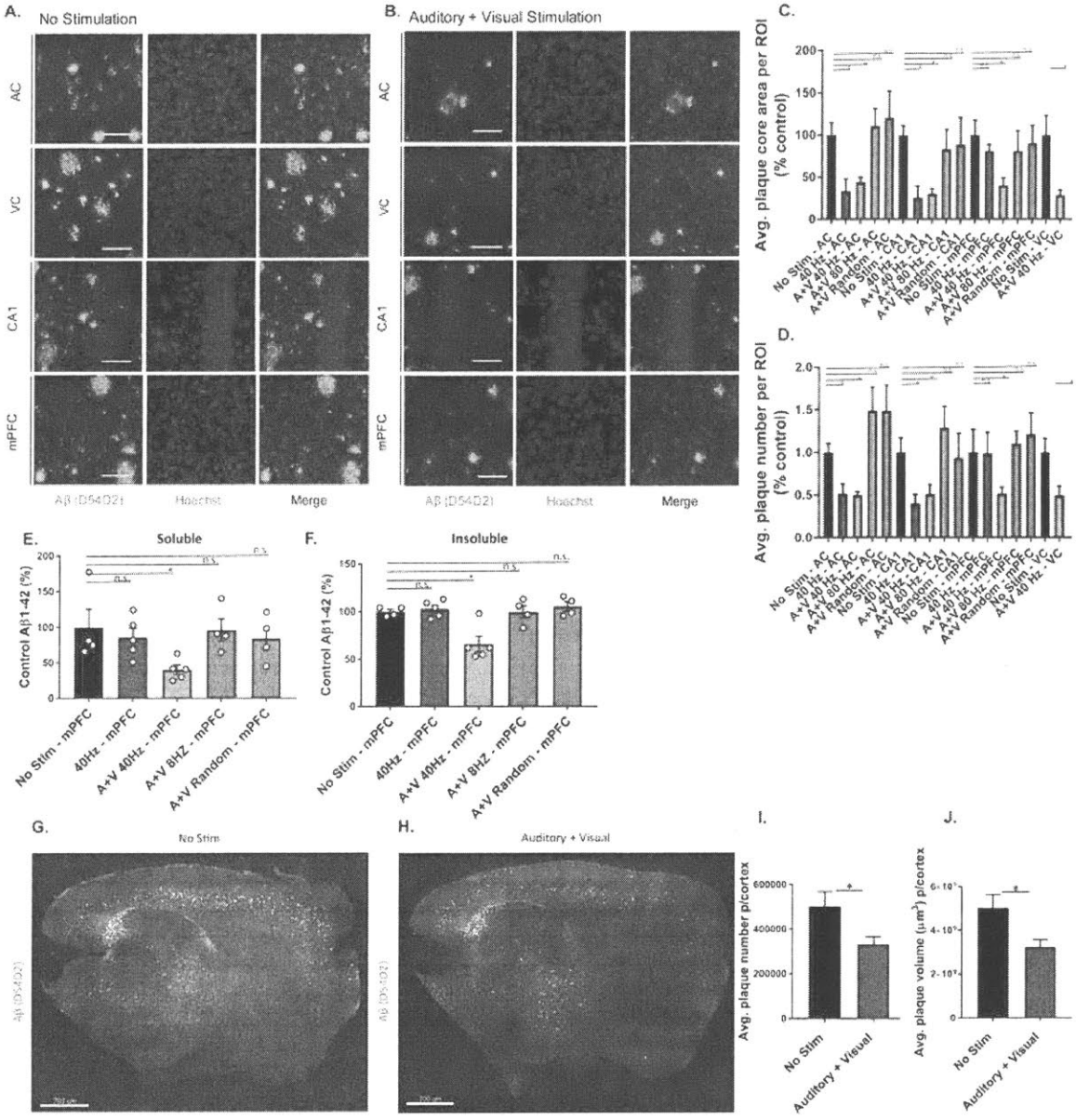
A.
No Stimulation
B.
Auditory + Visual Stimulation
AC
VC
CA1
mPFC
Aβ (D54D2)
Hoechst
Merge
C.
Avg. plaque core area per ROI (% control)
D.
Avg. plaque number per ROI (% control)
No Stim - AC
40 Hz - AC
A+V 40 Hz - AC
A+V 80 Hz - AC
A+V Random - AC
No Stim - CA1
40 Hz - CA1
A+V 40 Hz - CA1
A+V 80 Hz - CA1
A+V Random - CA1
No Stim - mPFC
40 Hz - mPFC
A+V 40 Hz - mPFC
A+V 80 Hz - mPFC
A+V Random - mPFC
No Stim - VC
A+V 40 Hz - VC
E.
Soluble
Control Aβ1-42 (%)
F.
Insoluble
No Stim - mPFC
40Hz - mPFC
A+V 40Hz - mPFC
A+V 8HZ - mPFC
A+V Random - mPFC
G.
No Stim
H.
Auditory + Visual
I.
Avg. plaque number p/cortex
J.
Avg. plaque volume (μm³) p/cortex
No Stim
Auditory + Visual

**Figure 7. Combined auditory and visual GENUS reduces amyloid load in the mPFC and neocortex**

A) Immunohistochemistry of anti-Aβ plaques (D54D2, green) antibodies in AC, VC, CA1, and mPFC of 6-month-old 5XFAD mice after 7 days of 1 hr/day (1-week) no stimulation (40x objective, scale bar, 50 μm). B) As in A for combined GENUS. C) Average plaque core area in AC, CA1, mPFC, and VC in 6-month old 5XFAD mice following 1-week no stimulation, 40 Hz auditory stimulation, combined GENUS, combined 80 Hz, and combined random frequency stimulation, normalized to no stimulation control (n=12 mice/group, *P<0.05, Kruskal-Wallis test with Dunn's multiple comparison test). D) Average plaque number in AC, CA1, mPFC, and VC in 6-month old 5XFAD mice following 1-week no stimulation, 40 Hz auditory stimulation, combined GENUS, combined 80 Hz, and combined random frequency stimulation, normalized to no stimulation control (n=12 mice/group, *P<0.05, Kruskal-Wallis test with Dunn's multiple comparison test). E) Relative soluble Aβ1-42 levels in mPFC of 6-month-old 5XFAD mice following 1-week 40 Hz auditory stimulation, combined GENUS, combined 8 Hz, or combined random frequency stimulation, normalized to non-stimulation control (n=4-5 mice per group, *P<0.05, Kruskal-Wallis test with Dunn's multiple comparison test). F) As in E for insoluble Aβ1-42 (*P<0.05). G) Immunohistochemistry of SHIELD treated whole brain (sagittal plane of 25 μm section of brain) of anti-Aβ plaques (D54D2, white) antibodies of 6-month-old 5XFAD mice after 1-week no stimulation (light-sheet microscope, scale bar, 700 μm). H) As in G for combined GENUS. I) Average cortical plaque number following no stimulation or combined GENUS (n=6 mice/group, *P<0.05; unpaired Mann-Whitney Test). J) Average cortical plaque volume (μm3) following combined GENUS (n=6 mice/group, *P<0.05; unpaired Mann-Whitney Test). Circles indicate 'n', mean +/- s.e.m. in bar graphs unless otherwise noted, n.s. = not significant.

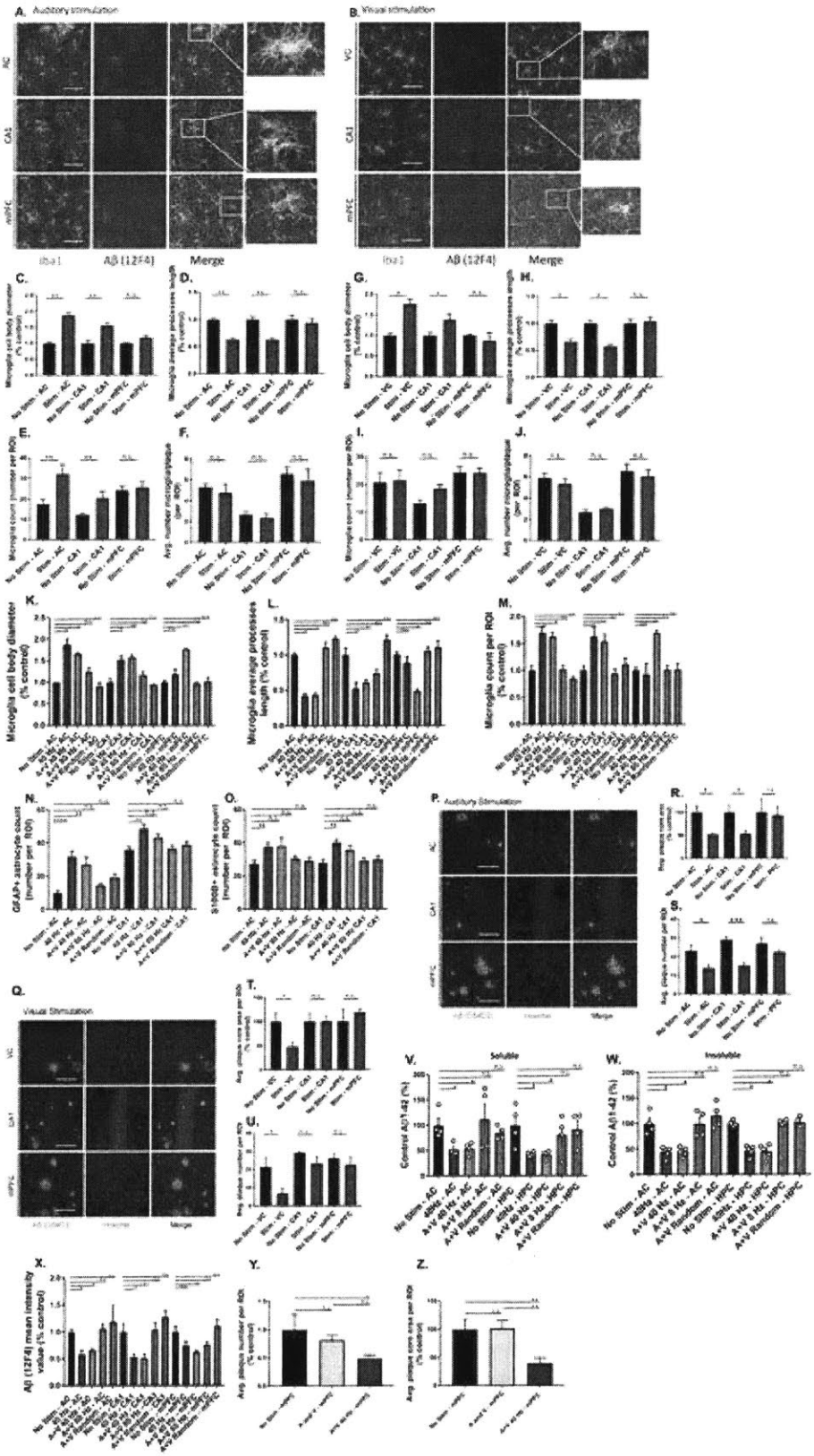

**Supplement Figure 7. 1-week of Auditory or Visual GENUS only do not affect mPFC pathology**

A) Immunohistochemistry of anti-Iba1 (019-19741, green) and anti-Aβ (12F4, red) antibodies in AC, CA1, and mPFC of 6-month-old 5XFAD mice after 7 days of 1 hour per day of auditory GENUS (inset magnification, 100x; scale bar, 50 μm). B) Immunohistochemistry of anti-Iba1 (019-19741, green) and anti-Aβ (12F4, red) antibodies in VC, CA1, and mPFC of 6-month-old 5XFAD mice after 7 days of 1 hour per day of visual GENUS (inset magnification, 100x; scale bar, 50 μm). C) Average microglia cell body diameter in AC, CA1, and mPFC of 6-month-old 5XFAD mice after 7 days of 1 hour per day of auditory GENUS, normalized to no stimulation control (n=6 mice per group, mean s.e.m. in bar graphs, n.s.= not significant, **P<0.01, unpaired Mann-Whitney test). D) Average microglia process length in AC, CA1, and mPFC of 6-month-old 5XFAD mice after 7 days of 1 hour per day of auditory GENUS, normalized to no stimulation control (n=6 mice per group, mean s.e.m. in bar graphs, n.s.= not significant, **P<0.01, unpaired Mann-Whitney test). E) Microglia count per region of interest in AC, CA1, and mPFC of 6-month-old 5XFAD mice after 7 days of 1 hour per day of auditory GENUS (n=6 mice per group, mean s.e.m. in bar graphs, n.s.= not significant, **P<0.01, unpaired Mann-Whitney test). F) Average number of microglia surrounding 25 μm radium of a plaque in AC, CA1, and mPFC following no stimulation or auditory GENUS (n=6 mice per group, mean s.e.m. in bar graphs, n.s.= not significant, unpaired Mann-Whitney test). G) Average microglia cell body diameter in VC, CA1, and mPFC of 6-month-old 5XFAD mice after 7 days of 1 hour per day of visual GENUS, normalized to no stimulation control (n=6 mice per group, mean s.e.m. in bar graphs, n.s.= not significant, *P<0.05; unpaired Mann-Whitney test). H) Average microglia process length in VC, CA1, and mPFC of 6-month-old 5XFAD mice after 7 days of 1 hour per day of visual GENUS, normalized to no stimulation control (n=6 mice per group, mean s.e.m. in bar graphs, n.s.= not significant, *P<0.05; unpaired Mann-Whitney test). I) Microglia count per region of interest in VC, CA1, and mPFC of 6-month-old 5XFAD mice after 7 days of 1 hour per day of visual GENUS (n=6 mice per group, mean s.e.m. in bar graphs, n.s.= not significant, unpaired Mann-Whitney test).

J) Average number of microglia surrounding 25 μm radium of a plaque in VC, CA1, and mPFC following no stimulation or visual GENUS (n=6 mice per group, mean s.e.m. in bar graphs, n.s.= not significant, unpaired Mann-Whitney test). K) Average microglia cell body diameter in AC, CA1, and mPFC of 6-month-old 5XFAD mice following 7 days of 1 hour per day 40 Hz auditory stimulation, combined (A+V) GENUS, combined (A+V) 80 Hz, or combined (A+V) random frequency stimulation, normalized to non-stimulation control (n=6 mice per group, mean s.e.m. in bar graphs, n.s.= not significant, *P<0.05, **P<0.01; unpaired Mann-Whitney test). L) Average microglia process length in AC, CA1, and mPFC of 6-month-old 5XFAD mice following 7 days of 1 hour per day 40 Hz auditory stimulation, combined (A+V) GENUS, combined (A+V) 80 Hz, or combined (A+V) random frequency stimulation, normalized to non-stimulation control (n=6 mice per group, mean s.e.m. in bar graphs, n.s.= not significant, *P<0.05, unpaired Mann-Whitney test).

M) Microglia count per region of interest in AC, CA1, and mPFC of 6-month-old 5XFAD mice following 7 days of 1 hour per day 40 Hz auditory stimulation, combined (A+V) GENUS, combined (A+V) 80 Hz, or combined (A+V) random frequency stimulation, normalized to non-stimulation control (n=6 mice per group, mean s.e.m. in bar graphs, n.s.= not significant, *P<0.05, unpaired Mann-Whitney test). N) Number of GFAP-positive astrocytes in AC and CA1 (n=6 mice per group, mean s.e.m. in bar graphs, n.s.= not significant, **P<0.01, ****P<0.0001; Kruskal-Wallis test with Dunn's multiple comparison test). O) Number of S100B-positive astrocytes in AC and CA1 (n=6 mice per group, mean s.e.m. in bar graphs, n.s.= not significant, **P<0.01; Kruskal-Wallis test with Dunn's multiple comparison test). P) Immunohistochemistry of anti-Aβ plaques (D54D2, green) antibodies in AC, CA1, and mPFC of 6-month-old 5XFAD mice after 7 days of 1 hour per day of auditory GENUS (n=6 mice per group, scale bar, 50 μm). Q) Immunohistochemistry of anti-Aβ plaques (D54D2, green) antibodies in VC, CA1, and mPFC of 6-month-old 5XFAD mice after 7 days of 1 hour per day of visual GENUS (n=6 mice per group, scale bar, 50 μm). R) Average plaque core area per region of interest, normalized to no stimulation control (n=6 per group, mean s.e.m. in bar graphs, n.s.= not significant, *P<0.05, unpaired Mann-Whitney test). S) Average number of plaques in AC, CA1, and mPFC following auditory GENUS normalized to no stimulation control (n=6 per group, mean s.e.m. in bar graphs, n.s.= not significant, *P<0.05, ***P<0.001, unpaired Mann-Whitney test). T) Average plaque core area per region of interest, normalized to no stimulation control (n=6 per group, mean s.e.m. in bar graphs, n.s.= not significant, *P<0.05, unpaired Mann-Whitney test). U) Average number of plaques in VC, CA1, and mPFC following visual GENUS normalized to no stimulation control (n=6 per group, mean s.e.m. in bar graphs, n.s.= not significant, *P<0.05, unpaired Mann-Whitney test). V) Relative soluble Aβ1-42 levels in AC and HPC in 6-month-old 5XFAD mice after 7 days of 1 hour per day no stimulation, 40 Hz auditory stimulation, combined (A+V) GENUS, combined (A+V) 8 Hz, and combined (A+V) random frequency stimulation, normalized to no stimulation control (n=4-5 per group, mean s.e.m. in bar graphs, n.s.= not significant, *P<0.05, Kruskal-Wallis test with Dunn's multiple comparison test). W) Relative insoluble Aβ1-42 levels in AC and HPC in 6-month-old 5XFAD mice after 7 days of 1 hour per day no stimulation, 40 Hz auditory stimulation, combined (A+V) GENUS, combined (A+V) 8 Hz, and combined (A+V) random frequency stimulation, normalized to no stimulation control (n=4-5 per group, mean s.e.m. in bar graphs, n.s.= not significant, *P<0.05, Kruskal-Wallis test with Dunn's multiple comparison test). X) Aβ (12F4) mean intensity value (12F4 antibody) in AC, CA1, and mPFC in 6-month old 5XFAD mice following 7 days of 1 hour per day no stimulation, 40 Hz auditory stimulation, combined (A+V) GENUS, combined (A+V) 80 Hz, and combined (A+V) random frequency stimulation, normalized to no stimulation control (n=4-5 mice per group, mean s.e.m. in bar graphs, n.s.= not significant, *P<0.05, Kruskal-Wallis test with Dunn's multiple comparison test). Y) Average number of plaques in mPFC following combined GENUS, summed auditory and visual alone GENUS, normalized to non-stimulation control (n=6-8 per group, mean s.e.m. in bar graphs, n.s.= not significant, *P<0.05, one-way ANOVA with Tukey's multiple comparison test). Z) Average area of plaques in mPFC following combined GENUS, summed auditory and visual alone GENUS, normalized to non-stimulation control (n=6-8 per group, mean s.e.m. in bar graphs, n.s.= not significant, **P<0.01, one-way ANOVA with Tukey's multiple comparison test).

## Chapter 6: Discussion

In this thesis, we demonstrated the ability to elicit gamma frequency neural activity in AC and CA1 following auditory Gamma ENtrainment Using Sensory stimulus (GENUS). A key finding in our study was the improvement in hippocampal-dependent recognition and spatial memory tasks in 5XFAD mice following auditory GENUS. A significant reduction in amyloid load was also observed alongside a glia and vasculature response in the auditory cortex (AC) and hippocampus (HPC). In addition, we show that combined auditory and visual GENUS prompts a broad microglia-clustering effect and amyloid reduction in multiple brain regions including the mPFC.

### Auditory GENUS modulates neuronal activity in AC, CA1, and mPFC

Prior research has demonstrated the ability of a 40 Hz auditory click-train stimuli to elicit a 40 Hz auditory steady state response (ASSR) in human and animal models (Nakao and Nakazawa, 2014; Presacco et al., 2010). Specifically, EEG studies in humans have shown the ability to evoke a range of response frequencies to auditory click-stimuli, including increases in 40 Hz power following 40 Hz click-trains (Presacco et al., 2010). Similar to visual flicker synchronization, ASSRs are shown to entrain neuronal spiking to the click-train sound with millisecond range precision (Presacco et al., 2010). This is observed in auditory cortex during in vivo electrophysiological recordings in rodents following a range of frequency stimuli using auditory clicks (Nakao and Nakazawa, 2014). AC neurons respond to slow click trains of auditory stimuli with synchronized, phase-locked spiking. However, as these click trains become faster, the effect of the stimulus on the neuronal responses becomes more modulatory, eliciting a smaller change in firing rate relative to the onset of each click (Ma et al., 2013; Rennaker et al. 2007). These

findings are consistent with our results. We find that in AC, we are able to entrain neural activity to stimulus frequency using 20 Hz, 40 Hz, and 80 Hz stimulus frequencies using auditory flicker. While the exact response varies across neurons, we find that for faster flicker frequencies neurons fire in response to a smaller fraction of stimulus tones and they fire at a wider range of phases following the stimulus both of which may be because the stimulus cycle is short. Here we use the term modulation to mean that the entrainment we observe in response to auditory and auditory-visual flicker stimulation is not on-off synchrony to the stimulus, and that single units do not fire in response to every pulse. The vector strengths of the spiking responses of individual neurons to 40 Hz flicker we report are similar to those observed in other studies (Ma et al., 2013).

Additionally, we find that modulation is significantly stronger in response to lower frequencies of stimulation. Modulation of single units during all frequencies of periodic stimulation examined here is significantly higher than no stimulation or random controls and is thus indicative of entrainment. Our results agree with previous literature on neural responses to sensory stimuli in many ways. However, differences may be due to the length of our stimulation paradigm (10s long as opposed to short trains of stimuli, like 500ms), our inclusion of all isolated single units (instead of only units that meet some auditory selective criteria), and inherent bias of circular statistic measures towards narrow unimodal responses.

Furthermore, we show for the first time that trains of 40 Hz auditory tones entrain 40 Hz neural activity in CA1 and mPFC. There is extensive evidence that auditory stimuli can elicit neural responses in mPFC and CA1; neurons in both regions respond to paired auditory stimuli, and CA1 neurons respond to auditory cues in an auditory navigation environment (Aronov et al., 2017; Mears et al., 2006; Miller et al., 1995). However, neural responses to trains of auditory stimuli

have customarily been studied in primary auditory regions. In this study, we find that single neurons in CA1 and mPFC are modulated by 40 Hz trains of auditory tones. The modulation observed in CA1 and mPFC is a small but clear entrainment of firing rate, where neurons fire as a function of stimulus phase although they do not fire in response to every pulse. The vector strengths of the spiking responses of individual neurons to 40 Hz flicker are significantly higher than the spiking responses to random or no stimulation conditions. Sensory inputs reach HPC and mPFC through multiple indirect pathways which likely low-pass filter spiking entrainment; thus, we expect spiking modulation observed in HPC and mPFC to be somewhat weak.

Prior studies show neurons can encode click trains using firing rate without synchronizing to the click train, also called rate coding (Lu et al., 2001; Ma et al., 2003; Wang, 2007). While we were not specifically examining how click train rate is encoded, we found across all neurons recorded that firing rate differences over multiple frequencies were a unimodal distribution around zero. Similarly, we found that firing rate differences between flicker stimulation, random stimulation, and no stimulation conditions were also a unimodal distribution around zero. While some neurons fire at a different rate depending on the frequency of flickering stimuli, the population as a whole did not fire more or less to different frequencies of flicker stimulation. Indeed, mean firing rates did not differ across conditions. Therefore, we conclude that changes in amyloid levels, microglia, and vasculature in response to 40 Hz flicker, but not other frequencies, cannot be explained by overall changes in firing rate.

Due to differences in recording methods, it is difficult to predict exactly how our results showing single neuron spiking modulation by 40 Hz stimulation will translate to other species. Prior work in primates has shown that neurons in auditory cortex are able to entrain to auditory

click trains at frequencies around 40 Hz (Beiser et al. 1995; Lu et al. 2001). Thus, it is reasonable to expect that neural populations in primates could be modulated by 40 Hz auditory stimulation. As such, we would expect neural entrainment at 40 Hz, even if the entrainment is less pronounced than would be expected with stimuli at lower frequencies. Prior studies have reported differences between species in how neurons encode repetitive stimuli, particularly in the proportion of neurons that show synchronization or rate coding. Previous work shows that in primates, smaller numbers of neurons synchronize to high frequency repetitive stimuli than in rats (Lu et al., 2001; Ma et al., 2013).

While these observations are interesting for understanding how neuron encode auditory stimuli, our primary interest lies in driving entrainment of neuronal spiking to flickering stimuli not how neurons encode specific stimulus features. Accordingly, we have shown that our flicker stimulation paradigm results in modulation of the neural population at the stimulus frequency. Exactly how the combination of results described in this study translate to other species will require further studies.

**Auditory GENUS improves cognitive function**

A significant finding from our study was the improvement in hippocampus-dependent cognitive function in spatial and recognition memory tasks following auditory GENUS (**Figure 2**). Deficiencies in spatial and recognition memory have been presented in human AD subjects (Arnold et al., 1991, Seeley et al., 2009, Sperling et al., 2010, Han et al., 2017). We employed widely used behavioral tests, including novel object recognition, location, and the Morris water maze, to examine the effects of auditory GENUS on cognition. Considering our ability to entrain

40 Hz spiking activity in CA1 following auditory GENUS, and the importance of hippocampus function in spatial and recognition memory, our results demonstrate the ability of auditory GENUS to potentially improve network function and therefore cognitive tasks in 5XFAD mice.

The role of gamma rhythms in information processing and its implications in cognition remains, however, an open question. Various groups have proposed gamma oscillations to be a broad and non-specific signal of low-level cortical interactions involving excitation and inhibition, arguing that its low power, conduction delays, and biased spike-related activity make it unsuitable for a role in cognitive functions (Jia et al., 2013, Ray and Maunsell, 2015). In contrast, multiple studies have shown that various cognitive functions, such as working and associative memory tasks, involve enhanced gamma activity (Spellman et al., 2015, Yamamoto et al., 2014). It is hypothesized that one of the functions of enhanced gamma activity is to improve the capacity for information transmission and sensory processing between neuronal systems (Fries et al., 2001, Fries, 2009, Knoblich et al., 2010). It is thus possible that non-invasive GENUS has the ability to enhance gamma activity and improve cognitive abilities in AD and neurodegeneration mouse models.

**Prolonged GENUS elicits specific microglia and vasculature responses**

We show that gamma entrainment via auditory GENUS results in a microglia morphological response indicative of an increased Aβ-uptake state (**Figure 4A and B**). This finding is complementary to a number of reports detailing the receptive nature of microglia to changes in the environment, including the presence of oligomeric amyloid and fibrillar plaque deposits, and their unique position to respond to such changes (Allen and Barres, 2005, Ransohoff and

Perry, 2009, Wang et al., 2015). Indeed, microglia can display a spectrum of responses, ranging from neurotoxic inflammatory immune responses to phagocytic to neuroprotective responses (Heneka et al., 2014, Wolf et al., 2017). We have previously reported the ability to use visual GENUS to induce microglia morphological changes and increase microglia Aβ-uptake in the visual cortex in 5XFAD mice (Iaccarino et al., 2016). In this study, however, we show that auditory GENUS can elicit a microglia response in brain regions downstream from primary sensory cortices. In hippocampal CA1, in addition to AC, we saw microglia with increased cell body size, reduced projection length, and higher number of Iba1-positive cells co-localized with Aβ (**Figure 4C-G**). This data suggests that auditory GENUS induces a morphological response indicative of increased phagocytic response in brain regions downstream from primary sensory cortices.

A surprising physiological response observed in addition to microglia morphology changes was an increase in vascular dilation following auditory GENUS in both AC and CA1 (**Figure 5A-C**). Astrocytes are known to be intermediaries between neuronal activity and microcirculation by bridging neuronal synapses and blood vessels through their extended projections (Filosa and Iddings, 2013). Changes in blood vessel diameter, indicative of a dilation response, are known to be regulated by neuronal activity and astrocyte-mediated interactions (Attwell et al., 2010). Indeed, we detected an increase in GFAP and S100B-positive astrocytes in both AC and CA1 following auditory GENUS (**Figure 4H-K**), which may be one possible reason for our observed increase in blood vessel diameter. However, what could potentially account for the change in astrocyte activation following auditory GENUS? One hypothesis states that changes in microglia activity can potentially influence changes in astrocyte activity, and vice-versa (Lee et al., 2011, Liddelow and Barres, 2017). Additionally, astrocytes express GABA receptors, activation of which

has been shown to cause changes in intracellular calcium transients, potentially eliciting local vasodilatory responses through the production and release of secreted factors (Losi et al., 2014, Bazargani and Attwell, 2016). Because GABA has been shown to be involved in the generation of gamma oscillations, astrocytes are thus likely to be influenced by changes in GENUS. These hypotheses are intriguing because our results show a reduction in GFAP-positive astrocytes in 6-month-old 5XFAD mice when compared to wild-type littermate controls, thus indicating that auditory GENUS may also induce the migration of astrocytes and/or promote astrocyte survival (**Supplement Figure 4G and H**). Delineating further mechanistic insight into how glia increase clearance of extracellular material following GENUS is critical however, and will continue to be investigated.

**Prolonged Auditory GENUS increases amyloid-vasculature associations**

Reduced amyloid levels and changes in blood vessel dilation led us to investigate whether auditory GENUS could affect Aβ interactions with the vasculature. Endothelial cells, which are connected by tight junctions to form the walls of blood vessels, make up part of the blood-brain-barrier (BBB). Selective transport through transcellular routes of the BBB provides major pathways for Aβ to clear from interstitial fluid in the brain into blood circulation for eventual systemic degradation in the liver, kidneys, and spleen (Kyrtsos and Baras, 2015). Low density lipoprotein receptor-related protein 1 (LRP1) has been reported to be involved in Aβ transcytosis through the brain endothelium, with various reports demonstrating LRP1 dysfunction in AD-subjects (Kanekiyo et al., 2013, Storck et al., 2016). Consistent with our hypothesis, we observed increased Aβ-LRP1 co-localization following auditory GENUS, potentially indicating an increase in

Aβ transcytosis and clearance through the vasculature (**Figure 5D-F**), and suggests that decreased Aβ transport across the BBB may contribute to Aβ aggregation and plaque development in the AD brain. Interestingly, Aβ along the vasculature did not completely co-localize with LRP1 but also appeared along the paravascular space surrounding blood vessels, potentially suggesting solute clearance through paravascular drainage along the venous efflux (Iliff et al., 2012). This method of clearance has been implicated as part of the 'glymphatic' pathway as a normal method for brain solute clearance, and has also been shown to be disrupted in AD (Kyrtsos and Baras, 2015). These results, in addition to increased Aβ-uptake via microglia, support our hypothesis that auditory GENUS can potentially increase Aβ clearance through increased Aβ co-localization with the vasculature.

**Prolonged GENUS reduces phosphorylated tau and seeding in P301S mice**

AD is not solely an Aβ aggregation problem; a requisite for the diagnosis of AD in humans is the formation of hyperphosphorylated tau protein aggregates (Hyman et al., 2012). It is hypothesized that phosphorylated tau at specific residues weakens the stability and functionality of microtubule assemblies in neurons, leading to an array of neuronal insults (Lindwall and Cole, 1984, Bramblett et al., 1993) . Moreover, many studies have indicated the accumulation of hyperphosphorylated tau as a greater predictor of cognitive dysfunction in AD subjects (Bancher et al., 1993, Lee et al., 2001, Ballatore et al., 2007). Our results show that auditory GENUS reduces the phosphorylation of specific residues known to be hyperphosphorylated on the tau protein in AD in both AC and whole hippocampus (**Supplement Figure 5A-L**). Moreover, we demonstrated a reduction in tau seeding, a proteopathic activity indicated to be involved in the progression of

tau protein aggregation (Holmes et al., 2014) (**Supplement Figure 5M**). This highlights the ability of auditory GENUS to elicit reductions of more than one pathogenic protein in more than one brain region. These results indicate the potential of GENUS to ameliorate tau-related AD pathology.

**Prolonged Combined GENUS induces microglia clustering effect in AC, CA1, VC, and mPFC**

Our observations following auditory GENUS on microglia morphology and its interactions with amyloid led us to examine whether combining auditory and visual flicker stimulation, or combined GENUS, could result in any changes associated with microglia activation. Following combined GENUS, a unique microglia- Aβ phagocytic clustering effect, illustrated by the increased number of microglia and their encapsulation of amyloid plaques (**Figure 6D, E, I**), was observed in AC and VC when compared to no stimulation control. Coupled with our observed morphological changes in cell body size and process length, this suggests a potential change in the activation state of microglia following combined GENUS (Ransohoff and Cardona, 2010). This hypothesis is supported by accumulating evidence suggesting that microglia are heterogeneous and can display a spectrum of activated states (Walker and Lue, 2015, Mathys et al., 2017). Specifically, a recent study using sub-tissue-focused single-cell RNA sequencing identified a potential protective disease-associated microglia (DAM) type in proximity to Aβ plaques; these microglia were found to have phagocytic pathways upregulated (e.g. increased expression of Lpl, Cst7, and CD9), and concomitant downregulation of homeostatic factors (e.g. P2ry12/P2ry13) (Keren-Shaul et al., 2017). DAM was also shown to positively co-stain for Aβ particles in 5XFAD mice and human AD postmortem brains. This analysis suggests that combined GENUS may

involve the induction of a spectrum of protective microglial states, as demonstrated by the increased uptake of Aβ and morphological similarities to DAM.

Surprisingly, we observed the effect of combined GENUS on microglia response extended to the mPFC (**Figure 6D-I**), whereas auditory or visual stimulation alone did not (**Supplement Figure 7A-M**). Indeed, higher-order association areas, such as the mPFC, have been shown to process multiple sensory stimuli, and include inputs from auditory and visual cortices (Shore et al., 2016, Gilbert and Li, 2013). These observations indicate a robust microglia clustering response in AC, VC, and mPFC following combined GENUS.

**Combined GENUS reduces amyloid throughout the cortex**

Alzheimer's is a complex disease because it has a pathological impact in many brain regions important for a variety of cognitive functions. Thus, treatments with any considerable therapeutic potential would need to affect downstream brain regions other than the primary sensory areas in order to have a systems-wide effect (Canter et al., 2016). Notably, we found that 1-week of auditory GENUS impacts the hippocampus of multiple AD mouse models, including 5XFAD, APP/PS1, and tau P301S mice. This is significant because acute 1 hr visual GENUS was unable to elicit changes in amyloid levels in hippocampus. However, our study showed (**Supplement Figure 7G and H**) that 1-week of visual GENUS did elicit changes in microglia cell body area and projection length. Therefore, prolonged treatment of visual GENUS has the ability to affect multiple higher-order brain areas in AD-mouse models.

The robust microglia clustering effects around amyloid deposits following combined GENUS led us to investigate whether such stimulation could elicit reductions in amyloid as well.

We found that combined GENUS resulted in a significant reduction in amyloid load in the AC, VC, CA1, and mPFC (**Figure 7A-F).** This reduction in the mPFC was not observed following 1-week of auditory or visual GENUS alone (**Supplement Figure 7N-S**). The effects of combined GENUS were striking when we examined amyloid plaques using whole brain SHIELD which showed a reduction in amyloid plaque number and total plaque volume in the whole cortex following combined GENUS when compared to no-stimulation controls (**Figure 7G-J**). Our results demonstrate the ability of combined GENUS to ameliorate AD-like pathology in brain regions spanning a large circuit network, an effect not observed with visual or auditory stimulation alone when stimulated for 1-week **(Supplement Figure 7N-S**).

An important question that remains is why do different 40 Hz sensory stimuli, or combinations thereof, elicit differences in circuit pathology and behavior in 5XFAD mice? Studies have shown that when comparing auditory versus visual cues during appetitive conditioning, mice that have auditory cues perform significantly better at the task than those with visual cues alone (Sanderson et al., 2016). This effect is potentially due to differences in circuit projections between the auditory and visual pathways, where auditory projections to the hippocampus are shorter and more direct than those from visual cortex (Newton et al., 2004; Shore et al., 2016). These results support our findings demonstrating the ability of auditory GENUS to elicit microglia transformation in hippocampus and hippocampus-dependent cognitive effects, whereas visual GENUS requires prolonged stimulation to elicit hippocampal and cognitive changes.

Together, these findings suggest that GENUS elicits circuit-wide effects on microglia activation and the phagocytosis of Aβ, driving the attenuation of AD-related pathology and is correlated with cognitive improvement. Importantly, because our experiments were performed

in AD-mouse models, future studies are essential to determine whether the benefits of GENUS are translatable in humans, especially considering our non-invasive approach.

## Contributions

Anthony J. Martorell, Annabelle C. Singer, Abigail L. Paulson, Emery N. Brown., Edward S. Boyden, Kwanghun Chung, and Li-Huei Tsai designed experiments. Annabelle C. Singer and Abigail L. Paulson performed and analyzed electrophysiology data. Stephanie M. Prince assisted with electrophysiology experiments. Anthony J. Martorell and David Nam-Woo Kim performed and analyzed ELISA experiments. Oleg Kritskiy performed western blots. Anthony J. Martorell performed behavior experiments. David Nam-Woo Kim and Fatema Abdurrob analyzed behavior experiments. Anthony J. Martorell, David Nam-Woo Kim, and Fatema Abdurrob performed and analyzed imaging experiments. Fatema Abdurrob performed and analyzed 3D microglia clustering quantification. Gabi Drummond, Webster Guan, and Vamsi Mangena performed and analyzed whole brain SHIELD experiments. Anthony J. Martorell, David Nam-Woo Kim, and Fatema Abdurrob performed auditory and combined GENUS experiments. Ho-Jun Suk and Annabelle C. Singer engineered auditory and combined GENUS sounds and equipment. Anthony J. Martorell, Annabelle C. Singer, Abigail L. Paulson, Jennie Z. Young, and Li-Huei Tsai wrote the manuscript. All authors read and revised the manuscript.

## Funding Acknowledgments

We are grateful to Hannah Iaccarino, members of the Tsai, Singer, and Boyden laboratories, M. Asaf, H. Meharena, F.X. Peña, S. Barker, K. Vodehnal, E. Demmons, and Y. Zhou for methods development, technical assistance, and comments on the paper. A.C.S. acknowledges the Packard Foundation, Friends and Alumni of Georgia Tech, and the Lane Family. A.L.P. acknowledges the Fulton County Elder Health Science Fellowship and the Wright Family. L.H.T. acknowledges the Robert and Renee Belfer Family Foundation, Halis Family Foundation, the JPB Foundation, and NIH RF1 AG047661. K.C. was supported by Burroughs Wellcome Fund Career Awards at the Scientific Interface, the Searle Scholars Program, Packard award in Science and Engineering, NARSAD Young Investigator Award, JPB Foundation (PIIF and PNDRF), NCSOFT Cultural Foundation, and NIH (1-U01-NS090473-01). Resources that may help enable general users to establish the methodology are freely available online (http://www.chunglabresources.org). A.J.M. was supported by T32 GM007484 Integrative Neuronal Systems, MIT Champions of the Brain Fellowship, and Henry E. Singleton Fellowship. W.G. was supported by the William C. and Margaret H. Rousseau Fellowship. V.M. was supported by the SITA Foundation Fellowship. H-J.S. acknowledges the Samsung Fellowship. E.S.B. acknowledges the MIT Aging Brain Initiative, John Doerr, Edward and Kay Poitras, the HHMI-Simons Fellowship, Open Philanthropy, Charles Hieken, and NIH 1R01EY023173. E.N.B. acknowledges NIH R01-GM104948, DP1-OD003646, and funds from the Department of Anesthesia, Critical Care and Pain Medicine, Massachusetts General Hospital, Boston, Massachusetts.

## Methods

### Experimental Model and Subject Details

### Animals

All animal work was approved by the Committee for Animal Care of the Division of Comparative Medicine at the Massachusetts Institute of Technology and by the Institutional Animal Care and Use Committee at Georgia Institute of Technology. Mice were housed in groups no larger than five on a standard 12-hour light/12-hour dark cycle; all experiments were performed during the light cycle. Electrophysiology experiments were performed at Georgia Institute of Technology, male (1-3 month-old) WT mice (C57Bl/6) were obtained from the Jackson laboratory. Mice were housed on a reverse 12 h light/12 h dark cycle and all experiments were performed during the dark cycle. Food and water were provided without restriction. For all experiments, mice from the same litter were divided into different conditions, respectfully. If additional groups were added, respective controls were always repeated concurrently.

### Method Details

### Surgical procedures

Adult (2-3 month-old) mice were anesthetized with isoflurane and fixed in a stereotaxic frame. Ophthalmic ointment (Puralube Vet Ointment, Dechra) was applied to the eyes, and the scalp was shaved and sterilized with povidone-iodine (Dynarex) and 70% ethanol. A custom stainless steel headplate was fixed using dental cement (C&B Metabond, Parkell) and the target craniotomy site for LFP recordings was marked on the skull (in mm, from bregma: −2.0 anterior/ posterior, +/-1.8 medial/lateral for targeting CA1, −2.0 to -3.0 anterior/ posterior, +/-1.8

medial/lateral for targeting auditory cortex, and +1.3 to +1.4 anterior/posterior, +/- 1.0 medial/lateral for targeting prefrontal cortex). A craniotomy was later performed in 3-8 month-old mice. The day before or day of the first recording session, craniotomies (200-500μm diameter) were made by thinning the skull with a dental drill and then making a hole with a 27-gauge needle. When not recording, the craniotomy was sealed with a sterile silicon elastomer (Kwik-Sil WPI).

**Electrophysiology recordings**

During recordings, head-fixed animals ran on an air-floating 8-inch spherical treadmill. All animals had previously learned to maneuver on the treadmill until they were comfortable while occasionally receiving sweetened condensed milk (1:2 water dilution). Animals were on the ball for a maximum of 5 hours and had multiple periods of running and rest during this time. Single shank 32-channel probes (NeuroNexus) were advanced to the target location. Recording sites spanned 250 μm. For auditory cortex recordings, the probe was advanced at a 45° angle from vertical parallel to the coronal plane to a depth of 3-4.15mm. A series of 50 ms tones of 5, 10, 15, and 20 kHz were presented to detect auditory response in the mean LFP. For CA1 recordings, the probe was advanced vertically through the craniotomy to a depth of 1.14 – 2.05mm until hippocampal pyramidal layer electrophysiology characteristics were observed (large theta waves and sharp wave ripples, 150+ μV spikes on multiple channels). For prefrontal cortex recordings, the probe was advanced at a 20° angle from vertical, at a 49° angle from the coronal plane to a depth of 1.48-2.15mm. If data were collected at multiple depths during the same recording session; new depths were mapped in order to ensure the location of the recording sites remained

in the target location (n = 9 recording depths from 9 sessions in 5 mice for AC and 12 recording depths from 10 sessions in 5 mice for CA1, n = 7 recording depths from 7 sessions in 4 mice for mPFC). Data were acquired with a sampling rate of 20 kHz using an Intan RHD2000 Evaluation System using a ground pellet as reference.

**Auditory and visual stimuli for electrophysiology recordings**

Animals were presented with 10 s stimulation blocks interleaved with 10 s baseline periods. Stimulation blocks rotated between auditory-only or auditory and visual stimulation at 20 Hz, 40 Hz, 80 Hz, or with random stimulation (pulses were delivered with randomized inter-pulse intervals determined from a uniform distribution with an average interval of 25 ms). Stimuli blocks were interleaved to ensure the results observed were not due to changes over time in the neuronal response. 10 s long stimulus blocks were used to reduce the influence of onset effects, and to examine neural responses to prolonged rhythmic stimulation. All auditory pulses were 1 ms-long 10 kHz tones. All visual pulses were 50% duty cycle of the stimulation frequency (25 ms, 12.5 ms, or 6.25 ms in length). For combined stimulation, auditory and visual pulses were aligned to the onset of each pulse.

**Prefrontal cortex histology**

During the final mPFC recording in each animal, the probe was coated with DiI and inserted to target depth. Mice were transcardially perfused with 4% paraformaldehyde in phosphate buffered saline (PBS) under anesthesia (isoflurane), and the brains were post-fixed overnight in 4% paraformaldehyde in 1xPBS. Brains were sectioned 100 μm thick with a Leica VT1000S

vibratome (Leica). Sections were stained with 0.2% 1mMol DAPI in 1xPBS and mounted onto microscopy slides with Vectashield mounting medium. Images were acquired on a Zeiss Axio Observer Z1 inverted epifluorescent microscope with the accompanying Zen Blue 2 software.

**Spike sorting and single unit stability**

Spike detection and sorting was carried out using MountainSort automated spike sorting followed by manual curation based on visual inspection of waveforms and cross-correlograms (Chung et al., 2017). Prior to manual curation, quality thresholds were applied to only include units with peak SNR greater than or equal to 1, less than 10% overlap with noise, and greater than 95% isolation against other units which resulted in well-isolated single units. To account for periods of instability in the recordings during which single units were lost, stability criteria were applied such that only stable periods (no sudden loss of a single unit's firing rate) would be considered in analysis. Firing rate (FR) for each unit was computed over the course of the recording session. Firing rate was clustered into two distributions, low FR and high FR, using k-means clustering. For units with FR that dropped below 10% of the high FR mean, further analyses identified a stable recording period defined as the longest length of time that the FR was 2 standard deviations above the low FR mean.

**LFP**

LFP was obtained by downsampling raw traces to 2kHz and bandpass filtering between 1-300Hz.

**Power spectrum**

Power spectral density analysis was performed using multitaper methods from the Chronux toolbox (time-bandwidth product = 3, number of tapers = 5). LFP traces were divided into 10s trials of each stimulation condition. The average power spectral density was computed for each animal (within the same recording day and recording depth) over these trials, referencing to a ground pellet in saline above the skull. Power spectral density analysis was initially computed for all recording sites in AC, CA1, and mPFC. From each recording depth, the traces with the largest 40 Hz peak in response to 40 Hz flicker stimuli were included in the analysis. The per-depth traces displayed in the presented data had the largest 40 Hz peak in response to auditory flicker stimuli.

**Firing during flicker stimulation**

The single unit peri-stimulus time histograms (PSTH) for each stimulus frequency encompassed two stimulus cycles (where one cycle = $\frac{1}{stimulus\ frequency}$ sec), with 10 bins per cycle, to show spiking across trains of stimuli. Displaying spiking modulation over multiple cycles is typical for displaying modulation by oscillations (Csicsvari et al., 1999). PSTHs were computed for all single units by binning spikes for 1 stimulus cycles before and after the start of each light-on or audio-on pulse. No stimulation (baseline) histograms were calculated using randomly distributed pulse times, as in the random stimulation condition. Firing rate was computed in each bin by dividing the number of spikes per bin by the total time in that bin (the total number of pulses times the bin size). To quantify firing rate periodicity in relation to the stimulus frequency, the time interval between firing rate peaks was calculated for all single unit histograms. The peaks of each PSTH was the maximum firing rate within one stimulus interval. To quantify firing rate modulation by the stimulus and compute circular statistics, peri-stimulus spike times were converted into

radians: $(peri - stimulus\ spike\ time) * 2\pi * (stimulus\ frequency)$ and vector strengths and Rayleigh statistics were computed. Vector strength was computed using methods from the CircStat toolbox; the Rayleigh statistic was computed using the equation $RS = 2nVS^2$, where *n* is total spike count, and *VS* is vector strength (Berens, 2009), Ma et al. 2013). Differences in vector strength and Rayleigh statistic values were computed by taking the differences in these values between stimulus conditions for each unit. Heat maps showing the firing rate response to flicker for all recorded single units were computed over four consecutive stimulus cycles. In order to show the response of all neurons, we show four consecutive stimulus cycles of each stimulation period. To do this, we aligned the 10s presentation periods of each stimulus condition, and then excluded the first 100ms of each presentation period to prevent onset effects from obscuring entrainment. Then, we averaged spiking response over the next four stimulus cycles (200 ms for 20 Hz, 100 ms for 40 Hz, and 50 ms for 80 Hz) to obtain the firing rate response to flicker. Firing rate for each single unit was computed in 1ms bins, smoothed with a gaussian windows proportional to each stimulus frequency (N = $\frac{1}{Stimulus\ frequency}$ sec, $\alpha = 3$), and z-scored. Neurons were aligned by their average stimulus phase preference in the analyzed four cycles.

**Mean Firing Rate**

Mean firing rate was computed for each single unit for each stimulus condition. Only stable periods for each unit contributed to the mean FR calculation (see **Spike sorting and single unit stability**, above). Difference in mean firing rate between stimulus conditions was computed within each unit by taking the difference in mean FR in each condition for that unit.

**40 Hz visual flicker stimulation protocol**

For biochemical and Immunohistochemical analysis, 5XFAD mice were placed in a dark chamber illuminated by a light-emitting diode (LED) bulb and were exposed to one of four stimulation conditions: dark, 8 Hz, 40 Hz (12.5 ms light on, 12.5 ms light off, 60 W), or random (light pulses were delivered with a random interval determined by a uniform distribution with a mean of 25 ms) stimulation for 1-hour for seven days.

**40 Hz auditory tone train stimulation protocol**

For biochemical, Immunohistochemical, or behavioral analysis, 5XFAD, APP/PS1, or P301S mice were placed in a dimly lit chamber in a quiet room insulated with sound-proof foam (McMaster-Carr, 5692T49). Speakers (AYL, AC-48073) were placed out-of-reach from the mouse above the chambers. Mice were exposed to one of five stimulation conditions: no tones, tones at 8 Hz, tones at 40 Hz, tones at 80 Hz, or tone delivered at random (auditory tones were delivered with a random interval determined by a uniform distribution with a mean of 25ms) stimulation. Tones for the stimulation conditions consisted of a 10 kHz tone that was 1 ms in duration and delivered at 60 dB. For electrophysiology recordings, after probe placement, the lights in the room were turned off and the animals were presented with alternating 10 s periods of audio-only and visual-audio stimulation interleaved with 10 s periods of no light or tones. For audio-only stimulation, a 10 kHz tone was played at 40 Hz with a 4% duty cycle. For visual-audio stimulation, the audio stimulation was accompanied with surrounding light flickered at 40 Hz for 10 s periods with a 50% duty cycle. Stimuli were presented in this manner for 20 min sessions, with 1-10 min pauses in between sessions to check on the animals' behavior.

**Concurrent 40 Hz auditory and visual stimulation protocol**

For biochemical, Immunohistochemical, or behavioral analysis, 5XFAD mice were placed in a dark chamber illuminated by an LED bulb and exposed to an auditory tone train, simultaneously. Mice were exposed to one of four stimulations: dark/quiet, 40 Hz light flicker, 40 Hz auditory tone train, concurrent 40 Hz light flicker and auditory tone, or random light flicker/tone stimulations.

**Immunohistochemistry**

Mice were transcardially perfused with 4% paraformaldehyde in phosphate buffered saline (PBS) under anesthesia (2:1 of ketamine/xylazine), and the brains were post-fixed overnight in 4% paraformaldehyde in PBS. Brains were sectioned 40 μm thick with a Leica VT1000S vibratome (Leica). Sections were permeabilized and blocked in PBS with 0.3% Triton X-100 and 10% donkey serum at room temperature for 2-hours. Sections were incubated overnight at 4°C in primary antibody containing PBS with 0.3% Triton X-100 and 10% donkey serum. Primary antibodies were: anti-β -amyloid (Cell Signaling Technology; D54D2), anti-Iba1 (Wako Chemicals; 019-19741), anti-glial fibrillary acidic protein (GFAP)(Abcam; ab4674), anti-S100B (Abcam; ab868), anti-LRP1 (Abcam; 28320), DyLight 488 labeled Lycopersicon Esculentum (tomato) lectin (Vector laboratories; DL-1174), anti-amyloid oligomer (Millipore Sigma; AB9234), anti-phospho-tau (Ser396) (Cell Signaling Technology; 9632), anti-phospho-tau (Thr181) (Cell Signaling Technology, 12885), Hoechst 33342 (Thermo Fisher Scientific; H3570). The anti-Aβ antibody 12F4 was used because it does not react with APP, allowing us to determine whether our labelling was specific to Aβ, as well as allowing for co-labelling with Iba1. Anti-amyloid oligomer antibody AB9234 was

used for co-labelling with LRP1. The following day, brain sections were incubated with fluorescently conjugated secondary antibodies (Jackson ImmunoResearch) for 2 hours at room temperature, and nuclei were stained with Hoechst 33342 (Invitrogen). Images were acquired using a confocal microscope (LSM 710; Zeiss) with a 40× objective at identical settings for all conditions. Images were quantified using ImageJ 1.42q by an experimenter blind to treatment groups. For each experimental condition, two coronal sections from each animal were used for quantification. Scale bars are 50 μm unless otherwise noted in figure legends. ImageJ was used to measure the diameter of Iba1+ cell bodies and to trace the processes for length measurement. In addition, the Coloc2 plugin was used to measure co-localization of Iba1 and Aβ. Microglia processes arborization was quantified using Imarisx64 8.1.2 (Bitplane, Zurich, Switzerland). The 'analyze particles' function in ImageJ was used for counting plaque number and area, deposits of at least 10 μm were included and a set threshold was used for both control and experimental groups.

**Vasculature- Aβ colocalization analysis**

ImarisColoc module was used to quantify colocalzation of signal between two separate source channels (i.e. Lectin and AB, Lectin and LRP1) in 3D. These source channels were thresholded to mask any intensity coming from noise or background signal. ImarisColoc then generates a new channel containing only voxels that colocalize within the thresholds set for the source channels, and presents the associated statistical analyses.

**Microglia-Aβ clustering analysis**

IMARIS was used to analyze the microglial clustering pattern around amyloid plaques in 40uM slices. The surfaces module was utilized to detect and 3D render plaques (red) based on 12F4 signal. Iba1-positive microglia were then counted using the spots module, placing a sphere at the soma of each cell (green). Finally, the Spots Close To Surface XTension was run to find the subset of spots that are closer to the surface objects than the defined 25uM threshold, and exclusion of spots that fall outside this range. The algorithm measures the distance from the center of the spot to the nearest point of the surface object in 3D space, allowing for the quantification of microglial aggregation near plaques.

**CLARITY immunostaining in brain slices**

Mice were perfused with ice-cold PBS (1X) followed by ice-cold 4% PFA, 1% glutaraldehyde in 1xPBS. Brains were dissected out and post-fixed in 4% PFA/1% glutaraldehyde solution for 72 hours at 4°C. Fixation was terminated by incubating brains in inactivation solution (4% acrylamide, 1 M glycine, 0.1% triton-X100 in 1X PBS) for 48 hours at RT. After washing in 1xPBS, brains were sliced into 100uM coronal sections on a vibratome (Leica VT100S) in 1xPBS. Sections containing regions of interest (i.e. auditory cortex and hippocampus) were selected, with reference to the Allen Mouse Brain Atlas, and incubated in clearing buffer (pH 8.5-9.0, 200mM sodium dodecylsulfate, 20mM lithium hydroxide monohydrate, 4mM boric acid in ddH2O) for 2-4 hours, shaking at 55°C. Cleared sections were washed 3 x15mins in 1xPBST (0.1% Triton-X100/1XPBS) and put into blocking solution (2% bovine serum albumin/1xPBST) overnight at RT. Subsequently, three 1hour washes in 1x PBST were performed, shaking at RT. Sections were incubated in weak binding buffer (pH 8.5-9.0, 37.75 mM Na2HPO4, 3.53 mM KH2PO4, 0.02%

sodium azide in PBST) for 1 hour at RT, then transferred to primary antibody, diluted to 1:100 in 1x weak binding buffer for 12 hours at 37°C. Reversal buffer (pH 7.4, 37.75 mM Na2HPO4, 3.53 mM KH2PO4 in 0.02% sodium azide in PBST) is then added in even hourly aliquots over 6 hours, to equal the volume of primary antibody solution plus the volume of the tissue. Another set of 3x1 hour washes in 1xPBST was conducted before sections were incubated for 12 hours at RT, in a mixture of Hoechst 33258 (1:250) (Sigma-Aldrich, 94403) and secondary antibody (1:100) in 1xPBS. Sections were then washed overnight in 1xPBS and incubated in RIMS (Refractive Index Matching Solution: 75g Histodenz, 20mL 0.1M phosphate buffer, 60mL ddH2O) for 1 hour at RT prior to mounting. Brain sections were mounted onto microscopy slides with coverslips (VWR VistaVision, VWR International, LLC, Radnor, PA) in RIMS.

Images were acquired on a Zeiss LSM 880 microscope with the accompanying Zen Black 2.1 software (Carl Zeiss Microscopy, Jena, Germany). Z-stack images were taken with a step size of 0.4-0.5 µm, pixel dwell 4.1 ms, averaging of 2, resolution 1024x1024 suitable for 3D reconstruction. Imarisx64 8.3.1 (Bitplane, Zurich, Switzerland) was used for 3-D rendering and analysis.

**Whole mouse brain processing and clearing**

5XFAD mouse brains were processed according to the SHIELD protocol (Park et al., 2018). Briefly, 5XFAD mice were transcardially perfused with ice-cold PBS followed by 20 mLs of SHIELD-OFF solution containing 4% PFA. Brains were dissected and post-fixed in the same solution for 24 hours at 4°C. Brains were then incubated overnight in SHIELD-OFF solution without PFA at 4°C. Brains were then incubated in the SHIELD-ON solution for 24 hours at 37°C. Following fixation,

brains were incubated in an aqueous clearing solution containing 200mM sodium doedecyl sulfate (SDS), 20mM lithium hydroxide monohydrate, 40mM boric acid, pH 8.5-9.0. Brains were then cleared using SmartClear Pro (LifeCanvas Technologies, Cambridge, MA) based on stochastic electrotransport (Kim et al., 2015) for several days, until transparent.

**Immunostaining of cleared whole hemispheres**

Cleared hemispheres were stained with 15ul of beta-amyloid antibody conjugated with Alexa Fluor-488 (CST, #51374) over 2 days, using a eTANGO, a modified stochastic electrotransport method (Kim et al., PNAS, 2015).

**Light-sheet microscopy**

Immunostained samples were incubated with hProtos (3g diatrizoic acid, 5g N-methyl-d-gludamine, 125g iohexol in 105ml DI-water) for optical clearing and then mounted to acrylic holder using 2% low-temperature melting agarose in hProtos. Custom-made light-sheet microscope equipped with 10× CLARITY-optimized objective was used to image whole hemispheres using the 488 channel for beta-amyloid visualization and the 647 channel for autofluorescence.

**Cleared whole brain image processing, plaque detection, and atlas alignment**

Acquired image data were illumination corrected using CIDRE, an open-source software package implemented in Matlab, and the resulting processed images were stitched together using Terastitcher. Imaris (Bitplane, http://www.bitplane.com/imaris/imaris) was used for 3D

visualizations, and ImageJ (NIH, http://imagej.nih.gov/ij/) was used to create representative slice-by-slice 2D visualizations. Automated plaque detection was performed using a combination of the open-source ClearMap software, a custom cell classification neural network model, and Elastix. Candidate plaques were located as "spots" with ClearMap's spot detection module. First, background subtraction was done slice-by-slice by using a grey-scale morphological top-hat transformation with a disk structure element with major and minor diameter pixel sizes of (21,21). Next, local maxima of the data are detected by applying a 3D maxima filter with disk structure element of size (7,7,4), and these local maxima are filtered with an intensity threshold of 100. The pixel volumes corresponding to each spot center location are also computed using a 3D watershed transform with spot centers as seed points. All candidate plaques with volume less than a sphere with 10-micron diameter were then filtered out. True plaques were identified from the candidate plaques using a convolutional neural network (CNN) model as a categorical plaque / non-plaque classifier implemented in Keras (https://keras.io/) with a Theano backend (https://github.com/Theano/Theano). The CNN input is a 32-by-32 pixel bounding box centered at a candidate plaque center, and the output is a two element one-hot vector representing the plaque and non-plaque categories. The architecture consists of 12 total convolutional layers, each with a rectified linear unit (ReLU) activation and followed by batch normalization: 3 with 64 2x2 kernels, 3 with 128 2x2 kernels, followed by 3 with 192 2x2 kernels, 1 with 256 2x2 kernels, 1 with 256 1x1 kernels, and 1 with 2 1x1 kernels. 2x2 subsampling is done after the third, sixth, and ninth convolutional layer, and Dropout with a rate of 0.5 is applied after the last nine convolutional/batch normalization layers for regularization. After the final convolutional layer, global average pooling followed by softmax activation is applied to generate the final categorical

vector. During training, a categorical cross entropy loss was used with the Adam optimizer with default parameters. The CNN was trained for 400 epochs with batch size of 64 on ~10,000 manual plaque annotations augmented with random rotations, shears, and reflections using the Keras Image Data Generator. The resulting model was then used to classify plaques from detected spots for all samples. To perform atlas alignment, autofluorescence channel images were first downsampled to the atlas resolution, and then Elastix was used to calculate affine and B-spline transformation parameters to do 3D image registration, with the resampled autofluorescence image as the fixed image and the atlas as moving image. The resulting alignment parameters were applied on the plaque locations (output from the CNN model) to transform the plaques into the atlas space, after which a CSV file with plaque count and volume information for each brain region (segmentation according to the Allen Brain Atlas) is generated.

**Western blot**

Hippocampus and auditory cortex from 6-month-old tau P301S mice were dissected and homogenized in RIPA buffer (50 mM Tris, pH 8.0, 150 mM NaCl, 1% NP-40, 0.5% sodium deoxycholate, 0.1% SDS) containing protease and phosphatase inhibitors. Lysates were incubated on ice for 15 min and spun at 12,000 RPM for 15 minutes. Then, supernatants were transferred to fresh tubes and analyzed for protein concentration (Bio-Rad Protein Assay). Equal amounts of protein (20 ug/lane) was resolved on a SDS-polyacrylamide gel and blotted onto a PVDF membrane. This membrane was incubated in blocking buffer containting 20 mM Tris-HCl (pH 7.4), 150 mM NaCl, and 0.1% (v/v) Tween 20 (TBS-T) plus 5% dry milk (m/v) for 1 h at room temperature followed by incubation overnight at 4 °C in primary antibodies and then secondary

antibodies at room temperature for 1 hour. Primary antibodies were anti-phospho-tau (Ser396) and anti-phospho-tau (Thr181). Secondary antibodies were LI-COR IRDye secondary antibodies. Signal intensities were quantified using ImageJ 1.46a and normalized to values of total tau Tau5 (Thermo Fisher Scientific; AHB0042).

**Tau seeding activity assay**

2-month old tau P301S brain sections were homogenized in 1× TBS supplemented with protease inhibitors (Roche complete mini tablets) using a probe sonicator (30% power; 15 pulses). After sonication, the lysates were centrifuged at 14,000 × g for 15 min to eliminate large, insoluble material. The supernatant was stored at −80°C and used for all future experiments. Protein concentration was determined using a Bio-Rad Protein Assay Dye. Fluorescence resonance energy transfer (FRET) biosensor cell lines described previously (Holmes et al., 2014) were provided by Marc I. Diamond. Cells were grown in DMEM (Invitrogen) augmented with 10% FBS and 1× penicillin/streptomycin and maintained at 37°C and 5% CO2 in a humidified incubator. For the assay, cells were plated in a 96-well plate at a density of 40,000 cells/well. Sixteen hours later, at 50% confluence, brain homogenate samples were transduced into cells using 1.2 µl Lipofectamine/well. After a 24 h incubation at 37°C, cells were harvested with 0.25% trypsin, fixed in 2% PFA (Electron Microscopy Services) for 15 min, and then resuspended in PBS. An LSR II HST-2 flow cytometer was used to measure the FRET signal within each cell. FRET quantification was accomplished using FlowJo version 10 software (TreeStar). Integrated FRET density was

derived by multiplying the percentage of FRET-positive cells in each sample by the median FRET intensity of those cells.

**ELISA**

Primary auditory cortices, medial prefrontal cortices, and hippocampi were isolated from 6-month-old 5XFAD males and subjected to Aβ measurement using $A\beta_{42}$ or $A\beta_{40}$ ELISA kits (Invitrogen) according to the manufacturer's instructions. Insoluble Aβ was treated with 5M guanidine/50 mM Tris HCL (pH 8.0) buffer before ELISA measurement.

**Behavioral Experiments**

**Novel Object Recognition**

The novel object recognition (NOR) task consisted of a habituation phase followed by training and testing performed the following day, as previously described (Leger et al., 2013). 24 hours before training, mice were habituated to an open testing arena (40 cm L x 40 cm W x 35 cm H) for 5 min, during which total distance (cm), time in the center (s), and velocity (cm/s) were calculated (TSE Systems). During training, mice were placed into the same box with two identical objects placed in opposite corners. Mice were allowed a total of 20 seconds of object interaction time (within a maximum time frame of 10 minutes), and then immediately removed from the arena. Object memory was tested 1 hr later using the same procedure during training, except one object was replaced with a novel one in its place. Object exploration was recorded when the snout contacted either object and was calculated by a recognition index, $RI=T_{novel}/(T_{novel}+T_{familiar})$, where $T_{novel}$ and $T_{familiar}$ indicate the time spent with the novel and familiar object, respectively.

**Novel Object Location**

The novel location recognition (NOL) task was performed using the same procedure as the object recognition task, except two identical objects were used for both training and testing, and one object was displaced to a novel location during testing.

**Morris Water Maze Test**

Spatial reference memory testing was performed in a circular tank (diameter, 1.2m) filled with white opaque water at approximately 22°C. Reference cues consisting of different colors and shapes were placed along the walls surrounding the tank. Within the tank was a fixed platform (diameter, 10cm) located in a target quadrant. During testing, the platform was submerged and the mice were placed into the tank at one of seven points randomly facing the wall of the tank. Mice were provided 60 s to search for the platform, which if not found, were gently guided to it. Animals were kept on the platform for 15 s. Two trials a day were conducted with a 1 hour intertrial interval. Between the trails, mice were gently padded dry and warmed on a heating pad. Mouse behavior was video-recorded using TSE Systems. The escape latency, or the time it took for the mouse to reach the platform, was scored for each trial and averaged per testing day. On day 6, the platform was removed and a memory test (probe test) was performed. The time spent in each of the 4 quadrants and the number of crossing of the area where the platform used to be was recorded. Swimming velocity was recorded automatically.

**Quantification and Statistical Analysis**

**Statistical analysis**

Statistical significance between two groups for non-electrophysiology experiments was calculated by two-tailed unpaired Mann-Whitney test. Significance between three groups or more was calculated by Kruskal-Wallis test with Dunn's multiple comparisons test. Prism 7 software was used to calculate the values. For electrophysiology data, differences between two stimulus conditions were assessed using non-parametric, two-sample Kolmogorov-Smirnov goodness of fit tests to compare circular statistic value distributions or using z-Test for two proportions to compare proportions. The significance of difference distributions was assessed using two-sided Wilcoxon signed rank test for zero median (e.g. differences in firing rates between stimulus conditions). Multiple comparisons were controlled for using the Bonferroni correction. Significance values are $p < 0.05$ (*), $p < 0.01$ (**), and $p < 0.001$ (***) unless otherwise specified. Specific statistical parameters are detailed in the figure legends.

## References


ALLEN, N. J. & BARRES, B. A. 2005. Signaling between glia and neurons: focus on synaptic plasticity. *Curr Opin Neurobiol,* 15**,** 542-8.

ARNOLD, S. E., HYMAN, B. T., FLORY, J., DAMASIO, A. R. & VAN HOESEN, G. W. 1991. The topographical and neuroanatomical distribution of neurofibrillary tangles and neuritic plaques in the cerebral cortex of patients with Alzheimer's disease. *Cereb Cortex,* 1**,** 103-16.

Aronov, D., Nevers, R., and Tank, D.W. (2017). Mapping of a non-spatial dimension by the hippocampal-entorhinal circuit. Nature*543*, 719-722.

BALLATORE, C., LEE, V. M. & TROJANOWSKI, J. Q. 2007. Tau-mediated neurodegeneration in Alzheimer's disease and related disorders. *Nat Rev Neurosci,* 8**,** 663-72.

BANCHER, C., BRAAK, H., FISCHER, P. & JELLINGER, K. A. 1993. Neuropathological staging of Alzheimer lesions and intellectual status in Alzheimer's and Parkinson's disease patients. *Neurosci Lett,* 162**,** 179-82.

BAZARGANI, N. & ATTWELL, D. 2016. Astrocyte calcium signaling: the third wave. *Nat Neurosci,* 19**,** 182-9.

Berens, P. (2009). CircStat: A MATLAB Toolbox for Circular Statistics. Journal of Statistical Software *Vol 31*, 1-21.

BERO, A. W., YAN, P., ROH, J. H., CIRRITO, J. R., STEWART, F. R., RAICHLE, M. E., LEE, J. M. & HOLTZMAN, D. M. 2011. Neuronal activity regulates the regional vulnerability to amyloid-β deposition. *Nat Neurosci,* 14**,** 750-6.

BRAMBLETT, G. T., GOEDERT, M., JAKES, R., MERRICK, S. E., TROJANOWSKI, J. Q. & LEE, V. M. 1993. Abnormal tau phosphorylation at Ser396 in Alzheimer's disease recapitulates development and contributes to reduced microtubule binding. *Neuron,* 10**,** 1089-99.

CANTER, R. G., PENNEY, J. & TSAI, L. H. 2016. The road to restoring neural circuits for the treatment of Alzheimer's disease. *Nature,* 539**,** 187-196.

CARDIN, J. A., CARLÉN, M., MELETIS, K., KNOBLICH, U., ZHANG, F., DEISSEROTH, K., TSAI, L. H. & MOORE, C. I. 2009. Driving fast-spiking cells induces gamma rhythm and controls sensory responses. *Nature,* 459, 663-7.

Chung, J.E., Magland, J.F., Barnett, A.H., Tolosa, V.M., Tooker, A.C., Lee, K.Y., Shah, K.G., Felix, S.H., Frank, L.M., and Greengard, L.F. (2017). A Fully Automated Approach to Spike Sorting. Neuron *95*, 1381-1394.e1386.

Chung, W.S., Allen, N.J., and Eroglu, C. (2015). Astrocytes Control Synapse Formation, Function, and Elimination. Cold Spring Harb Perspect Biol *7*, a020370.

CIRRITO, J. R., YAMADA, K. A., FINN, M. B., SLOVITER, R. S., BALES, K. R., MAY, P. C., SCHOEPP, D. D., PAUL, S. M., MENNERICK, S. & HOLTZMAN, D. M. 2005. Synaptic activity regulates interstitial fluid amyloid-beta levels in vivo. *Neuron,* 48, 913-22.

Csicsvari, J., Hirase, H., Czurkó, A., Mamiya, A., and Buzsáki, G. (1999). Oscillatory coupling of hippocampal pyramidal cells and interneurons in the behaving Rat. J Neurosci *19*, 274-287.

DAVIES, D. S., MA, J., JEGATHEES, T. & GOLDSBURY, C. 2016. Microglia show altered morphology and reduced arborization in human brain during aging and Alzheimer's disease. *Brain Pathol.*

ENG, L. F., VANDERHAEGHEN, J. J., BIGNAMI, A. & GERSTL, B. 1971. An acidic protein isolated from fibrous astrocytes. *Brain Res,* 28, 351-4.

EUSTON, D. R., GRUBER, A. J. & MCNAUGHTON, B. L. 2012. The role of medial prefrontal cortex in memory and decision making. *Neuron,* 76, 1057-70.

Filosa, J.A., and Iddings, J.A. (2013). Astrocyte regulation of cerebral vascular tone. Am J Physiol Heart Circ Physiol *305*, H609-619.

FRIES, P. 2009. Neuronal gamma-band synchronization as a fundamental process in cortical computation. *Annu Rev Neurosci,* 32, 209-24.

FRIES, P., REYNOLDS, J. H., RORIE, A. E. & DESIMONE, R. 2001. Modulation of oscillatory neuronal synchronization by selective visual attention. *Science,* 291, 1560-3.

GILBERT, C. D. & LI, W. 2013. Top-down influences on visual processing. *Nat Rev Neurosci,* 14, 350-63.

GILLESPIE, A. K., JONES, E. A., LIN, Y. H., KARLSSON, M. P., KAY, K., YOON, S. Y., TONG, L. M., NOVA, P., CARR, J. S., FRANK, L. M. & HUANG, Y. 2016. Apolipoprotein E4 Causes Age-Dependent Disruption of Slow Gamma Oscillations during Hippocampal Sharp-Wave Ripples. *Neuron,* 90, 740-51.

GRUNDKE-IQBAL, I., IQBAL, K., TUNG, Y. C., QUINLAN, M., WISNIEWSKI, H. M. & BINDER, L. I. 1986. Abnormal phosphorylation of the microtubule-associated protein tau (tau) in Alzheimer cytoskeletal pathology. *Proc Natl Acad Sci U S A,* 83, 4913-7.

HAN, Y., WANG, K., JIA, J. & WU, W. 2017. Changes of EEG Spectra and Functional Connectivity during an Object-Location Memory Task in Alzheimer's Disease. *Front Behav Neurosci,* 11, 107.

HARDY, J. A. & HIGGINS, G. A. 1992. Alzheimer's disease: the amyloid cascade hypothesis. *Science,* 256, 184-5.

HENEKA, M. T., KUMMER, M. P. & LATZ, E. 2014. Innate immune activation in neurodegenerative disease. *Nat Rev Immunol,* 14, 463-77.

HOLMES, B. B., FURMAN, J. L., MAHAN, T. E., YAMASAKI, T. R., MIRBAHA, H., EADES, W. C., BELAYGOROD, L., CAIRNS, N. J., HOLTZMAN, D. M. & DIAMOND, M. I. 2014. Proteopathic tau seeding predicts tauopathy in vivo. *Proc Natl Acad Sci U S A,* 111, E4376-85.

HYMAN, B. T., PHELPS, C. H., BEACH, T. G., BIGIO, E. H., CAIRNS, N. J., CARRILLO, M. C., DICKSON, D. W., DUYCKAERTS, C., FROSCH, M. P., MASLIAH, E., MIRRA, S. S., NELSON, P. T., SCHNEIDER, J. A., THAL, D. R., THIES, B., TROJANOWSKI, J. Q., VINTERS, H. V. & MONTINE, T. J. 2012. National Institute on Aging-Alzheimer's Association guidelines for the neuropathologic assessment of Alzheimer's disease. *Alzheimers Dement,* 8, 1-13.

IACCARINO, H. F., SINGER, A. C., MARTORELL, A. J., RUDENKO, A., GAO, F., GILLINGHAM, T. Z., MATHYS, H., SEO, J., KRITSKIY, O., ABDURROB, F., ADAIKKAN, C., CANTER, R. G., RUEDA, R., BROWN, E. N., BOYDEN, E. S. & TSAI, L. H. 2016. Gamma frequency entrainment attenuates amyloid load and modifies microglia. *Nature,* 540, 230-235.

IHARA, Y., NUKINA, N., MIURA, R. & OGAWARA, M. 1986. Phosphorylated tau protein is integrated into paired helical filaments in Alzheimer's disease. *J Biochem,* 99, 1807-10.

ILIFF, J. J., WANG, M., LIAO, Y., PLOGG, B. A., PENG, W., GUNDERSEN, G. A., BENVENISTE, H., VATES, G. E., DEANE, R., GOLDMAN, S. A., NAGELHUS, E. A. & NEDERGAARD, M. 2012. A paravascular pathway facilitates CSF flow through the brain parenchyma and the clearance of interstitial solutes, including amyloid β. *Sci Transl Med,* 4, 147ra111.

ITTNER, L. M. & GÖTZ, J. 2011. Amyloid-β and tau--a toxic pas de deux in Alzheimer's disease. *Nat Rev Neurosci,* 12**,** 65-72.

JIA, X., XING, D. & KOHN, A. 2013. No consistent relationship between gamma power and peak frequency in macaque primary visual cortex. *J Neurosci,* 33**,** 17-25.

KANEKIYO, T., CIRRITO, J. R., LIU, C. C., SHINOHARA, M., LI, J., SCHULER, D. R., HOLTZMAN, D. M. & BU, G. 2013. Neuronal clearance of amyloid-β by endocytic receptor LRP1. *J Neurosci,* 33**,** 19276-83.

KEREN-SHAUL, H., SPINRAD, A., WEINER, A., MATCOVITCH-NATAN, O., DVIR-SZTERNFELD, R., ULLAND, T. K., DAVID, E., BARUCH, K., LARA-ASTAISO, D., TOTH, B., ITZKOVITZ, S., COLONNA, M., SCHWARTZ, M. & AMIT, I. 2017. A Unique Microglia Type Associated with Restricting Development of Alzheimer's Disease. *Cell,* 169**,** 1276-1290.e17.

KIM, H., ÄHRLUND-RICHTER, S., WANG, X., DEISSEROTH, K. & CARLÉN, M. 2016. Prefrontal Parvalbumin Neurons in Control of Attention. *Cell,* 164**,** 208-18.

Kim, S.Y., Cho, J.H., Murray, E., Bakh, N., Choi, H., Ohn, K., Ruelas, L., Hubbert, A., McCue, M., Vassallo, S.L.*, et al.* (2015). Stochastic electrotransport selectively enhances the transport of highly electromobile molecules. Proc Natl Acad Sci U S A *112*, E6274-6283.

KITAMURA, T., OGAWA, S. K., ROY, D. S., OKUYAMA, T., MORRISSEY, M. D., SMITH, L. M., REDONDO, R. L. & TONEGAWA, S. 2017. Engrams and circuits crucial for systems consolidation of a memory. *Science,* 356**,** 73-78.

KNOBLICH, U., SIEGLE, J. H., PRITCHETT, D. L. & MOORE, C. I. 2010. What do we gain from gamma? Local dynamic gain modulation drives enhanced efficacy and efficiency of signal transmission. *Front Hum Neurosci,* 4**,** 185.

Kisler, K., Nelson, A.R., Montagne, A., and Zlokovic, B.V. (2017). Cerebral blood flow regulation and neurovascular dysfunction in Alzheimer disease. Nat Rev Neurosci *18*, 419-434.

KYRTSOS, C. R. & BARAS, J. S. 2015. Modeling the Role of the Glymphatic Pathway and Cerebral Blood Vessel Properties in Alzheimer's Disease Pathogenesis. *PLoS One,* 10**,** e0139574.

LEE, M., SCHWAB, C. & MCGEER, P. L. 2011. Astrocytes are GABAergic cells that modulate microglial activity. *Glia,* 59**,** 152-65.

LEE, V. M., GOEDERT, M. & TROJANOWSKI, J. Q. 2001. Neurodegenerative tauopathies. *Annu Rev Neurosci,* 24**,** 1121-59.

LEGER, M., QUIEDEVILLE, A., BOUET, V., HAELEWYN, B., BOULOUARD, M., SCHUMANN-BARD, P. & FRERET, T. 2013. Object recognition test in mice. *Nat Protoc,* 8**,** 2531-7.

LIDDELOW, S. A. & BARRES, B. A. 2017. Reactive Astrocytes: Production, Function, and Therapeutic Potential. *Immunity,* 46**,** 957-967.

LINDWALL, G. & COLE, R. D. 1984. Phosphorylation affects the ability of tau protein to promote microtubule assembly. *J Biol Chem,* 259**,** 5301-5.

LOSI, G., MARIOTTI, L. & CARMIGNOTO, G. 2014. GABAergic interneuron to astrocyte signalling: a neglected form of cell communication in the brain. *Philos Trans R Soc Lond B Biol Sci,* 369**,** 20130609.

Lu, T., Liang, L., and Wang, X. (2001). Neural representations of temporally asymmetric stimuli in the auditory cortex of awake primates. J Neurophysiol *85*, 2364-2380.

Ma, L., Tai, X., Su, L., Shi, L., Wang, E., and Qin, L. (2013). The neuronal responses to repetitive acoustic pulses in different fields of the auditory cortex of awake rats. PLoS One *8*, e64288.

MATHYS, H., ADAIKKAN, C., GAO, F., YOUNG, J. Z., MANET, E., HEMBERG, M., DE JAGER, P. L., RANSOHOFF, R. M., REGEV, A. & TSAI, L. H. 2017. Temporal Tracking of Microglia Activation in Neurodegeneration at Single-Cell Resolution. *Cell Rep,* 21**,** 366-380.

MAVIEL, T., DURKIN, T. P., MENZAGHI, F. & BONTEMPI, B. 2004. Sites of neocortical reorganization critical for remote spatial memory. *Science,* 305**,** 96-9.

Mears, R.P., Klein, A.C., and Cromwell, H.C. (2006). Auditory inhibitory gating in medial prefrontal cortex: Single unit and local field potential analysis. Neuroscience *141*, 47-65.

Miller, C.L., and Freedman, R. (1995). The activity of hippocampal interneurons and pyramidal cells during the response of the hippocampus to repeated auditory stimuli. Neuroscience *69*, 371-381.

MORRIS, R. 1984. Developments of a water-maze procedure for studying spatial learning in the rat. *J Neurosci Methods,* 11**,** 47-60.

MOSHER, K. I. & WYSS-CORAY, T. 2014. Microglial dysfunction in brain aging and Alzheimer's disease. *Biochem Pharmacol,* 88, 594-604.

OAKLEY, H., COLE, S. L., LOGAN, S., MAUS, E., SHAO, P., CRAFT, J., GUILLOZET-BONGAARTS, A., OHNO, M., DISTERHOFT, J., VAN ELDIK, L., BERRY, R. & VASSAR, R. 2006. Intraneuronal beta-amyloid aggregates, neurodegeneration, and neuron loss in transgenic mice with five familial Alzheimer's disease mutations: potential factors in amyloid plaque formation. *J Neurosci,* 26, 10129-40.

PALOP, J. J., CHIN, J., ROBERSON, E. D., WANG, J., THWIN, M. T., BIEN-LY, N., YOO, J., HO, K. O., YU, G. Q., KREITZER, A., FINKBEINER, S., NOEBELS, J. L. & MUCKE, L. 2007. Aberrant excitatory neuronal activity and compensatory remodeling of inhibitory hippocampal circuits in mouse models of Alzheimer's disease. *Neuron,* 55, 697-711.

Park, Y.G., Sohn, C.H., Chen, R., McCue, M., Yun, D.H., Drummond, G.T., Ku, T., Evans, N.B., Oak, H.C., Trieu, W., *et al.* (2018). Protection of tissue physicochemical properties using polyfunctional crosslinkers. Nat Biotechnol.

RAGER, G. & SINGER, W. 1998. The response of cat visual cortex to flicker stimuli of variable frequency. *Eur J Neurosci,* 10, 1856-77.

RANSOHOFF, R. M. & CARDONA, A. E. 2010. The myeloid cells of the central nervous system parenchyma. *Nature,* 468, 253-62.

RANSOHOFF, R. M. & PERRY, V. H. 2009. Microglial physiology: unique stimuli, specialized responses. *Annu Rev Immunol,* 27, 119-45.

RAY, S. & MAUNSELL, J. H. 2015. Do gamma oscillations play a role in cerebral cortex? *Trends Cogn Sci,* 19, 78-85.

RODRÍGUEZ, J. J., OLABARRIA, M., CHVATAL, A. & VERKHRATSKY, A. 2009. Astroglia in dementia and Alzheimer's disease. *Cell Death Differ,* 16, 378-85.

ROSSANT, C., KADIR, S. N., GOODMAN, D. F. M., SCHULMAN, J., HUNTER, M. L. D., SALEEM, A. B., GROSMARK, A., BELLUSCIO, M., DENFIELD, G. H., ECKER, A. S., TOLIAS, A. S., SOLOMON, S., BUZSAKI, G., CARANDINI, M. & HARRIS, K. D. 2016. Spike sorting for large, dense electrode arrays. *Nat Neurosci,* 19, 634-641.

SAIJO, K. & GLASS, C. K. 2011. Microglial cell origin and phenotypes in health and disease. *Nat Rev Immunol,* 11, 775-87.

SEELEY, W. W., CRAWFORD, R. K., ZHOU, J., MILLER, B. L. & GREICIUS, M. D. 2009. Neurodegenerative diseases target large-scale human brain networks. *Neuron,* 62, 42-52.

SELKOE, D. J., YAMAZAKI, T., CITRON, M., PODLISNY, M. B., KOO, E. H., TEPLOW, D. B. & HAASS, C. 1996. The role of APP processing and trafficking pathways in the formation of amyloid beta-protein. *Ann N Y Acad Sci,* 777, 57-64.

SHORE, S. E., ROBERTS, L. E. & LANGGUTH, B. 2016. Maladaptive plasticity in tinnitus--triggers, mechanisms and treatment. *Nat Rev Neurol,* 12, 150-60.

SOHAL, V. S. 2016. How Close Are We to Understanding What (if Anything) γ Oscillations Do in Cortical Circuits? *J Neurosci,* 36, 10489-10495.

SOHAL, V. S., ZHANG, F., YIZHAR, O. & DEISSEROTH, K. 2009. Parvalbumin neurons and gamma rhythms enhance cortical circuit performance. *Nature,* 459, 698-702.

SPELLMAN, T., RIGOTTI, M., AHMARI, S. E., FUSI, S., GOGOS, J. A. & GORDON, J. A. 2015. Hippocampal-prefrontal input supports spatial encoding in working memory. *Nature,* 522, 309-14.

SPERLING, R. A., DICKERSON, B. C., PIHLAJAMAKI, M., VANNINI, P., LAVIOLETTE, P. S., VITOLO, O. V., HEDDEN, T., BECKER, J. A., RENTZ, D. M., SELKOE, D. J. & JOHNSON, K. A. 2010. Functional alterations in memory networks in early Alzheimer's disease. *Neuromolecular Med,* 12, 27-43.

STORCK, S. E., MEISTER, S., NAHRATH, J., MEIßNER, J. N., SCHUBERT, N., DI SPIEZIO, A., BACHES, S., VANDENBROUCKE, R. E., BOUTER, Y., PRIKULIS, I., KORTH, C., WEGGEN, S., HEIMANN, A., SCHWANINGER, M., BAYER, T. A. & PIETRZIK, C. U. 2016. Endothelial LRP1 transports amyloid-β(1-42) across the blood-brain barrier. *J Clin Invest,* 126, 123-36.

TAKEHARA, K., KAWAHARA, S. & KIRINO, Y. 2003. Time-dependent reorganization of the brain components underlying memory retention in trace eyeblink conditioning. *J Neurosci,* 23, 9897-905.

TAKEUCHI, H., IBA, M., INOUE, H., HIGUCHI, M., TAKAO, K., TSUKITA, K., KARATSU, Y., IWAMOTO, Y., MIYAKAWA, T., SUHARA, T., TROJANOWSKI, J. Q., LEE, V. M. & TAKAHASHI, R. 2011. P301S mutant human tau transgenic mice manifest early symptoms of human tauopathies with dementia and altered sensorimotor gating. *PLoS One,* 6, e21050.

VANMECHELEN, E., VANDERSTICHELE, H., DAVIDSSON, P., VAN KERSCHAVER, E., VAN DER PERRE, B., SJÖGREN, M., ANDREASEN, N. & BLENNOW, K. 2000. Quantification of tau

phosphorylated at threonine 181 in human cerebrospinal fluid: a sandwich ELISA with a synthetic phosphopeptide for standardization. *Neurosci Lett,* 285, 49-52.

VERRET, L., MANN, E. O., HANG, G. B., BARTH, A. M., COBOS, I., HO, K., DEVIDZE, N., MASLIAH, E., KREITZER, A. C., MODY, I., MUCKE, L. & PALOP, J. J. 2012. Inhibitory interneuron deficit links altered network activity and cognitive dysfunction in Alzheimer model. *Cell,* 149, 708-21.

VORHEES, C. V. & WILLIAMS, M. T. 2006. Morris water maze: procedures for assessing spatial and related forms of learning and memory. *Nat Protoc,* 1, 848-58.

WALKER, D. G. & LUE, L. F. 2015. Immune phenotypes of microglia in human neurodegenerative disease: challenges to detecting microglial polarization in human brains. *Alzheimers Res Ther,* 7, 56.

WANG, Y., CELLA, M., MALLINSON, K., ULRICH, J. D., YOUNG, K. L., ROBINETTE, M. L., GILFILLAN, S., KRISHNAN, G. M., SUDHAKAR, S., ZINSELMEYER, B. H., HOLTZMAN, D. M., CIRRITO, J. R. & COLONNA, M. 2015. TREM2 lipid sensing sustains the microglial response in an Alzheimer's disease model. *Cell,* 160, 1061-71.

WOLF, S. A., BODDEKE, H. W. & KETTENMANN, H. 2017. Microglia in Physiology and Disease. *Annu Rev Physiol,* 79, 619-643.

YAMAMOTO, J., SUH, J., TAKEUCHI, D. & TONEGAWA, S. 2014. Successful execution of working memory linked to synchronized high-frequency gamma oscillations. *Cell,* 157, 845-57.

YANKNER, B. A. & LU, T. 2009. Amyloid beta-protein toxicity and the pathogenesis of Alzheimer disease. *J Biol Chem,* 284, 4755-9.

YOSHIYAMA, Y., HIGUCHI, M., ZHANG, B., HUANG, S. M., IWATA, N., SAIDO, T. C., MAEDA, J., SUHARA, T., TROJANOWSKI, J. Q. & LEE, V. M. 2007. Synapse loss and microglial activation precede tangles in a P301S tauopathy mouse model. *Neuron,* 53, 337-51.